Universidad de Navarra

Facultad de Ciencias

"TARGETING OF XBP1/*HAC1* mRNA TO ENDOPLASMIC RETICULUM STRESS SIGNALING CENTERS"

Silvia Gómez Puerta

Universidad de Navarra

Facultad de Ciencias

Memoria presentada por Dª Silvia Gómez Puerta para aspirar al grado de Doctor por la Universidad de Navarra

El presente trabajo ha sido realizado bajo mi dirección en el Departamento de Terapia Génica y Regulación de la Expresión Génica y autorizo su presentación ante el Tribunal que lo ha de juzgar.

Pamplona, 26 de abril de 2016.

Dr. Tomás Aragón Amonarriz

Acknowledges

La realización del trabajo de investigación que se expone en este este documento no hubiera sido posible sin el apoyo del Ministerio de Economía y Competitividad del Gobierno de España y de la Universidad de Navarra, por lo cual les estamos muy agradecidos.

Igualmente, agradezco al Dr. Tomás Aragón Amonarriz por darme la oportunidad de participar en este excitante proyecto de investigación y por su acertada dirección científica; así como al Dr. Josepmaría Argemí Balbé y al Ing. Roberto Ferrero Laborda, por todo el apoyo brindado y por el buen ambiente de trabajo.

También quisiera agradecer a nuestros colaboradores, sin los cuales este trabajo de investigación no hubiese sido posible. A la Dra. Encarnación Martínez-Salas y a la Dra. Gloria Lozano del Centro Biología Molecular “Severo Ochoa”, al equipo de investigación del Dr. Eelco van Anken de la Università Vita-Salute San Raffaele, a Dr. Alfredo Castello y a la Dra. Aino Jarvelin de la Universidad de Oxford, al Dr. Rafael Aldabe, a la Dra. Montserrat Arrasate y al Dpto. De Imagen del Centro de Investigación Médica Aplicada (CIMA).

Incluyo en estos agradecimientos a todas las personas del Departamento de Terapia Génica y Regulación de la Expresión Génica del CIMA, por la cooperación y la solidaridad ofrecida en todo momento, especialmente al grupo de investigación de la Dra. Carmen Berasain y a la Dra. Gloria González por su apoyo y colaboración.

Por último, quisiera agradecer la excelente preparación recibida en mi país de origen, Cuba, sin la cual no hubiese podido acceder a los estudios de doctorado.

A todos y todas doy las gracias por lo aprendido durante estos 4 años.

Silvia Gómez Puerta.

A mis padres,

A Iván.

INDEX

List of Abbreviations:

ATF4: Activating Transcription Factor-4

ATF6: Activated Transcription Factor-6

BiP: Immunoglobulin-Binding Protein

b-ZIP: Basic Leucine Zipper

eIF2α: eukaryotic Translation Initiation Factor-2

ER: Endoplasmic Reticulum

ERAD: ER-Associated Degradation

FISH: Fluorescent *in situ* Hybridization

FS: Frame shift

GFP: Green Fluorescent Protein

HR2: Hydrophobic Region 2

IRE1: Inositol Requiring-Protein-1

LE: Localization Element

ORF: Open Reading Frame

PERK: Protein Kinase RNA (PKR)-like ER kinase

RBP: RNA Binding Protein

RIDD: Regulated IRE1-Dependent Decay

RNase: Ribonuclease

SHAPE: Selective 2′-Hydroxyl Acylation analyzed by Primer Extension

SRP: Signal Recognition Particle

Tg: thapsigargin

Tm: tunicamycin

TMD: Transmembrane Domain

UPR: Unfolded Protein Response

XBP1: X-Box Binding Protein 1

XBP1s: spliced XBP1

XBP1u: unspliced XBP1

1. INTRODUCTION

Cells constitute the structural and functional unit of life. We are interested in figuring out how cells work in order to understand how life functions. So, a better understanding of life was my main motivation to join to the Tomás Aragón research group at the Gene Therapy and Regulation of Gene Expression Department of CIMA.

The aim of study of Tomás Aragón team is the study of the Unfolded Protein Response (UPR) that stars at the endoplasmic reticulum (ER) organelle, and its implications in neurological and hepatological pathologies. If we think that cells are a protein factory, the ER would be the specialized site where secreted and membrane proteins are correctly assembled before their final destination. External stimuli could increase the protein production demand and therefore the capacity of the ER could be compromised. When this happens a situation known as ER stress triggers the UPR, which constitute the intracellular signaling pathway that communicates this toxic situation to the cell nucleus, in order to restore protein folding homeostasis.

To transduce the signal from the ER lumen to the cell nucleus, an unconventional splicing reaction dedicated to a single mRNA molecule, *HAC1* in yeast and XBP1 in mammalian cells takes place. This reaction is initiated by the ER stress sensor centers formed by IRE1 protein. Previous research has revealed the existence of a mechanism that allows *HAC1*/XBP1 mRNAs to encounter with IRE1 protein at the ER membrane. In this research work, we are interested in understanding better the molecular mechanism that governs the *HAC1*/XBP1 mRNA transport to the ER sites where IRE1 initiates the response to stress.

1.1. The Unfolded Protein Response

The ER is the eukaryotic cell organelle where most secreted and transmembrane proteins are folded before they travel to their final destination. Approximately 30% of the cellular proteins (Rutkowski & Hegde 2010) are translocated into the ER lumen as unfolded polypeptide chains to undergo folding into the ER lumen (Keenan et al. 2001). The global load of polypeptides to be folded into the ER fluctuates in response to external stimuli and the physiological state of the cell. To ensure the quality of protein folding at the ER, cells have evolved a “quality control” pathway to ensure that the ER folding machinery fits the cellular folding needs. The UPR is an intracellular signaling pathway that senses deficiencies in protein folding within the ER and turns on a coping gene expression program to upgrade capacity. As such, the UPR is in principle a homeostatic pathway. However,

the UPR is more widely known as a coping response to stress. As mentioned above, UPR signaling is activated when an imbalance between unfolded and folded polypeptides occurs in the ER. This imbalance produces a dysfunctional state of the ER known as ER stress. For this reason, I will commonly refer to UPR-inducing conditions as “ER stress conditions”.

To alleviate ER stress, UPR activates transcriptional and translational responses elicited to achieve two mains actions:

1) Reduce the load of unfolded proteins in the ER lumen. Such reduction is achieved by the inhibition of overall translation. Also, unfolded polypeptides are sent back from the ER to the cytosol – or retrotranslocated – to be degraded by the proteasome via ER-associated degradation (ERAD) (Meusser et al. 2005). To shut down the expression of specific proteins, the UPR also reduces the amount of a subset of ER-associated mRNAs by activating the regulated IRE1-dependent decay (RIDD) (Hollien & Weissman 2006).

2) Increase the size and folding capacity in the ER lumen by transcriptional activation of genes that encode the chaperones and protein-modifying enzymes needed to fold proteins and to increase the size of the ER.

3) If the ER stress is prolonged the cell commits apoptosis (Ron & Walter 2007).

Under specific conditions, the UPR can be regulated to anticipate increased demand on the ER to fold proteins. For example, the differentiation of B lymphocytes into antibody-producing plasma cells requires UPR activation (Iwakoshi et al. 2003), presumably to increase the size and protein folding capacity of the ER to handle the markedly increased secretory pathway load generated by up-regulated immunoglobulin’s synthesis. Further, it has been shown that the UPR is controlled in a circadian clock dependent manner in hepatic cells (Cretenet et al. 2010), to guarantee the correct regulation of lipid metabolism. Also, it has been shown that the UPR is modulated by external stimuli such as infection, in which UPR activity is tuned by signaling through the Toll like receptors (TLR) that recognize the presence of pathogens (Woo et al. 2009).

In mammalian cells, three different transmembrane ER resident proteins have been described that constantly sense the equilibrium between the folded and unfolded proteins in the lumen of the ER. These proteins transduce a stress signal to the cytosol and trigger the UPR in the case of an ER perturbation. Each

transmembrane protein defines one of the UPR signaling mechanisms: the inositol requiring-protein-1 (IRE1) mechanism; the activating transcription factor-6 (ATF6) mechanism; and the protein kinase RNA (PKR)-like ER kinase (PERK) mechanism (Fig.1). The three UPR mechanisms work in parallel to activate, by different mechanisms, the basic leucine zipper (b-ZIP) transcription factors that induce the UPR gene expression program (Walter & Ron 2011).

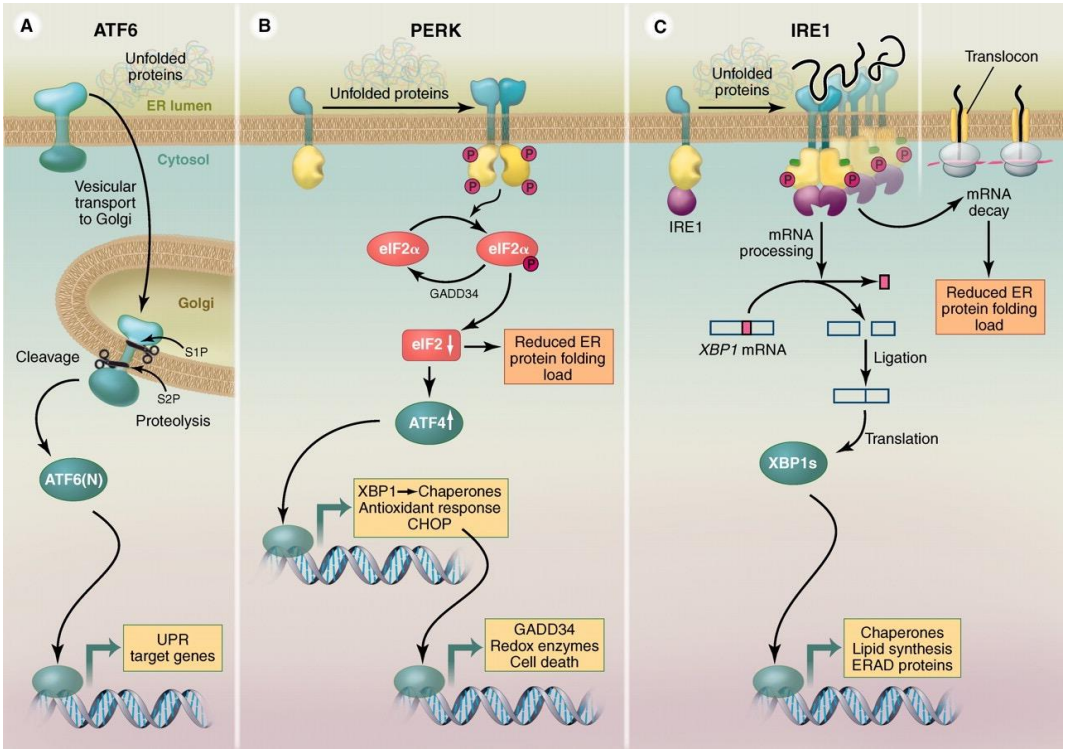

Figure 1. The three signaling mechanisms of the UPR. Three families of signal transducers (ATF6, PERK, and IRE1) sense the protein-folding conditions in the ER lumen and transmit that information, resulting in production of bZIP transcription regulators that enter the nucleus to drive transcription of UPR target genes. Each pathway uses a different mechanism of signal transduction: ATF6 by regulated proteolysis, PERK by translational control, and IRE1 by nonconventional mRNA splicing. In addition to the transcriptional responses that largely serve to increase the protein-folding capacity in the ER, both PERK and IRE1 reduce the ER folding load by down-tuning translation and degrading ER-bound mRNAs, respectively.

Source: Walter, P. & Ron, D., 2011. Science, 334(6059), pp.1081–1086.

1.1.1. How is ER stress sensed?

Since most ER protein folding substrates enter into the ER lumen as unfolded polypeptides, the molecular mechanism to sense the buildup of misfolded proteins has to be properly regulated. To sense ER stress, the transducer proteins ATF6, PERK and IRE1 contain a luminal domain that senses the protein folding status and transduces this information to the cytosol (Walter & Ron 2011). Three different

mechanisms have been proposed to explain how the luminal domains of these proteins sense ER stress (Ron & Walter 2007).

The first model proposes that the direct binding of folded proteins to the luminal ER stress sensing domains triggers UPR activation (Fig.2a). This model is based on the structure of the ER stress sensing luminal domain of yeast Ire1 protein (Ire1p). Credle and colleagues identified a cavity in the luminal domain, which possesses a major histocompatibility complex (MHC)–like architecture and has the adequate dimension to accommodate an extended polypeptide (Credle et al. 2005). In fact, a follow up study demonstrated that the luminal domain of yeast Ire1p could directly bind unfolded peptides with a relaxed specificity (Gardner & Walter 2011). Furthermore, the crystal structure of the luminal domain of mammalian IRE1α revealed a closed binding groove conformation (Zhou et al. 2006), suggesting that the binding of an extended peptide to the open groove structure could induce a conformational change that could in turn trigger IRE1α oligomerization and UPR activation.

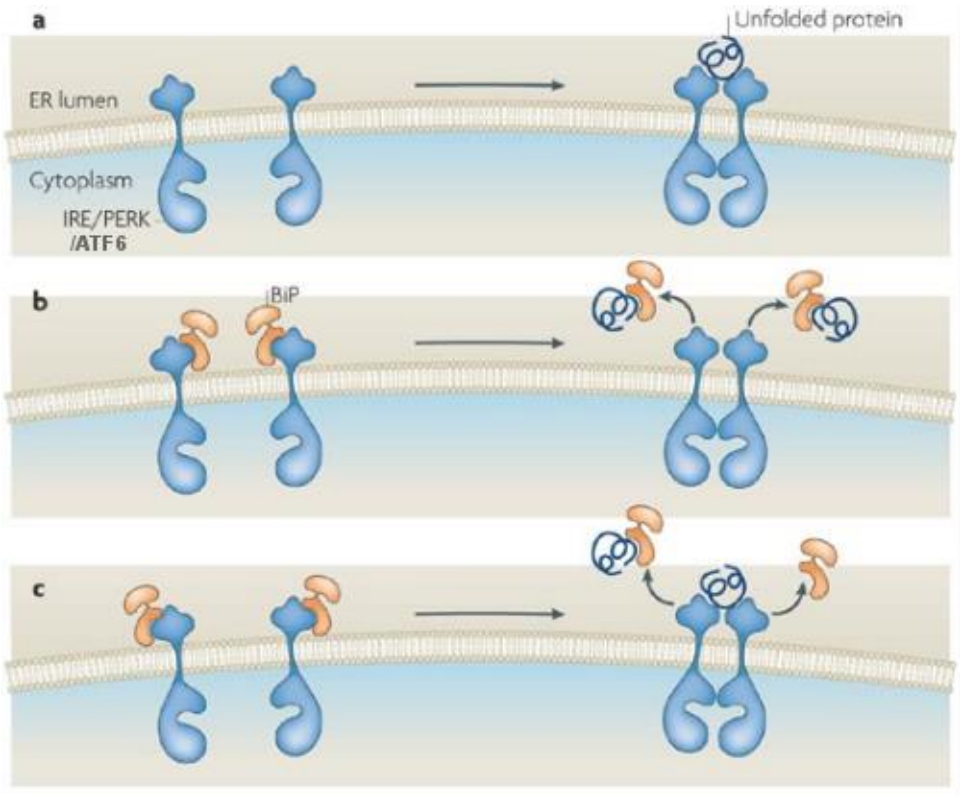

Figure 2. Models of UPR activation. a) Model I described that a direct binding of the unfolded proteins promote the oligomerization and activation of IRE1, PERK and ATF6 b) Model II, based in the direct binding of the chaperone resident protein BiP to the luminal domains of IRE1/PERK/ATF6 in the absence of ER stress, retaining them in the monomers state. In the presence of ER stress the BiP chaperone binds to the unfolded proteins, allowing the oligomerization of the IRE1/PERK luminal domains.c) a combination of Model I and Model II.

Source: Adapted from Ron, D. & Walter, P., 2007. Molecular cell biology, 8(7), pp.519–529.

The second model proposes that the immunoglobulin-binding protein (BiP), one of the most abundant ER chaperones, associates to the luminal domain of ATF6, PERK and IRE1 proteins and keeps them in an inactive state in the absence of ER stress. It has been shown that BiP dissociation from the IRE1 and PERK luminal domains allows the oligomerization and enzymatic activation of IRE1 and PERK (Walter & Ron 2011)(Fig.2b). This model is in agreement with the observation that BiP overexpression inhibits UPR, whereas reducing BiP expression levels activates the UPR (Bertolotti et al. 2000; Okamura et al. 2000). A fragment containing the regions II-IV of the luminal domains of PERK and yeast Ire1p bind directly to the ATPase domain of BiP, with Kd = 1.97 μM and 2.05 μM, respectively, consistent with a typical low affinity, transient protein–protein interaction. This low association constant could still be of high functional relevance, given the high concentration of BiP in the ER lumen. Binding of misfolded polypeptides to the substrate binding domain of BiP promotes the dissociation of IRE1/BiP and PERK/BiP complexes, thereby allowing the oligomerization of the transducer proteins and the initiation of UPR signaling (Carrara et al. 2014).

The third, most plausible model combines the two first models (Fig.2c). The idea is that both stimuli, the direct binding of misfolded proteins and the dissociation of BiP are sequentially needed for UPR activation. The release of BiP from the luminal domain of IRE1 and PERK would allow the oligomerization of the transducer proteins, followed by stabilization of IRE1/PERK foci by the direct binding of the unfolded proteins to the luminal domains (Ron & Walter 2007).

1.1.2. The ATF6 mechanism

Activated transcription factor-6 (ATF6) is synthesized as an ER resident transmembrane protein bearing a transcription factor moiety at its cytosolic side and a luminal ER stress sensing domain (Haze et al. 1999). The luminal ER stress sensing domain provides the mechanism to retain ATF6 at the ER under non stress conditions. Under ER stress, ATF6 is packaged into COP-II transport vesicles in the ER and transported to the Golgi apparatus. Translocation to the Golgi makes ATF6 accessible to proteases SP1 and SP2, which sequentially cleave ATF6 at its transmembrane domain (TMD), releasing an N-terminal cytosolic ATF6 fragment (ATF6f) to the cytosol (Schindler & Schekman 2009). Once liberated from its

membrane attachment, ATF6f acts as a functional transcription factor that enters the nucleus and activates the transcription of UPR target genes (Haze et al. 1999). ATF6f enhances the transcription of the ER folding machinery, such us the chaperone BiP, the protein disulfide isomerase (PDI), and glucose regulated protein 94 (GRP94) (Walter & Ron 2011). ATF6f also induces transcription of the X-box Binding Protein 1 (XBP1) mRNA (Yoshida et al. 2001) (Fig.1A).

1.1.3. The PERK mechanism

The protein kinase RNA (PKR)-like ER kinase (PERK) protein is a type I transmembrane ER protein specific to mammalian cells. As all ER transducers proteins, PERK has a luminal domain that senses the protein folding status at the ER lumen, followed by the transmembrane domain and a kinase domain located in the cytosolic compartment (Harding et al. 1999) (Fig.1B). PERK remains inactive in a monomeric state in the absence of ER stress. Under ER stress conditions, PERK oligomerizes and trans-authophosphorylates. In this state, PERK phosphorylates the α-subunit of eukaryotic translation initiation factor-2 (eIF2α) at Ser51 residue. Phosphorylation of eIF2α inhibits the capacity of the guanine nucleotide exchange factor eIF2B to recycle eIF2 to its active GTP-bound form. Thereby, PERK-induced eIF2α phosphorylation inhibits translation initiation and acutely inhibits global protein synthesis (Harding et al. 2000) (Fig.1B).

A second consequence of eIF2α phosphorylation is the privileged translation of a subset of specific mRNAs. Under eIF2α phosphorylation conditions the translation of mRNAs containing short upstream open reading frames at their 5´-untranslated region (or uORFs), which is normally not efficient, is greatly enhanced. One of the main mRNAs regulated by this mechanism encodes the activating transcription factor-4 (ATF4) protein (Lu et al. 2004) (Fig.1B). As a secondary messenger of the PERK activation, ATF4 activates the transcription of a substantial part of the UPR transcriptome (Harding et al. 2003). CHOP (transcription factor C/EBP homologous protein) is the best known ATF4 target gene. CHOP is a transcription factor that controls genes encoding components involved in apoptosis (Harding et al. 2000). CHOP reduces the amount of Bcl-2 protein (Mccullough et al. 2001), resulting thereby in the mitochondrial cytochrome c release, apoptosome formation, and activation of caspases pathway that lead to cell death (Bernales, Papa, et al. 2006).

Therefore, PERK signaling can both contribute in the coping responses to stress by reducing global translation, but it also can promote cell death by apoptosis, most likely under conditions of chronic or excessive ER stress. Interestingly, to control the phosphorylation levels of eiF2α, the PERK-induced CHOP gene activates the transcription of GADD34 (growth arrest and DNA damage inducible 34), which encodes the regulatory subunit of protein phosphatase 1 C (PP1C), which dephosphorylated the eIF2α subunit, as a negative feedback loop (Connor et al. 2001) (Fig.1B) to limit the extent of PERK signaling.

1.1.4. The IRE1 mechanism

IRE1 initiates the most conserved UPR signaling mechanism present in all eukaryotes, from yeast to human. IRE1 is a type I ER transmembrane protein with a luminal ER stress sensing domain and a cytoplasmic portion containing kinase and endoribonuclease domains (Cox et al. 1993; Mori et al. 1993) (Fig.1C). In *Saccharomyces cerevisiae* cells grown under standard laboratory conditions Ire1p is in a monomeric or low oligomeric form, while under ER stress Ire1p oligomerizes in the plane of the ER membrane. Oligomerization is a requisite for the activation of the kinase and RNase enzymatic domains. Once activated, Ire1p transduces the ER stress signal to the cytosol by cleaving mRNAs, *HAC1* mRNA in lower eukaryotes (Cox & Walter 1996) and XBP1 mRNA in metazoans (Calfon et al. 2002; Yoshida et al. 2001). *HAC1*/XBP1 mRNAs encode active b-ZIP transcription factors that activate the UPR expression program (Fig.1C).

1.1.4.1. IRE1 ER stress sensing and activation

Oligomerization of the Ire1p luminal domain is a crucial step for the activation of the Ire1 RNase domain (Korennykh et al. 2009; Aragón et al. 2009) (Fig.3A). The oligomerization of Ire1p luminal domains induces a conformational change that juxtaposes the kinase domains in a face-to-face configuration, facilitating trans-autophosphorylation. (Lee et al. 2008). The entry of ATP into the kinase pocket promotes a positive feedback loop for Ire1p oligomerization (Korennykh et al. 2009). After the trans-autophosphorylation, the RNase domain is activated by ensambling in a back-to back dimer conformation that further stacks into higher-order oligomers (Korennykh et al. 2009) (Fig.3 A&B).

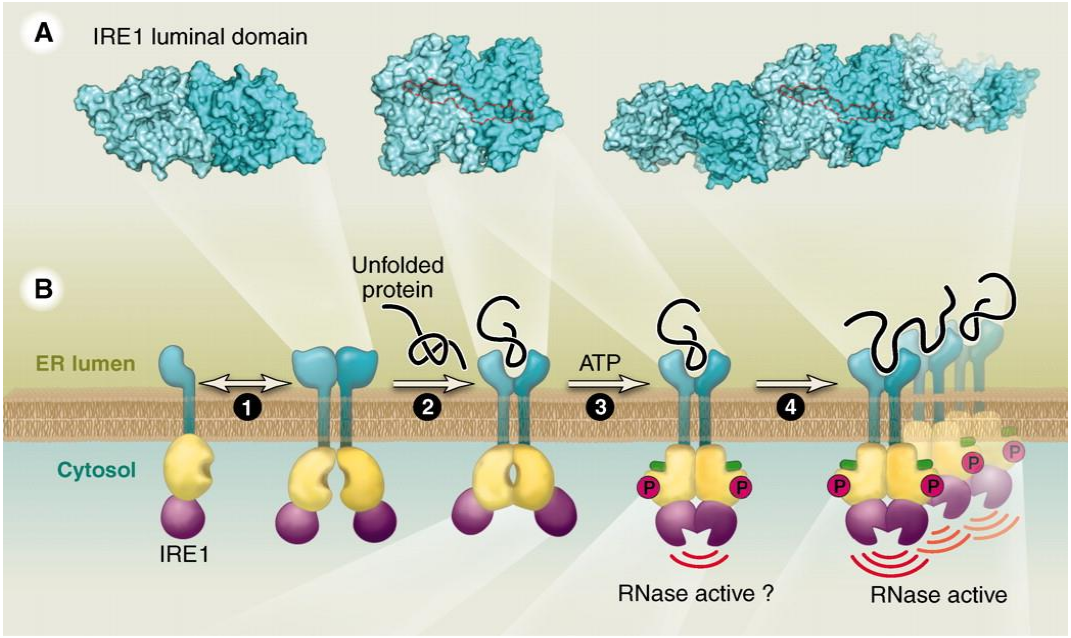

Figure 3. A speculative model of IRE1 activation. The figure depicts multiple structures of the IRE1 luminal ER stress–sensing domain (A) IRE1 cytosolic kinase and RNase domains (B). IRE1 monomers (step 1) engage homotypically in the plane of the membrane. ER luminal domains may form a closed dimer in which the proposed peptide-binding groove is occluded and further oligomerization is prevented. In response to protein misfolding (step 2), the luminal domain rearranges, allowing unfolded protein binding and further oligomerization, leading to front-to-front interactions of the kinase/RNase domains on the other, cytosolic side of the ER membrane. After trans-autophosphorylation, IRE1 forms back-to-back dimers (step 3) that stack into oligomers (step 4).

Source: Adapted from Walter, P. & Ron, D., 2011. Science, 334(6059), pp.1081–1086.

In mammalian cells two IRE1 genes have been identified, IRE1α and IRE1β, being IRE1α the most abundant protein, which is ubiquitously expressed, whereas IRE1β is only expressed in specialized epithelia from the gastrointestinal and respiratory tracts (Gardner & Walter 2011). As in yeast, mammalian IRE1α oligomerizes under ER stress conditions (Fig.3B) and requires the formation of a cluster of up to four or more monomers to activate the RNase domain. It has been demonstrated that the IRE1α RNase activity depends on the oligomerization of its luminal domain (Li et al. 2010). Furthermore, IRE1α phosphorylation is correlated with the formation of IRE1 foci and the splicing levels of XBP1, indicating that the trans-authophosphorylation in mammalian cells is a necessary step for the activation of the RNase domain, as in yeast (Li et al. 2010). Interestingly, it has been shown that nonmuscle myosin IIB heavy chain, a subunit of nonmuscle myosin IIB, is required for mammalian IRE1α aggregation and foci formation under ER stress (He et al. 2012).

1.1.4.2. *HAC1*/XBP1 mRNA splicing reaction by IRE1

Active IRE1 splices a unique substrate RNA target, *HAC1* mRNA in yeast (Sidrauski et al. 1996) and XBP1 mRNA in mammalian cells (Calfon et al. 2002; Yoshida et al. 2001), at the cytoplasmic surface of the ER. In yeast, *HAC1* contains a long, 252 nucleotide intron sequence that represses in *cis* the translation of *HAC1* mRNA by means of a long range RNA: RNA interaction with the 5' untranslated region of its own mRNA (Rüegsegger et al. 2001). The functional consequence is that there are no detectable Hac1p levels unless the intron is removed by splicing: After Ire1p cleavage of *HAC1* mRNA and ligation by the tRNA ligase Trl1 (Sidrauski et al. 1996), the transcription factor can be translated (Rüegsegger et al. 2001) (Fig.4).

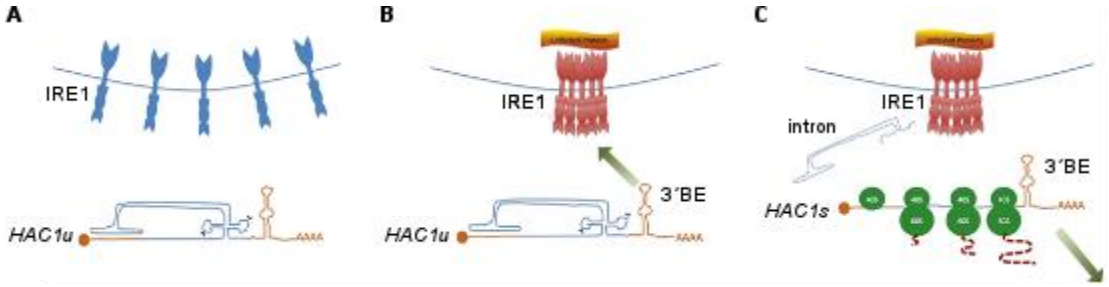

Figure 4 Recruitment of *HAC1* mRNA to ER membranes in yeast. (A) In the absence of ER stress, Ire1p is distributed throughout the ER membrane in a monomeric state. The unspliced *HAC1u* mRNA is cytosolic and translationally repressed by base-pairing between the 50 untranslated region (orange) and the intron. (B) Accumulation of misfolded proteins in the ER lumen (ER stress) activates Ire1p and leads to its clustering in foci that attract the translationally repressed *HAC1u* mRNA by a process that depends on the 3´ bipartite element (3´BE). (C) Ire1-dependent excision of the intron derepresses translation of the spliced *HAC1s* mRNA and release from the ER membrane.

Source: Adapted from Ron, D., 2009. Molecular Cell, 34(2):133-4.

In mammalian cells, the XBP1 intron is inserted within the coding sequence of the mRNA but is much shorter (only 26 nucleotides-long) and does not contribute to the translational silencing of XBP1 mRNA. In fact, unspliced XBP1 mRNA can be translated into a 33 kDa protein, Xbp1u, which is unstable and not efficient as a transcriptional factor (Calfon et al. 2002; Yoshida et al. 2001). Removal of the intron sequence by IRE1α and the subsequent exons ligation by the RtcB ligase (Lu et al. 2014) produces a translational frameshift that changes the carboxy-terminal half of XBP1 protein, yielding a larger protein, Xbp1s (54KDa) protein. Xbp1s protein encodes a potent transcription factor that regulates the transcription of some of the UPR target genes (Calfon et al. 2002) (Fig.5).

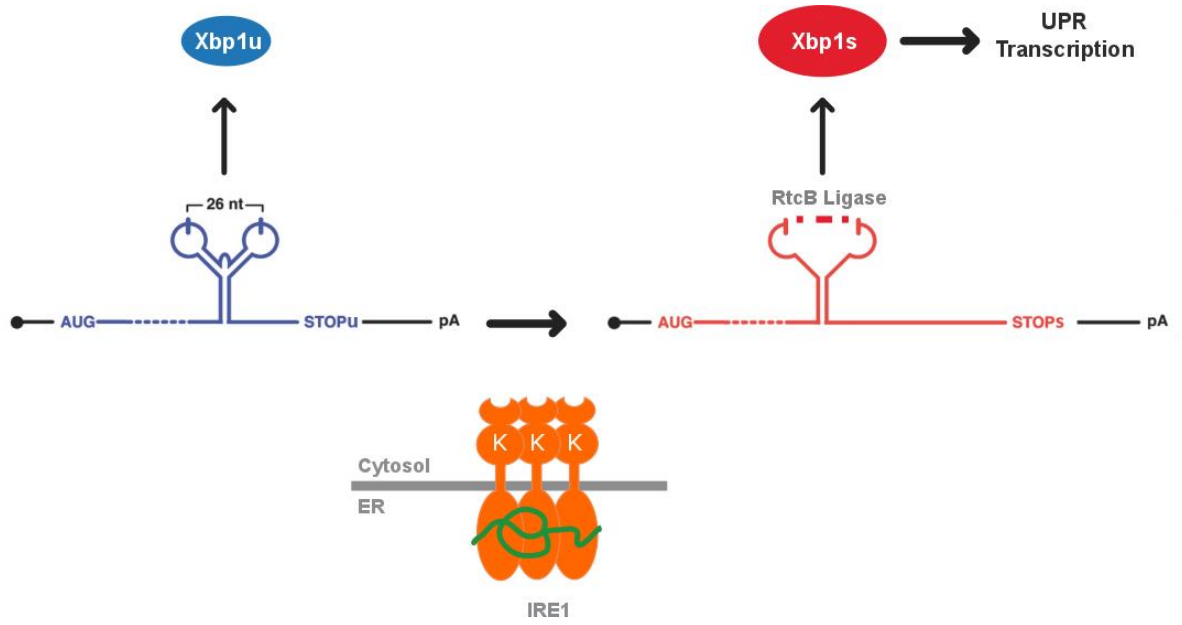

Figure 5 Illustrative scheme of the XBP1 transcripts and proteins variants. Unspliced XBP1 mRNA (XBP1u) encode for an approximately 33 kDa protein named Xbp1u. In the presence of ER stress active endoribonuclease IRE1 removed 26 nucleotides from XBP1u mRNA. The RtcB ligase joined the exons and produced the spliced XBP1 mRNA (XBP1s). The XBP1s mRNA encode for an approximately 54kDa protein named Xbp1s.

Altogether, from yeast to human, UPR splicing promotes changes in the translation of the XBP1/*HAC1* messenger RNAs, such that splicing makes them competent to express a functional transcription factor that will provide a strong response to ER stress.

1.1.4.3. Regulated IRE1-dependent decay pathway

Apart from the splicing of XBP1 mRNA, metazoan IRE1 can recognize other substrates to catalyze their cleavage and decay: This mechanism has been named the Regulated IRE1-Dependent Decay (RIDD). In this mechanism, IRE1 catalyzes the cleavage of mRNAs bound to the ER membrane, leading to their degradation (Hollien & Weissman 2006). The RIDD pathway is conserved in mammalian, Drosophila, and plant cells (Tam et al. 2014; Hollien & Weissman 2006; Hollien et al. 2009; Mishiba et al. 2013). RIDD target mRNAs encode secretory and plasma membrane proteins that, in most cases, are delivered to the ER by means of their signal peptide sequence; this requirement indicates that probably IRE1-mediated mRNA decay occurs during co-translational translocation (Hollien & Weissman 2006).

Recent work demonstrated that the catalytic mechanism of cleavage of the RIDD target mRNAs by IRE1 differs from the mechanism described for the splicing of

XBP1/*HAC1* mRNA (Tam et al. 2014). Although the activation of the nuclease and the kinase domain of IRE1 is required for both pathways, IRE1 oligomerization is only required for the splicing of XBP1/*HAC1* mRNAs (Tam et al. 2014). The authors further showed that the selective inhibition of XBP1 splicing by IRE1 leaves the RIDD pathway intact, promoting cell death (Tam et al. 2014).

It has been proposed that the RIDD pathway serves to mitigate ER stress by reducing the load of unfolded polypeptides that translocate into the ER lumen under ER stress. However this may not be the only function of RIDD. In mice lacking hepatic XBP1, IRE1 activity is exacerbated by the lack of ER homeostasis. In such situation, hepatic IRE1α is able to promote the degradation of lipogenic mRNA, which results in a significant drop in the levels of serum cholesterol and triglycerides (So et al. 2012). This observation demonstrates that XBP1 insufficiency could promote RIDD with distinct cell/tissue-specific consequences.

1.1.4.4. Molecular mechanism of IRE1 and XBP1/*HAC1* mRNA encounter

UPR splicing provides a very rapid response to sudden ER stress. A key step to warrant the rapid splicing kinetics is the mechanism that facilitates the encounter of active IRE1 and *HAC1*/XBP1 mRNA substrates in the ER stress response centers at the cytosolic side of the ER. Two different mechanisms with convergent features have been proposed in yeast and mammalian cells.

HAC1 mRNA transport mechanism

In yeast, ER stress causes the rapid concentration of Ire1p in a discrete number of foci (2-10 per cell) at the ER. Whether these clustering sites are arranged randomly or correspond to a specific ER subdomain is still unknown, but the oligomerization of Ire1p molecules driven by the luminal ER stress sensing domain of Ire1p is critical for the formation of the foci. Mutations disrupting dimerization interfaces impair Ire1p clustering and *HAC1* splicing. From these foci, Ire1p recruits *HAC1* mRNA and excises its intron (Korennykh et al. 2009; Aragón et al. 2009) .

The selective recruitment of *HAC1* mRNA is encoded in two independent determinants in *cis*. First, a stem-bulge domain near the tip of an extended stem at the 3’ untranslated region was identified as a key determinant for the co-localization of *HAC1* mRNA and Ire1p in foci. This element was initially identified as a sequence

conserved in all yeast *HAC1* mRNAs as a bipartite element and was therefore named 3' bipartite element (3'BE). While the 3'BE is essential to support efficient splicing *in vivo*, it was completely dispensable in *in vitro* cleavage assays, indicating that this element is not involved in Ire1p endonucleolytic catalysis (Aragón et al. 2009).

In addition to the 3´BE element, inhibition of translation through hybridization of the intron sequence to the 5´ untranslated region of *HAC1* mRNA (Rüegsegger et al. 2001), is required for the correct transport of *HAC1* mRNA to Ire1p foci. Removal of the intron sequence affects RNA recruitment efficiency. The requirement of the intron for targeting can be artificially bypassed by other translation inhibition mechanisms: Insertion of the 3'BE element together with a 5'-untranslated region stem loop, as a means to inhibit translation initiation, was sufficient to deliver the controls *PGK1* mRNA to Ire1p foci (Aragón et al. 2009).

The direct participation of the *HAC1* intron in the mRNA localization is interesting because it specifies the selective recruitment of unspliced, but not spliced *HAC1* mRNA molecules to the splicing centers, thereby preventing futile cycles of RNA recruitment to Ire1p, once splicing has taken place (Fig.4).

XBP1 mRNA transport mechanism

In higher eukaryotes, the XBP1 intron does not inhibit translation as the yeast intron does (Calfon et al. 2002). Still it plays a key role in the targeting model proposed, which is based in the preferential association of XBP1u mRNA to ER membranes. According to Yanagitani and colleagues, in the absence of ER stress, XBP1u mRNA displays a high level of association to membranes, which resembles binding efficiencies comparable to mRNAs encoding secreted proteins. In contrast, when ER stress was induced, the XBP1s mRNA behaves as a cytosolic mRNA (Yanagitani et al. 2009) (Fig.6). Of note, the association of XBP1 mRNA to membranes was determined by velocity sedimentation procedures.

The selective association of XBP1u to membranes requires the translation of the XBP1u mRNA. The systematic mutational analysis on the XBP1u mRNA sequence in combination with mRNA membrane association assays demonstrated that an aminoacidic determinant encoded in the open reading frame of the XBP1u, but not the frame of XBP1s mRNA, determines XBP1 mRNA association with the membranes. This determinant turned out to be a hydrophobic peptide region (HR2) that promotes the co-translational association of the ternary complex formed by the

XBP1 mRNA/ribosome and nascent chain to membranes. To be recruited to membrane as a complex, a translational pausing mechanism exists that provides the needed stability to this complex (Yanagitani et al. 2011); a C-terminal aminoacidic stretch located right after the HR2 peptide provides the transient pausing of the ribosomes before the STOP codon.

The original idea to explain how the HR2 peptide promotes membrane association suggested that, given the lipophilic nature of the HR2 peptide it could directly associate with membranes (Yanagitani et al. 2009). However, other alternatives seem also reasonable. A recent report from Plumb and colleagues demonstrated that IRE1α can associate with components of the translocon, which are the gates for the co-translational translocation of proteins to the ER lumen. Thus, one plausible explanation is that HR2 could be recognized by the signal recognition particle for the delivery to membranes. Independent on the transporting agent, the tethering of XBP1u mRNA to the ER does not require the presence of IRE1α in the cell.

After the splicing reaction has occurred, ribosomes translating XBP1s mRNA do not produce the HR2 peptide anymore, and therefore are not associated to the ER (Fig.6). Thus, as in the case of the targeting mechanism proposed for *HAC1* in yeast, this mode of recruitment selectively engages the unprocessed mRNA for targeting.

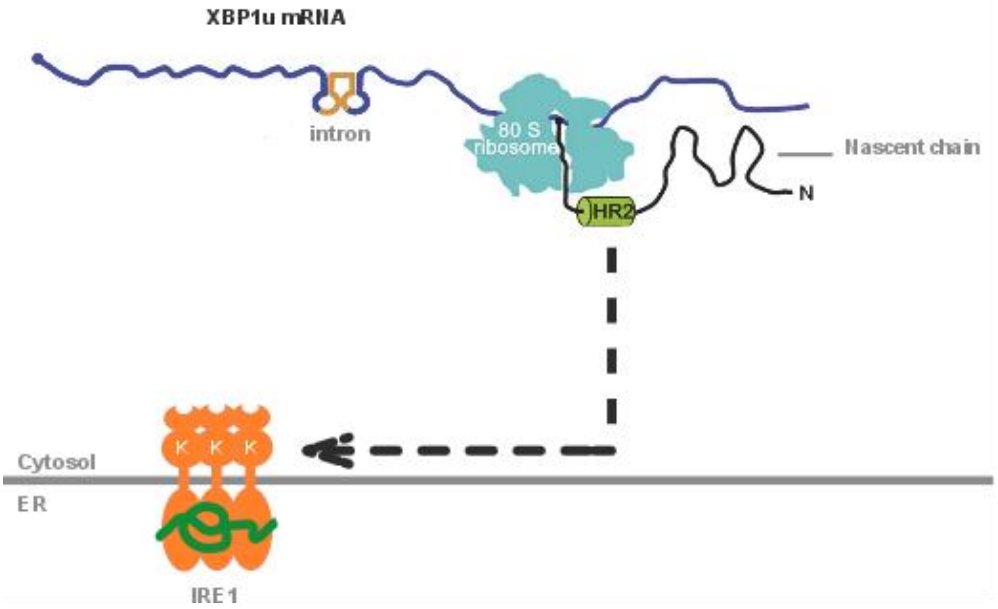

Figure 6 Illustrative scheme of the co-translational model proposed that describes the transport of the unspliced XBP1 mRNA (XBP1u mRNA) to the ER in mammalian cells, which facilitates the encounter with the endoribonuclease IRE1. In this model the nascent chain contains a hydrophobic peptide 2 (HR2) that promotes the association of the XBP1u mRNA/ribosome/nascent chain complex to the ER where IRE1 can process it.

Source: Adapted from: Yanagitani et al., 2009. Molecular Cell, 34(2):191-200

Two different mechanisms serving the same purpose

The splicing of XBP1/*HAC1* mRNA sets a unique paradigm in the regulation of gene expression, because transport of these transcripts is not meant to facilitate the localized translation of the mRNA, but instead serves to participate directly in signal transduction. Strikingly, eukaryotic cells have evolved very different mechanisms which provide the same essential properties: 1) While the yeast targeting mechanism is based on an RNA targeting element, mammalian XBP1 transport utilizes an peptide moiety for targeting 2) the translational inhibition is important to facilitate splicing in yeast, while translation is necessary to produce the targeting determinant in XBP1 mRNA, 3) Yeast *HAC1* recruitment is triggered by Ire1p clustering, but the tethering of XBP1 mRNA to membranes is *IRE1*-independent. Still, both mechanisms seem to facilitate the rapid and selective delivery of unspliced mRNA to IRE1 and foster splicing.

1.1.4.5. Biological relevance of XBP1 splicing

XBP1 mRNA splicing serves to enables the translation of the processed form of Xbp1 protein (Xbp1s). Considering that a highly conserved mechanism is dedicated to one single substrate, it is easy to understand the biological importance of this process for the function of the cell. In this section we will examine the consequences of XBP1 processing by IRE1.

Genetic manipulation of XBP1 in animal models has revealed some of its main functions in different tissues. The Xbp1s protein deficiency results in embryonic lethality owing to liver hypoplasia and anemia (Reimold et al. 2000). This lethality could be rescued by expression of XBP1 in the liver of Xbp1−/−, but these animals die shortly after birth due to the impairment of secretory organs, that is, the exocrine pancreas and salivary glands (Lee et al. 2005). Similarly, the targeted deletion of XBP1 in mice acinar gastric cells leads to the dysfunction of these cells (Huh et al. 2010).

XBP1 and transcription of the protein quality control machinery

Genome-wide transcriptomic profiling experiments revealed that, once produced, Xbp1s controls the transcription of a wide set of genes involved in a wide

range of cellular functions. Many of the processes transcriptionally controlled by Xbp1s are directly linked to ER homeostasis. For instance, many of the enzymes that enable N-linked glycosylation, a large fraction of ER resident chaperones and the redox components that ensure disulfide bond formation are regulated at least in part by Xbp1s. Likewise, degradation of ERAD substrates depends to a large extent on the transcription of its components by Xbp1s (Iwakoshi et al. 2003, Yoshida et al. 2003).

The transcriptional control of the core, conserved ER functions is conserved througt evolution. Genetic and transcriptomic evidence demonstrated that a) yeast Hac1p transcription factor directly participates in the transcriptional regulation of up to 5% of the *Saccharomyces cerevisiae* transcriptome comprising most of the ER functional components (Travers et al. 2000) and b) *IRE1/HAC1*-dependent transcription is essential for survival when specific processes in the ER were compromised. In particular, when protein N-glycosylation and ERAD components were genetically ablated UPR transcription was strongly activated (Jonikas et al. 2009). Moreover, ERAD components became essential for survival when *HAC1* or *IRE1* genes where knocked out, underscoring the close functional connection between UPR signaling and ER quality control (Travers et al. 2000; Friedlander et al. 2000).

Multiple myeloma cells are committed to synthesize and secrete high levels of immunoglobulins; according to this feature, they display a high level of UPR activation which is required to keep the folding homeostasis. Impairing ERAD-mediated degradation of misfolded proteins is particular toxic for these tumoral cells. In line with this idea, proteasome inhibition could increase the accumulation of misfolded proteins inside the ER and exacerbate ER stress, in a way that could not be alleviated. Such stress cannot be resolved and cells commit to apoptosis. This is rationale to treat Multiple Myeloma with the proteasomal inhibitor Bortezomib (Ling et al. 2012).

Severe alterations of ER protein folding can also activate autophagy, as a parallel/ alternative mechanism to clear misfolded proteins and re-use the resulting aminoacid pool in new cycles of translation. In line with this idea, transcription of many rate-limiting components of the autophagic machinery (like Beclin-1) is controlled by Xbp1s (Tian et al. 2015, Pehar et al. 2012). Again, the main principles that link UPR and autophagy were previously identified in yeast, where the selective

autophagy of the ER (or ER-phagy) has been documented in cells under ER stress (Bernales et al. 2006). Current work in yeast and mammals is identifying the main components involved in this process (Khaminets et al. 2015, Lipatova & Segev 2015). Of note, unpublished data from our group indicate that hepatic Xbp1s associates to the promoters of some of these components, like FAM134b.

As mentioned above, the increment of ER size constitutes one of the UPR activation consequences. It has been reported in different studies that Xbp1s contributes to ER expansion by promoting the transcription of genes involved in the maintenance and expansion of ER during the UPR (Acosta-alvear et al. 2007). For instance, Xbp1s induces the biosynthesis of phosphatidylcholine, the primary phospholipid of ER membrane (Sriburi et al. 2004; Sriburi et al. 2007).

XBP1 and disease

XBP1 has been related with cancer disease. For instance, the splicing and the subsequent production of Xbp1s correlates directly with an increase in the survival of breast cancer tumor cells (Davies et al. 2008). Similarly, XBP1 mRNA splicing is activated in human triple-negative breast cancer (TNBC), contributing to the tumorogenicity and disease progression (Chen et al. 2014). Additionally, Xbp1s transcription factor is essential for angiogenesis during early tumor growth in human pancreatic adenocarcinomas, thereby facilitating tumor growth (Romero-Ramirez et al. 2009). Xbp1s is also an essential transcription factor for B-lymphocytes differentiation and its overactivation has been associated with the survival and malignance of multiple myeloma tumor (Carrasco et al. 2007).

XBP1 activation seems to play a relevant role in several neurodegenerative disorders (Hoozemans et al. 2005; Hoozemans et al. 2007). However the role that UPR – and in particular XBP1 – plays in these diseases is not uniform. As a coping response to cellular stress, Xbp1s should play a protective role. In line with this notion, after spinal cord injury (SCI), the UPR is activated and the expression of Xbp1s enhances locomotor recovery (Valenzuela et al. 2012). Similarly, in Drosophila melanogaster and in mammalian cellular models of Alzheimer's disease, expression of Xbp1s decreases the toxicity of amyloid-β by preventing the accumulation of free (Ca+2) in the cytosol (Casas-Tinto et al. 2011).

In contrast, XBP1 may also contribute to neurodegeneration. In a murine model of amyotrophic lateral sclerosis (ALS), deletion of the XBP1 alleviated SOD1-induced neurodegeration by causing an increase of PERK and ATF6 UPR

mechanisms and the ensuing increase of autophagy in motoneurons (Hetz et al. 2009). In Parkinson disease the role of XBP1 is even less clear: The absence of Xbp1s produces different effects in the dopaminergic neurons depending on the stage when XBP1 is depleted. Knocking out Xbp1s during the development protects the cells against α-Synuclein toxicity, while in adults it seems to promote neurodegeneration, suggesting that Xbp1s plays an essential role in the maintainance of protein homeostasis in dopaminergic neurons (Valdés et al. 2014).

In secretory professional cells, like pancreatic β cells, Xbp1s is essential for cell function and survival. As pancreatic β cells are committed to secrete massive levels of insulin in response to glucose serum levels, the folding capacity of the ER in these cells needs to adapt constantly to the insulin requirement. Xbp1s deficiency in these cells caused a defect in the pro-insulin processing, insulin secretion and inhibited cell proliferation. These strong effects were not only due an inefficient UPR response, but also to the over-activation of IRE1α endoribonuclease, which degraded mRNAs encoding processing-proinsulin enzymes (Lee et al. 2011).

1.2. Localization of RNAs within the cell

Intracellular localization of RNAs constitutes a mode of post-transcriptional regulation, whereby in most cases the synthesis of specific proteins in their cytoplasmic site of function can be spatially and temporally controlled. The molecular mechanisms responsible for the proper RNA localization are better known in transcripts encoding proteins involved in specialized functions in well-defined cellular compartments (Martin & Ephrussi 2009).

One example is the *ASH1* (asymmetric synthesis of HO 1) mRNA, which encodes for a transcriptional repressor in yeast. During the late anaphase of the cell cycle, the *ASH1* mRNA is transported to the bud tip such that it is delivered only to the nucleus of the daughter cell where it functions as a transcriptional repressor of the HO endonuclease, inhibiting mating type switching in the daughter cell (Paquin & Chartrand 2008) (Fig.7A). Other classic examples occur during early development in Drosophila, where the localization of *oskar*, *gurken*, *bicoid* and *nanos* RNAs to the anterior and posterior poles of the oocyte is important to establish morphogen gradients that underlie the proper spatial patterning of the developing embryo (Johnstone & Lasko 2001) (Fig.7B). In a similar way, the mRNA encoding for the T-box transcription factor VegT in Xenopus oocytes localizes in the vegetal pole

inducing endodermal and mesodermal cell fates in the embryo (King et al. 2005) (Fig.7C). It has also been shown that the localization of β-*actin* mRNA in lamellipodia in motile chicken fibroblast cells is essential for cytoskeletal-mediated motility and directed cell migration (Condeelis & Singer 2005) (Fig.7D).

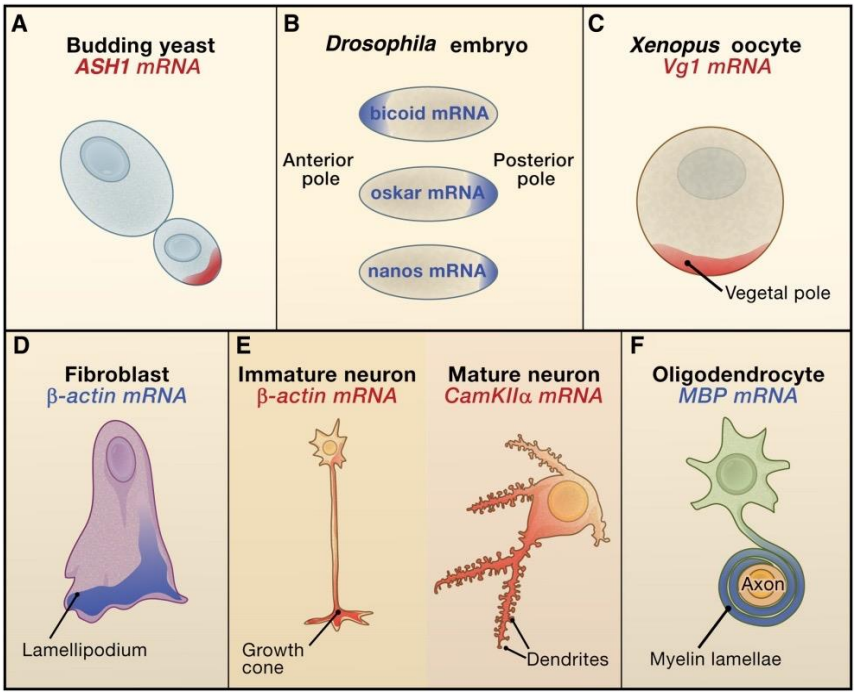

Figure 7. Classic examples of localized mRNAs. (A) In budding yeast, the *ASH*1 mRNA localizes to the bud tip. (B) In *Drosophila* embryos, *bicoid* mRNA localizes to the anterior pole; *oskar* and *nanos* mRNAs to the posterior pole. (C) In Xenopus oocytes (stage IV), Vg1 mRNA localizes to the vegetal pole. (D) In chick and mammalian fibroblasts, β-*actin* mRNA localizes to lamellipodia. (E) In developing, immature mammalian neurons, β-*actin* mRNA is present in distal growth cones and in mature, fully polarized pyramidal neurons, *CamKIIα* mRNA is present in distal dendrites. (F) In mammalian oligodendrocytes, myelin basic protein (MBP) mRNA localizes to myelinating processes that ensheath neuronal axons.

Source: Martin, K.C. & Ephrussi, A., 2009. Cell, 136(4): 719-730.

During brain development, the local translation of mRNAs in the axonal growth cone allows the immature neurons to respond to the local stimuli produced by their synaptic partners (Lin & Holt 2007) (Fig.7E). In the case of mature brain, local mRNA translation in one of the multiple synapse sites of a given neuron contributes to enhanced integration capacity and plasticity of the brain (Martin & Zukin 2006) (Fig.7E). Also, in oligodendrocytes, the mRNA encoding the myelin basic protein (MBP) is transported to the region where myelin assembly occurs and the protein is inserted directly into the nascent membrane (Chen et al. 2008) (Fig.7F).

Although large scale approaches have found the existence of localized RNAs in a variety of model systems such as *Drosophila* (Lécuyer et al. 2007), *Xenopus*

(Blower et al. 2007) and fibroblasts (Mili et al. 2008), in the majority of the cases, the molecular mechanisms of RNA transport to their cellular compartment is still unknown. However, some RNA transport mechanisms have been revealed from the in-depth studies of the classical localized RNA.

1.2.1. RNA transport depends on *cis*-acting elements

Cis-acting localization elements (LEs) or zipcode sequences have been found in localized mRNA as the sequence elements that determine the localization of a specific mRNA. Normally, LEs reside in the 3´ untranslated region (3´UTR), but they can also be found within the open reading frame. The length of the element can range from a few nucleotides to more than 1Kb (Jambhekar & Derisi 2007). These LEs or zipcode sequence are recognized by different RNA binding proteins (RBP) which connect the mRNA to specific transport relays.

For example, the zipcode regulatory sequence found in the 3´UTR of the β-*actin* mRNA mediates its localization to the cell leading edge in chicken fibroblasts (Kislauskis et al. 1994). The mutational analysis of this zipcode sequence identified a bipartite LE of 28 nucleotides, which is specifically recognized by the ZBP1 protein (zipcode-binding protein 1)(Chao et al. 2010; Patel et al. 2012). Another example is found in the *MBP* mRNA, which contains a LE of 11 nucleotides also located in its 3´UTR. This LE is recognized by the heterogeneous nuclear ribonucleoprotein (hnRNP) A2 to be properly transported in oligodendrocytes (Munro et al. 1999).

Several LEs have been identified and characterized in different biological systems (Jambhekar & Derisi 2007). However, a common pattern in the zipcode primary sequence or in their structure has not yet emerged, indicating heterogeneity of these motifs. RBPs could recognize both primary or secondary structures of LEs. For example, in *Drosophil*a, *bicoid* mRNA contains a helical region important for its proper transport (Macdonald & Kerr 1998). Interestingly, the primary LEs sequence of the *gurken*, *K10*, and the *I factor retrotransposon* mRNAs are all distinct, but could have similar three-dimensional structures. These LEs are recognized by the same RBP Egalitarian, an RNA adaptor protein involved in dynein-directed transport. Thus, different primary sequences can enable the recruitment of a similar localization machinery (Dienstbier et al. 2009). An interesting example of this principle is the yeast *ASH1* mRNA, in which four different zipcode sequences were found: E1, E2A, E2B, and E3 (Chartrand et al. 1999; Gonzalez et al. 1999). The LEs are distributed

throughout the transcript and do not show homology in their primary sequence, however, all of them can be recognized by the same RBP, the She2p protein (*SWI*5-dependent HO expression 2 protein), which mediates its localization to the bud tip (Long et al. 2000).

1.2.2. Nuclear events involved in cytoplasmic RNA localization

In the nucleus of cells, the pre-mRNAs undergo modifications such as the addition of the cap structure to the 5´-end, the addition of poly(A) to the 3´-end, and the deposition of the exon-exon junction complex proteins with the removal of introns during splicing (Hocine et al. 2010). These nuclear processes lead the association of different RBPs to the transcript, which can determine the final localization of the mRNA within the cytoplasm. For example, it has been shown that in *Drosophila*, the splicing of the first intron of *oskar* mRNA recruits Y14, a component of the exon junction complex, which is also an essential factor of the transport machinery and is required for the proper pole cytoplasmic localization of the transcript (Hachet & Ephrussi 2004). In rat hippocampal neurons, differential polyadenylation sites of two isoforms of brain-derived neurotrophic factor (BDNF), results in the selective association of localization elements in the long isoform, that deliver the transcript to dendrites (An et al. 2008). In yeast, the RBP She2p binds to the LEs sequence of the *ASH1* mRNA and promotes its nuclear export and the targeting to the daughter cell through cytoskeletal components (Long et al. 2000).

Once the mRNAs in complex with the RBP are in the cytosol, the associated proteins could then promote the binding of other proteins factors directly involved in RNA localization by the distinct types of transport mechanisms described below.

1.2.3. Types of RNA transport mechanism

Based on the experimental evidence from biochemical approaches and RNA visualization, different modes to carry the RNA to their properly subcellular localization have been proposed. These molecular mechanisms have been classified in 1) free diffusion and local anchored, 2) local protection from degradation 3) directional transport along the cytoskeletal components.

Free diffusion and local anchored

A mode of RNA localization is random diffusion of transcripts through the cytoplasm followed by their anchoring at their subcellular target site. For instance, during *Drosophila* development, the *nanos* mRNA is localized at the posterior pole of the oocytes (Johnstone & Lasko 2001). *In vivo* visualization of the *nanos* mRNA movement revealed that *nanos* mRNA is transported by diffusion and – once it gets to the posterior pole of the oocytes – it is anchored to this pole in an actin filaments dependent process (Forrest & Gavis 2003).

Selective RNA destabilization

Another way to achieve proper mRNA localization is through its selective stabilization in a specific site of the cell, while the same mRNA would be unstable (and therefore degraded) in the rest of the cell. In *Drosophila* development only 4% of *nanos* mRNA is protected and localized at the pole plasma by the local anchored mechanism described above, whereas the rest is degraded (Bergsten & Gavis 1999). The molecular mechanism that explains selective *nanos* degradation is based on the binding of the RBP Smaug to a zipcode sequence on the 3´UTR of *nanos* mRNA. The Smaug protein promotes the recruitment of the CCR4/POP2/NOT deadenylase complex, resulting in the deadenylation and destabilization of the transcript. In the posterior pole, *nanos* translation is possible thanks the presence of *oskar* protein, which precludes Smaug binding to *nanos* mRNA and thereby prevents the destabilization of *nanos* mRNA (Zaessinger et al. 2006).

Active transport of RNA within the cytosol

The mechanism of mRNA transport mediated by molecular motor proteins along the cytoskeleton fibers is the most common mechanism for localizing mRNA in most cell types. As explained above, often the localized RNAs contain LEs or zipcodes, which can be recognized by *trans*-acting factors such as RBPs within the nucleus. Once in the cytoplasm, the RBPs could bind to molecular motor proteins, which then promote the transport of the RNAs to their proper subcellular location along the cytoskeletal fibers. The mRNAs are either transported by the dynein or kinesin along microtubules or by myosin along actin filaments (Bullock 2007) (Fig.8).

During mid-oogenesis in *Drosophila*, the *bicoid*, *gurken* and *oskar* mRNAs are differentially confined within the cytoplasm by different molecular mechanisms. The *bicoid* mRNA is localized to the anterior pole, the *gurken* mRNA to the dorsal–

anterior, and the *oskar* mRNA to the posterior pole of the oocyte. In the case of the *bicoid* mRNA, localization depends on the microtubule network and requires the exposure to Exuparentia in the nurse cells (Cha et al. 2001). *gurken* mRNA localization depends only on cytoplasmic factors (MacDougall et al. 2003) and is statically anchored by dynein within large electron-dense cytoplasmic structures known as sponge bodies (Delanoue et al. 2007). By contrast, the localization of *oska*r mRNA at the posterior pole requires the heavy chain of kinesin 1 (KHC), a plus-end directed microtubule motor (Palacios & St Johnston 2002).

As mentioned above, the yeast *ASH1* mRNA is transported to the bud tip during cell division, and its transport depends on a zipcode sequence on the 3´UTR of *ASH1* mRNA, which is recognized by the She2p (Shen et al. 2009). The She2p protein interacts with She1p, which is a type V myosin, through a bridging protein She3p (Bookwalter et al. 2009). In the case of the β-actin mRNA, which localizes at leading edge of fibroblasts, the RNA is transported by both microtubules and actin filaments (Fusco et al. 2003), although it is predominantly dependent on actin and requires the function of myosin II-B (Latham et al. 2001). More than 50 transcripts have been found to localize at the leading edge of fibroblast cells and to require an intact microtubule cytoskeleton for this regional localization. These mRNAs are anchored in granules at the plus-ends of de-tyrosinated microtubules by the APC tumor- suppressor protein (Kertesz et al. 2010).

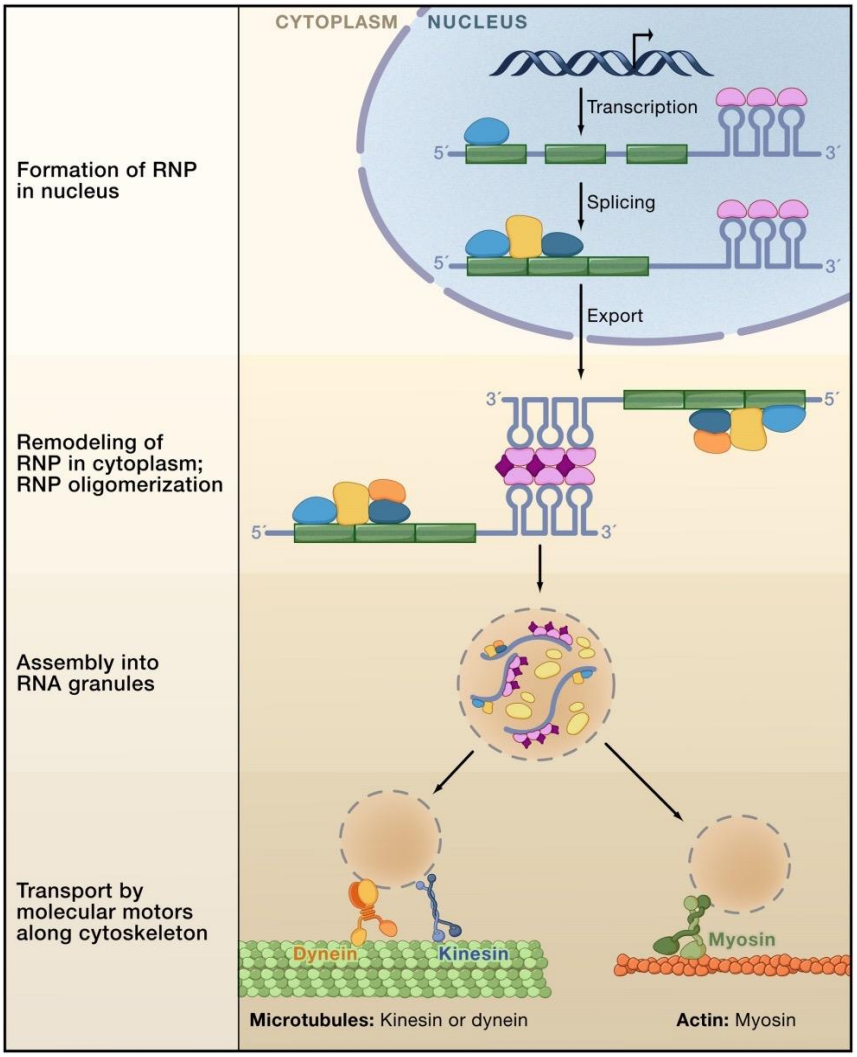

Figure 8. mRNA Localization is a multistep process. The pre-mRNA (exons in green; introns, 5′ and 3′UTRs in grey) has *cis*-acting localization elements in its primary sequence. These are usually in the 3′UTR and often form stem-loop structures. RNA-binding proteins (blue and purple) bind the pre-mRNA. During splicing, additional RNA-binding proteins (golden and dark blue) are added to form a ribonucleoprotein (RNP) complex. Following export into the cytoplasm, the RNP is remodeled as additional proteins (orange, dark purple) are added. In some cases, the RNP can form oligomers with other RNPs through protein-protein interactions. In the cytoplasm, RNPs are assembled into RNA granules that are likely a heterogeneous population of structures containing diverse RNAs, ribosomal subunits (yellow), as well as many factors involved in translational regulation. Recent studies suggest a dynamic relationship between RNA transport granules, P-bodies, and stress granules. The RNA granules associate with motor proteins and are transported by cytoskeletal elements to their final destination.

Source: Martin, K.C. & Ephrussi, A., 2009. Cell, 136(4): 719-730.

In the last years, the development of better methodologies to visualize the movement of individual RNA particles *in vivo* have allowed more accurate and quantitative measurements of RNA movement. For example, *in vivo* visualization of RNA reporters within the nucleus revealed that the movements of the transcripts were governed by the laws of diffusion and not active transport. The overall mRNA diffusion kinetics observed in the nucleus is approximately 0.005–0.02 $\mu m^2/s$ (Mor et

al. 2010). In the cytoplasm, mRNA movement has also been observed to occur by diffusion, although with faster kinetics due to the absence of chromatin (Mor et al. 2010).

The first study of RNA movement within the cytoplasm was done using the MS2 visualization system that allows the *in vivo* visualization of single molecules of RNA (Bertrand et al. 1998). Visualization of a lacZ mRNA reporter, without any zipcode sequence, showed that more than a half of the transcripts reporters diffused randomly trough the cytoplasm with a diffusion coefficient of 0.45 X 10^{-9} cm^2. The rest of the mRNA molecules remained in a static status, 20% of them associated to microtubules and microfilaments and 2-5% moved along microtubules in a directional manner at constant rate of 1.5 μm/s. When the β-actin zipcode sequence was inserted in the 3´UTR mRNA visualization reporters, the lacZ transcripts increased the frequency of active transport along the microtubules to 20% as well as the length of transport, implying that *cis*- acting elements may influence the probabilistic behavior of RNA populations (Fusco et al. 2003). *In vivo* visualization of localized mRNAs like *oska*r during *Drosophila* development revealed that the majority of this transcript diffused randomly and only 13% of the molecules were actively transported along the cytoskeleton (Doyle & Kiebler 2011). Thus, the idea that the most energetically efficient and thus preferred method of mRNA localization is diffusion and anchored has emerged. If the timing of mRNA localization is crucial, cells can use the active transport to recruit the RNA to the properly subcellular site.

1.2.4. Transport of mRNAs to the ER

The ER is the organelle where most secreted and membrane proteins have to be properly folded before being sorted to their destinations. By ultrastructure studies, Palade and colleagues demonstrated that secreted and membrane proteins are synthetized at ER-bound ribosomes (Caro & Palade 1964). To explain how mRNAs localize at the ER membrane a targeting model has been proposed and widely accepted in the research community. According to this model the translation of mRNAs that encode secreted and membrane proteins is initiated in the cytosol and the ribosome/mRNA complexes are specifically recruited to the ER membrane, thanks to a topogenic signal, either a signal sequence at the amino terminus of the nascent polypeptide chain or a transmembrane domain, as this signal emerges from the ribosome co-translationally. The Signal Recognition Particle (SRP), a

ribonucleoprotein complex universally conserved from bacterial to mammalian cells, mediatesthe co-translational targeting of mRNAs to the eukaryotic ER membrane or prokaryotic plasma membrane (Walter et al. 1984, Walter & Johnson 1994; Pool 2005).

1.2.5. mRNA transport by the Signal Recognition Particle

SRP-dependent targeting of mRNAs to the ER has been proposed to work in a strictly co-translational manner: when a nascent polypeptide that contains a topogenic signal, either a target signal or a transmembrane domain, emerges from the ribosome exit tunnel is recognized by the SRP complex. Then, the ribosome nascent chain complex (RNC) is transported to the proximity of Sec61p translocon in eukaryotes, or SecYEG in prokaryotes, through the interaction with the SRP receptor (SR). This process is controlled by GTPase activity present in both the SRP and SRP receptor. By interacting with the SRP receptor, SRP enhances the GTPase activity of the SRP receptor and vice versa such that each one of these components works as a guanine nucleotide exchange factor (GEF) for the other. The functional consequence of this mutual enhancement is the hydrolysis of GTP by both enzymes which is required to dissociate the SRP/SR complex. Once released, free SRP is able to start a new round of targeting. Once the nascent chain/ribosome/mRNA ternary complex is in the vicinity of the translocon the nascent polypeptide is either inserted in the lipid bilayer via the translocon or enters into the ER lumen to be folded (Akopian et al. 2013) (Fig.9).

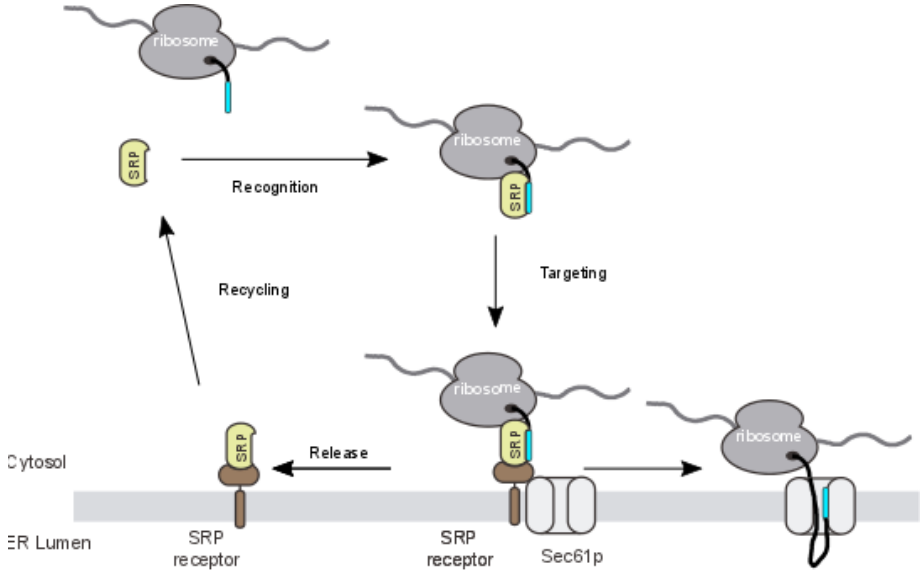

Figure 9. Shematic representation of the ER targeting by Signal Recognition Particle (SRP).

The SRP complex diverged in size and composition among different species but the functional core of this pathway is conserved (Pool et al. 2005). In fact, bacterial SRP can replace mammalian SRP and mediate the efficient co-translational targeting of mRNAs to the microsomal membranes *in vitro* (Powers & Walter 1997).

The eukaryotic SRP complex is composed by six proteins: the SRP9, SRP14, SRP19, SRP54, SRP68 and SRP72, named according to their molecular weights) and the 7S SRP RNA. The bacterial SRP complex is composed of only one protein subunit, the SRP54 component (named Ffh in bacteria), which binds to the SRP RNA. Ffh protein contains two structural and functional separated domains; one that recognizes the signal peptide and binds to the SRP RNA (Keenan et al. 1998) and the second, a GTPase NG domains that interacts with the GTPase NG domain located on the SR (Egea et al. 2004). The other SRP component universally is the SRP RNA, which serve as a scaffold that holds the SRP subunits and also provides additional interactions with the SR (Akopian et al. 2013).

The eukaryotic SRP complex could be divided in two principle domains; the S-domain, that involves the II–IV domains of the 7S RNA and the SRP 19, 54, and 68/72 protein subunits, and the Alu domain, comprised of domain I of the 7S RNA and the SRP 9/14 subunits (Fig. 10). The eukaryotic SRP assembly implies a cooperative binding in a consecutive order of its subunits. All the SRP subunits except the SRP54 are imported to the nucleus to bind the 7S RNA and then exported to the cytosol to load the SRP54 to complete the SRP assembly (Leung & Brown 2010). Further, it has been demonstrated that SRP19 is required for binding of SRP54 (Walter & Blobel 1983), but the structure and functions of the SRP68/72 subunits remain unclear.

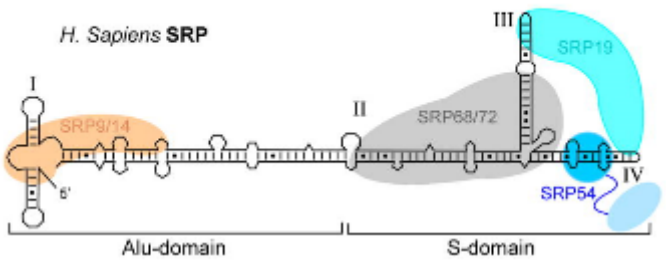

Figure 10. Organization of the mammalian SRP. The SRP54 M- and NG-domains are in dark and light *blue*, respectively, SRP19 is in *cyan*, SRP9/14 is in *orange*, and the SRP68/72 complex is represented as a *gray* sphere.

The core function of the SRP Alu domains is the arrest of the translation elongation just after the signal peptide emerges from the ribosome. Translational pausing imposed by the SRP is important because it provides the stability to the SRP/nascent chain/ribosome/mRNA required to deliver the whole complex to the SRP receptor; in line with this notion, SRP fails to target the RNC if the nascent polypeptide exceeds a critical length (Siegel & Walter 1988).

The Alu domain contacts with specific domains of the translating ribosome to mediate the elongation arrest. Cryo-EM studies revealed first that the Alu domain contacts the elongation binding site at the ribosome subunit interface (Halic et al. 2004). This finding was complemented by biochemical and crosslinking studies which demonstrated that the heterodimer formed by the SRP9/14 subunits interacts with ribosomal RNA and also with ribosomal proteins at the interface between the large and small ribosomal subunits (Mary et al. 2010), providing the molecular mechanism for the action of SRP in translation elongation. Along with this biochemical evidence, the *in vivo* deletion of the heterodimer SRP9/14 caused a defect in the protein targeting and in cell growth (Lakkaraju et al. 2008).

Altogether, the SRP targeting mechanism seems to operate the targeting of mRNA by a mechanism that requires translation, where the targeting determinant is a peptide (the signal sequence at the nascent chain) and where a translational pausing mechanism is necessary to stabilize the transported ribonucleoprotein particle. These main principles are shared by the XBP1 targeting mechanism proposed by Yanagitani and colleagues.

Partitioning of mRNAs into the ER. The ER as a specialized territory

According to co-translational SRP targeting model, mRNAs encoding for cytosolic proteins, which do not encode signal peptide or trasmembrane domains in their sequence should not be localized at the ER membrane. However, recent studies have documented the association of a broad set of mRNAs to the ER that includes mRNAs encoding cytosolic and the canonical ER-target proteins. Still it is unclear how much RNA is associated to ER membranes: While in HeLa approximately half of all ribosomes are ER-associated and a similar fraction of the total mRNA is ER-localized (Jagannathan et al. 2014), independent studies performed in HEK293 cells state that only 13% of total mRNAs is ER-bound (Reid et al. 2014).

mRNAs associated to the ER are translatable. In yeast, approximately 75% of all cellular translation activity may occur in association with the ER (Zhou et al. 2014). In mammalian cells, mRNAs encoding cytosolic, nuclear and peroxisomal proteins are also translated at the ER membrane (Chen et al. 2011, Reid & Nicchitta 2012, Jagannathan et al. 2014); translation at the ER surface does not affect the proper localization of the synthesized proteins (Pyhtila et al. 2008). Based on these data, some authors have proposed that the ER could behave as a general translation platform and not as a specialized translation site only for secreted and membrane proteins.

The mechanism by which mRNAs encoding cytosolic/nuclear proteins associate with the ER is unclear, but it seems clear that SRP is not necessary to mediate such partitioning. For specific mRNAs, *cis*-acting localization elements driving membrane association have been identified. For instance, a sequence at the 3´-end of the placental alkaline phosphatase open reading frame (ALPP) mRNA directs the localization to ER membrane, in a process mediated by the protein P180, an mRNA receptor present in the ER (Cui et al. 2013). In contrast, other mRNAs like the mRNA encoding calreticulin, which does not encode any TMD, associates with the ER in a p180-dependent manner and independently of translation (Cui et al. 2012). SRP-independent mRNA targeting is also detected in lower eukaryotes, where the PMP1 mRNA associates to the ER via a 3´UTR UG-rich element (Loya et al. 2008).

Co-trafficking of localized mRNAs and ER

In many biological systems, the localization of mRNA species at a given site takes place by means of a stable association to the ER, which serves as a vehicle that determines mRNA transport. Here are specific cases where this mode of transport is relevant.

Vg1 mRNA

Xenopus laevis Vg1 mRNA encodes a transforming growth factor (TGF) a-like molecule involved in mesoderm induction. By the end of stage II/beginning of stage III of the development, Vg1 mRNA – which at earlier stages displayed a diffuse cytosolic localization – and the ER become enriched in a wedge shaped region between the nucleus and the vegetal cortex. By the end of stage III, both Vg1 mRNA and ER are transported to the vegetal cortex in a microtubule dependent manner.

The coordinated transport of ER and Vg1 mRNA is the result of the association of both components in a globular substructure within the wedge of stages II and III (Deshler et al. 1997). The identification of the Vg1 localization element led to the biochemical discovery of Vera (Vg LE binding and ER association), or Vg1RBP (Vg1 RNA binding protein). Vera is essential for Vg1 localization and co-fractionates with an ER enriched fraction (Deshler et al. 1997). Although there is no direct evidence that Vera directly tethers Vg1 mRNA to the ER, conditions causing the release of Vera from the ER disrupt Vg1 mRNA ER association.

Budding yeast localized mRNAs

In *Saccharomyces cerevisiae* more than 30 mRNAs are transported to the bud tip using the She1p–She3p targeting components (Aronov et al. 2007; Shepard et al. 2003). Key in this mechanisms the RNA binding protein She2p that binds its target mRNAs as they are transcribed in the nucleus and shuttles them to the cytoplasm (Shen et al. 2009). Once in the cytosol, the mRNP complex associates to She3p, which is in turn complexed with the type V myosin motor protein Myo4p (She1p). Myo4p is required for the active transport of the mRNP to the bud tip (Heuck et al. 2010). Myo4p and She3p also participate in the proper segregation of a subclass of the ER – the cortical ER (cER) – to the daughter cell. The cER is the part of the yeast ER right underneath the plasma membrane, and needs to be inherited to the yeast bud along the cell division process. cER inheritance is initiated by the protrusion of ER tubules from the mother cell into the bud tip (West et al. 2011).

Several studies indicate that mRNA localization to the new bud is coordinated with cER segregation. Live imaging showed that bud localized *ASH1* mRNA and tubular ER can move in a coordinated way to the bud and that the mRNP is often seen at the tip of an ER tubule (Schmid et al. 2006). *ASH1* mRNA association to ER tubules does not require the motor protein Myo4p, but it does require the RNA binding protien She2p, which associates with ER membranes independent of Myo4p, She3p and ER-attached ribosomes. Taken together these results imply that She2p might tether mRNPs containing *ASH1* mRNA and other localized mRNAs to the ER.

Many, but not all of the mRNAs localized to the bud tip require the correct formation of tubular ER since loss of the reticulum Rtn1p in conjunction with loss of Yop1 (Filigheddu et al. 2007; Voeltz et al. 2006) not only disrupts tubular ER formation but also blocks mRNA localization. One exception to this requirement is the *ASH1* mRNA, which is localized independently of functional ER segregation

(Fundakowski et al. 2012). Thus, two alternative mechanisms of RNA targeting co-exist in yeast, one of which utilizes the She2p/She3p/Myo4p complex, which also contributes to cER inheritance. The RNA-binding protein She2p seems to play a key role in both attaching localized mRNA to cER but also in ER-independent mRNA localization, and could participate in either one or the other transport mechanisms depending on the cellular context.

Localization of mRNAs to specific ER subdomains

As mentioned above, the well-studied mRNAs like *oskar*, *α-actin* and *ASH1* are selectively localized and restricted to specific sites within the cell by different types of mechanisms where a *cis*-acting element on the mRNA sequence is recognized by trans-acting elements that bring the RNAs to their proper site.
SRP-dependent targeting is the main ER mRNA targeting mechanism of the cell, and provides the delivery of RNAs to the translocon pore dispersed evenly throughout the ER network. Although the ER is often considered as a continuous network where all the functional tasks are homogeneously represented, specific processes take place at distinct ER subdomains. To reach these sites, selected subsets of mRNAs are engaged in dedicated targeting mechanisms. The transport of XBP1 mRNA/*HAC1* mRNA to ER stress signaling centers described above is one of the best examples of selective mRNA transport mechanisms to ER locations, but other cases have been reported, and illustrate different possible targeting principles (Hermesh & Jansen 2013).

Rice seed storage protein mRNAs

Developing rice endosperm contains two distinct types of rough ER, cisternal ER (C-ER) and protein body ER (PB-ER). PB-ER contains aggregates of storage proteins and are delimited from the rough ER membranes, which are interconnected to the C-ER. Rice seeds, as most plants, contain two types of storage proteins: glutelin and prolamine. During rice development glutelin and prolamin are translated at the ER, translocated into the ER lumen and then trafficked to different compartments. Prolamines are retained in the ER lumen as PB whereas glutelins are transported to the protein storage vacuole (PSV). The correct sorting of prolamine and glutelin depends on the localization of their mRNAs to distinct ER domains, namely the PB-ER and C-ER (Li et al. 1993). Deletion analysis of the prolamine

mRNA revealed that its localization is independent of the region coding for the signal peptide sequence but required translation (Choi et al. 2000). RNA localization is carried out by two redundant localization elements (LEs) located within the ORF and the 3′UTR. A mutant RNA lacking both LEs is only delivered at the C-ER, which indicates the existence of a default mRNA localization pathway to the C-ER that must be overcome by specific LEs (Hamada et al. 2003).

It has been speculated that the selective regulation of these mRNAs in specific ER subdomains could be required to prevent deleterious protein interactions. Biochemical and cell biology studies indicate that the actin cytoskeleton could be involved in the transport of prolamine mRNA (Hamada et al. 2003). In addition, two RBPs associate to prolamine and glutelin mRNA and are supposed to participate in transport. OsTudor-SN binds both prolamine and glutelin mRNAs in vivo. This protein is found at the PB-ER and C-ER, but also in cytoplasmic particles and might therefore not mediate the specific localization of its bound RNA. The second protein associating with prolamine and glutelin mRNAs is RBP-A. However, since it can be found in several different compartments in the cell like the nucleus, at microtubules and at C-ER (Crofts et al. 2010), it is still not clear if it has any specific role in mRNA targeting to PB-ER or C-ER.

Drosophila gurken and *wingless* mRNAs

In the *Drosophila* oocyte, localization of *gurken* (*grk*) mRNA to the dorsal anterior corner of the oocyte in stages 9–10 specifies the anteroposterior and dorsoventral axes in the late embryo. *grk* encodes a TGF alpha-like protein that is secreted to the extracellular space. Newly synthesized gurken protein leaves the ER at specialized ER exit sites called transitional ER (Barlowe et al. 1994; Bonifacino & Glick 2004). Although stage 9 oocytes contain about 1000 transitional ER (tER) sites that are evenly distributed throughout the ooplasm, the majority of gurken protein can be found at tER sites and tER-Golgi units located at the dorsal anterior corner and in the intercellular place between the oocyte and the follicle cells. In *Drosophila* mutants causing a localization of *grk* mRNA at the posterior pole, only tER-Golgi units located at the posterior pole are positive for gurken protein (Delanoue et al. 2007), indicating that localization of *grk* mRNA to a specific fraction of ER determines the exocytic sites for the encoded protein.

In summary, SRP-independent mRNA targeting to the ER accounts for different modes of RNA recruitment to the ER. General modes of RNA recruitment could facilitate the association of all mRNAs to the ER, which could serve to foster translation or regulation. For specific mRNAs, distinct mechanisms account for the selectively delivery of mRNAs to specific subdomains within the ER. In this Project, we expect to gain insight into the targeting mechanism that brings XBP1 mRNA and *HAC1* mRNA to ER stress signaling centers.

2. AIMS

The XBP1 mRNA transport to ER splicing centers is a key step in the activation of the UPR. This doctoral thesis work tries to understand the mechanism by which this process takes place under physiological and endoplasmic stress conditions.

This mechanism will be explored in human cells and in the yeast *Saccharomyces cerevisiae*, where the recruitment of *HAC1* mRNA to signaling centers was identified for the first time. Different transport mechanisms have been proposed for XBP1/*HAC1* mRNAs in both species that result in the selective recruitment of mRNA to the ER. We will challenge the mammalian model to then explore the molecular components driving the transport, while we will take advantage of new findings in yeast UPR to get further insights in yeast *HAC1* mRNA targeting.

Specifically, we will,

1. Determine the contribution of the co-translational model based on the hydrophobic peptide HR2 to XBP1 splicing and XBP1 mRNA transport to ER membrane

2. Identify the element/s on the XBP1 mRNA sequence required to support the efficient XBP1 mRNA splicing under acute ER stress.

3. Explore the participation of the cytoskeleton on the XBP1 mRNA splicing/transport reaction.

4. Evaluate the role of the yeast Ire1 linker domain on the *HAC1* mRNA splicing reaction.

3. MATERIALS AND METHODS

3.1. Plasmid constructs

The cloning procedures were conducted following the standard Molecular Biology techniques and all the constructs were confirmed by sequencing analysis.

3.1.1. Site-directed mutagenesis

We used the *Quick Change Site-Directed Mutagenesis* kit (Stratagene Cloning Systems, Inc.) for site-specific mutations in the plasmid sequence. Briefly, the desired plasmid was amplified by PCR using a high-fidelity *PfuTurbo DNA polymerase* with two complementary specific primers, containing the mutation of interest in the middle of the sequence. The resulting PCR product was then treated with *DpnI* enzyme. *DpnI* is an endonuclease that recognizes the sequence 5´-Gm^{6}ATC-3´and digests methylated and hemymethylated DNA. Since DNA methylation occurs in bacteria *DpnI* treatment selectively degrades the original plasmid used as template and does not digest PCR-derived DNA. Mutagenized plasmids were transformed into *DH5α* chemically competent *Escherichia coli* cells. Plasmid DNA was isolated by the alkaline hydrolysis method using the *Nucleospin® Plasmid kit* (Macherey-Nagel). DNA sequence was verified by Sanger sequencing.

3.1.2. Plasmids used for mutational and functional analysis of XBP1 mRNA

A wild-type (WT), N-terminally FLAG-tagged version of the murine unspliced XBP1 (FLAG.mXBP1u) gene, published by Calfon et al., 2002 was used as WT control, and as the starting construct to generate XBP1 mutants (Fig.11A). The FLAG epitope sequence was inserted right after the XBP1 AUG codon. FLAG tagged murine XBP1 mRNA is efficiently spliced in human cells (Calfon et al., 2002). The pCMV.FLAGmXBP1u represented in Figure 11A, was acquired from Addgene platform (www.addgene.com). Schematic representation of the XBP1 mRNA splicing reaction and the protein translation products of the unspliced and the spliced variants of the murine XBP1 mRNA are represented in Figure 11B.

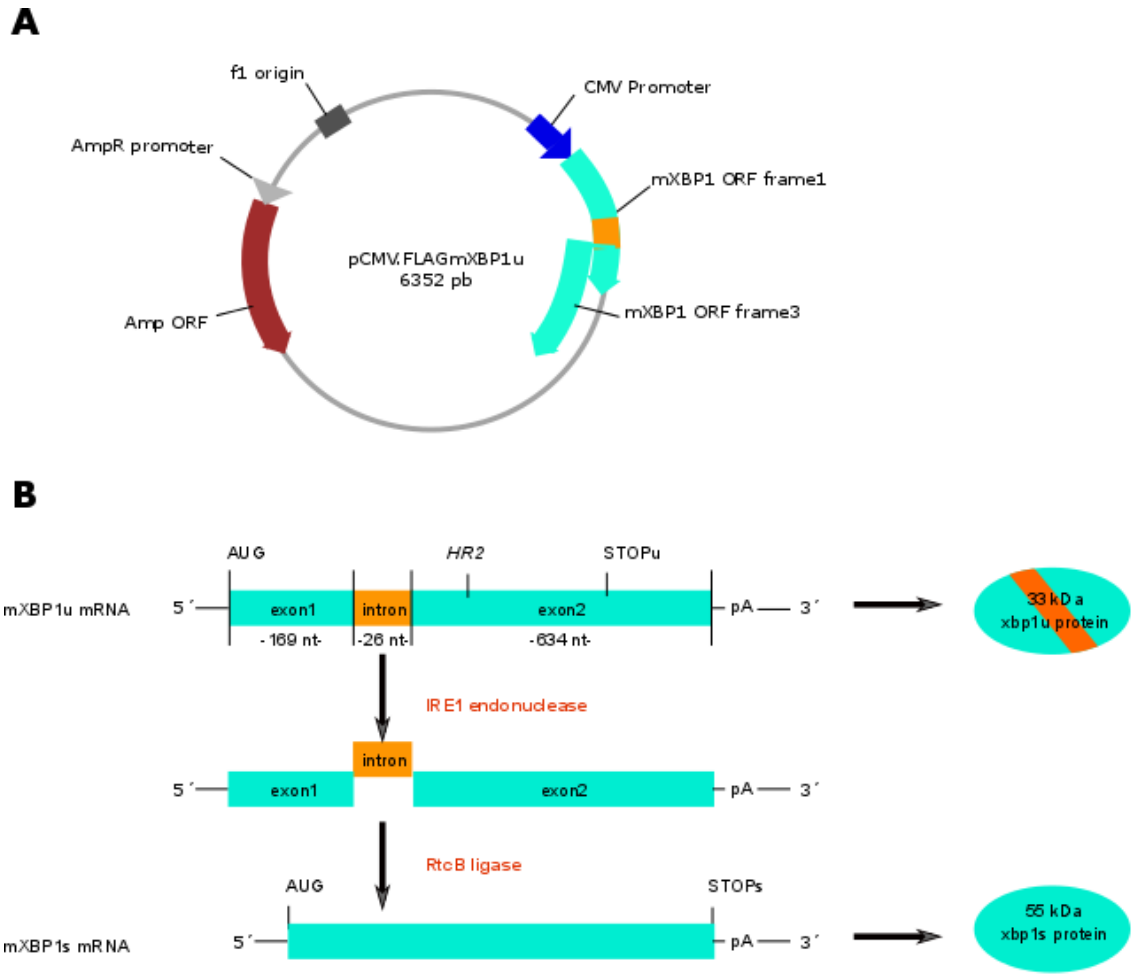

Figure 11. The unspliced XBP1 construct used as WT version. A) Schematic representation of the pCMV.FLAGmXBP1u plasmid of 6352 base pairs (pb), coding for the N-terminal Flag-tagged murine unspliced XBP1 mRNA (FLAG.mXBP1u) construct reported by Calfon et al., 2002. The expression of the XBP1 gene is controlled by the human cytomegalovirus (CMV) promoter. The XBP1 gene contains two open reading frames (ORF), the XBP1 ORF1 and the XBP1 ORF3. The f1 origin of replication and the Ampicillin (Amp) resistance gene cassette is shown in the plasmid scheme. B) Schematic representation of the XBP1 mRNA splicing reaction. The murine unspliced form of XBP1 mRNA (mXBP1u) is composed by 2 exons (exon1 and exon2) linked by a short intron sequence of 26 nucleotides (nt), highlighted in orange color. The XBP1u mRNA encodes a 33 kDa protein designed as Xbp1u. The Xbp1u protein contains the hydrophobic peptide (HR2). In the presence of ER stress, the endonuclease IRE1α can cleave the XBP1u mRNA causing the release of the intron. The spliced form of the XBP1 mRNA (XBP1s) emerges after the junction of the XBP1 exon1 and exon2 by the RtcB ligase. The elimination of the intron sequence produces a frameshift allowing the production of a larger Xbp1s protein (55 KDa).

3.1.3. Plasmid used to challenge the co-translational model

pCMV2_STOP

The plasmid pCMV2_STOP contains the sequence of the XBP1 mutant STOP, which bears a UGA stop codon within the intron of FLAG.mXBP1u mRNA (Calfon et al. 2002), introduced by mutating T481 to A. As this mutation

disrupts the stem of the 5' splice site, a compensatory mutation of A465 to T was also inserted. This second mutation, located in exon 1 of XBP1 does not alter XBP1u or XBP1s open reading frames. The insertion of a premature STOP codon interrupts the XBP1u mRNA open reading frame and produces a truncated version of xbp1u protein (tXbp1u) which does not contain the HR2 peptide, without affecting the open reading frame of the xbp1s protein. The insertion of the stop codon in XBP1 mRNA sequence was performed by site-directed mutagenesis (section 3.1.1) using the plasmid pCMV2_FLAG.mXBP1u as template and the oligonucleotides primers 1 and 2 described in Table 1.

pCMV2_FS (+1) int

The plasmid pCMV2_FS (+1) int encodes the XBP1 mutant FS (+1) int which contains one adenine inserted at position 485 of the intron sequence of the Flag.mXBP1u mRNA (Calfon et al. 2002). The insertion produces a (+1) frameshift that prevents the production of the HR2 peptide, without affecting the open reading frame of the spliced Xbp1 protein. To generate the mutant FS (+1) int, plasmid pCMV2_FLAG.mXBP1 was amplified by PCR using the *ExTaq* DNA polymerase (Takara) and the mutagenic oligonucleotide primers 3 and 4 (Table 1). The DNA fragment amplified replaced the *HindIII* / *PstI* fragment released from pCMV2_FLAG.mXBP1.

pCMV2_FS (+2) ex1

Plasmid pCMV2_FS (+2) ex1 encodes the XBP1 mutant FS (+2) ex1, which contains two nucleotides (CT) inserted at position 445 in the exon 1 of the Flag.mXBP1u mRNA (Calfon et al. 2002). The insertion of two nucleotides produces a (+2) frameshift that prevents the production of the HR2 peptide. To generate mutant FS (+2) ex1, pCMV2_FLAG.mXBP1 was amplified by PCR using the *ExTaq* DNA polymerase (Takara) and the mutagenic oligonucleotide primers 3 and 6 (Table 1). The DNA product replaced the *HindIII* / *PstI* fragment released from pCMV2_FLAG.mXBP1 plasmid.

pCMV2_FS (+2)ex2

Plasmid pCMV2_FS (+2) ex2 encodes the FS (+2) ex2 mutant, which contains two adenines inserted at position 544, in the exon2 of the Flag.mXBP1u mRNA (Calfon et al. 2002). The insertion of two nucleotides produces a (+2) frameshift that prevents the production of the HR2 peptide. To generate the mutant FS (+2) ex2, plasmid pCMV2_FLAG.mXBP1 was amplified by PCR using the *ExTaq* DNA polymerase (Takara) and the mutagenic oligonucleotide primers 3 and 7 (Table 1). The DNA product replaced the *PstI / EcoRV* fragment released from pCMV2_FLAG.mXBP1.

pCMV2_FS repaired

The plasmid pCMV2_FS repaired is a plasmid that combines two frameshifting mutations, FS (+2) ex1 and FS (+1) ex2, described previously. The combination of these two mutations restores HR2 synthesis from the unspliced version of the mRNA. To generate the mutant FS repaired, plasmid pCMV2_FLAG.mXBP1 was amplified by PCR using the *ExTaq* DNA polymerase (Takara) and the mutagenic oligonucleotide primers 3 and 8 (Table 1). The DNA product replaced the *PstI* / *EcoRV* fragment released from the pCMV2_FS (+1) ex2.

pCMV2_FS (+1) int repaired

The plasmid pCMV2_FS (+1) int repaired combines mutations XBP1 FS (+1) int and FS (+2) ex2. The combination of these two mutations restores HR2 synthesis from the unspliced version of the mRNA. To generate the mutant FS (+1) int repaired, a fragment extracted from the plasmid pCMV2_FS (+2) ex2 by digestion with *PstI* / *EcoRV* enzymes replaced the *PstI* / *EcoRV* released from pCMV2_FS (+1) int.

XBP1 mRNA deletion mutants

A series of deletion plasmids lacking either the 5’ or the 3’ end of XBP1 molecules were constructed based on modifications of pCMV_FLAGmXBP1u, or pCMV_STOP as an HR2-deficient “sensitized allele”. To generate 5’-end deletions, PCR products carrying a *HindIII* site at their 5’end and a *BamHI* at their 3’end were inserted in the

HindIII and *BamHI* sites located in the XBP1 plasmids right after the FLAG coding sequence and right before the XBP1 intron, respectively.

To generate 3' end deletions, a series of PCR products bearing an *EcoRV* site at their 5' end and a *BglII* site at the 3'end were inserted into the *EcoRV* and *BglII* sites of the XBP1 constructs described above.

Deletion mutants were numbered after the sequence of unspliced murine XBP1 (NM_013842.3) considering the +1 the first nucleotide of the coding sequence.

3.1.4. Plasmid for *in vitro* transcription

To perform *in vitro* transcription, template DNA was inserted into the multiple cloning site of pcDNA3.1(+) (Invitrogen). The pcDNA3.1(+) plasmid contains the T7 promoter which is recognized by the *T7 RNA polymerase* allowing *in vitro* transcription.

XBP1 mutants for the in vitro cleavage assay

To perform *in vitro* cleavage assays with recombinant IRE1α, we generated two plasmids by inserting a different fragment from either the WT version of XBP1 mRNA (nucleotides 30-581) or the FS (+1) int mutant (nucleotides 30-582) into pcDNA3.1(+) (Invitrogen). The former insertion produced the plasmid pcDNA3.1_mXBP1u. The latter insertion produced the plasmid pcDNA3.1_FS (+1) int. Both DNA fragments were isolated by enzymatic digestion with *HindIII* and *EcoRV* enzymes and inserted into the multicloning site of pcDNA3.1(+).

Plasmid used for Selective 2'-hydroxyl Acylation analyzed by Primer Extension (SHAPE)

To identify structural elements on the XBP1 mRNA sequence, a fragment of nucleotides 30-588 was inserted into plasmid pcDNA3.1(+) (Invitrogen). To this aim, plasmid pCMV2_FLAG.mXBP1u was amplified by the *ExTaq DNA polymerase* (Takara) using the oligonucleotide forward primer 3 and the reverse oligonucleotide 9 which contained the *BglII* restriction site at the 5´ end (Table 1). The resulting PCR product was purified, digested with

enzymes *HindIII* and *BglII* and inserted into the multiple cloning site of pcDNA3.1(+).

3.1.5. Plasmids for IRE1α visualization

To generate a fluorescent version of IRE1α we fused the coding sequence of human IRE1α to the coding sequence of mCherry or eGFP fluorescent proteins. Since N-terminal or C-terminal tagging of IRE1α interferes with its endonucleolytic capacity, we inserted fluorescent proteins as internal tags. To that aim, we inserted by site-directed mutagenesis (see section 3.1.1) an *AgeI* restriction site at nucleotide 1516 of the IRE1α coding sequence. This position corresponds to a cytoplasmic domain of human IRE1α immediately adjacent to its transmembrane domain. Plasmid hIRE1α.pcD – deposited by Dr. Randal Kauffman in the Addgene platform – expressing WT human IRE1α was used as a template for mutagenesis. Site-directed mutagenesis was performed using the oligonucleotide primers 10 and 11 (Table 1). Then, the coding sequences of mCherry or eGFP fluorescent proteins were inserted in the *AgeI* restriction site to generate the plasmids phIRE1α _mCherry and phIRE1α_eGFP, respectively.

3.1.6. Vimentin plasmid

The plasmid encoding peGFP-Vim1-myc was a generous gift from Dr. Edward Kuczmarski, from the Northwestern University Feinberg School of Medicine (Chicago, EE. UU).

3.1.7. Plasmid used in the generation of stable expression cell lines

To generate stable cell lines, we used the Flip-In System (Invitrogen), which allows the integration of the foreign DNA by the *Flp* recombinase specifically into a FRT recombination site, previously inserted into the genome of the host cell line. The transgene of interest was cloned into the expression vector pcDNA5/FRT (Fig.12). In this vector gene expression is controlled by CMV immediate-early enhancer/promoter. The expression vector also contains a Hygromycin resistance gene without promoter and ATG initiation codon, with an FRT site embedded in its 5´end of its coding sequence (Fig.12). Flp recombinase-assisted integration of the pcDNA5/FRT plasmid at the right genomic location is such that the Hygromycin gene

is inserted in front of a promoter-AUG cassette allowing Hygromycin expression and the positive selection of stable transfomant clones.

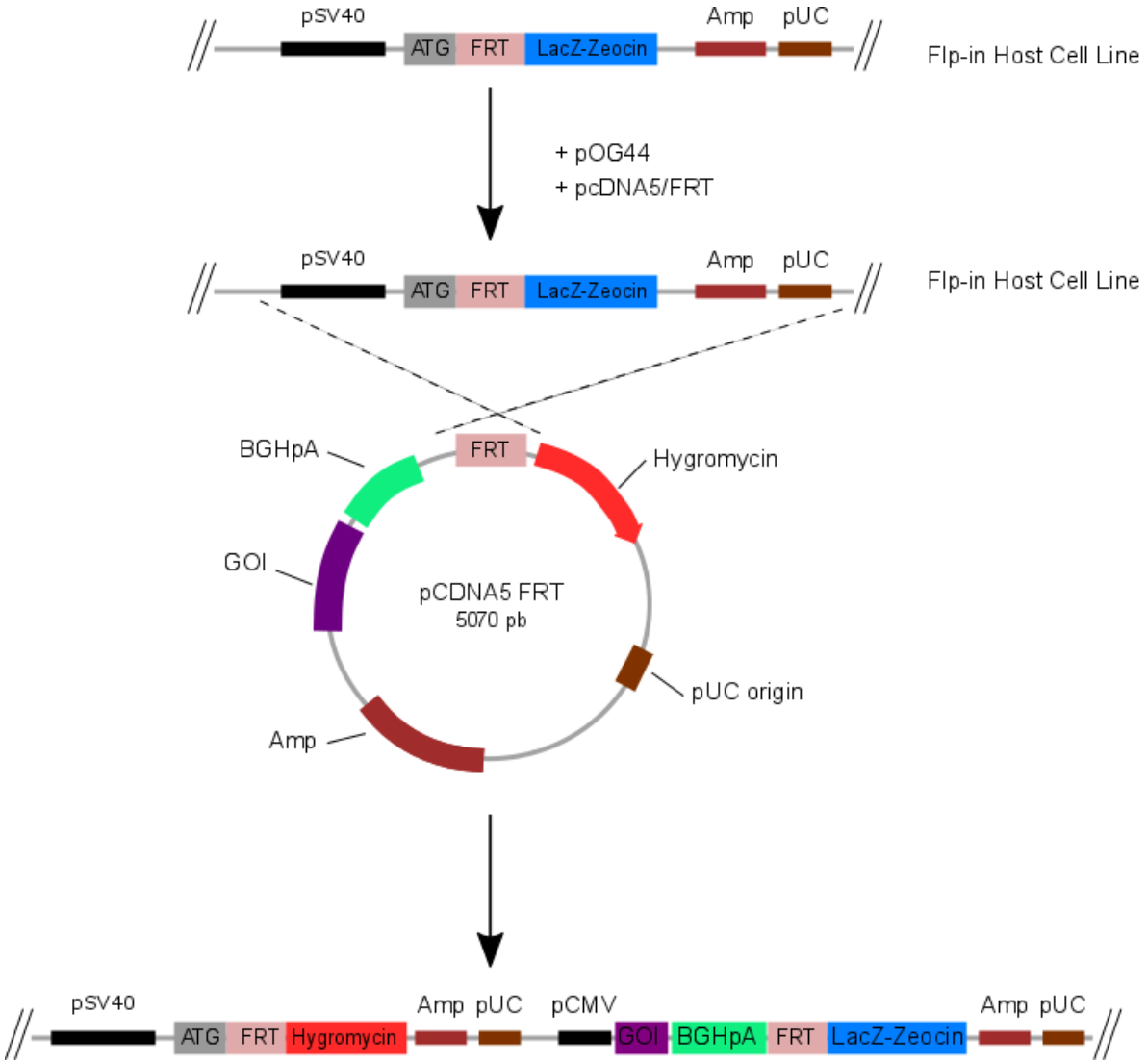

Figure 12. Schematic representation of Flp-in System (Invitrogen) used for the generation of stable cell lines. The pFRT/LacZeo was previously stably transfected into the mammalian host cell line of interest to generate the zeocin-resistant Flp-in Host Cell Line. The the pcDNA5 FRT containing the Gene Of Interest (GOI) and the pOG44 that codes for Flp recombinase are co-transfected in the Flp-in host cell line. The Flp recombinase catalyzes the homologous recombination between the FRT sites of pcDNA5 FRT expression vector and the host cell genome. The integrated DNA allows the expression of GOI and the Hygromycin resistant protein.

pcDNA5/FRT_ FLAG.mXBP1u

Plasmid pcDNA5/FRT_FLAG.mXBP1u encodes murine unspliced FLAG-tagged XBP1 mRNA (Flag.mXBP1u mRNA, see above). The sequence coding for XBP1 mRNA was extracted from the pCMV2_FLAG.mXBP1u by digestion with enzymes *SpeI* and *EcoRV* and

inserted into the multi cloning site of the pcDNA5 FRT expression vector (Invitrogen).

pcDNA5/FRT_STOP

pcDNA5/FRT_STOP encodes the XBP1 STOP mutant. A *SpeI* / *EcoRV* restriction fragment containing the STOP mutant was extracted from the pCMV2_STOP and subcloned into the pcDNA5/FRT_FLAG.mXBP1u.

pcDNA5/FRT_FS (+1) int

Plasmid pcDNA5/FRT_FS (+1) int encodes the XBP1 mRNA FS (+1) int mutant. A DNA fragment containing the mutation of the FS (+1) int XBP1 mutant was extracted from the plasmid pCMV2_FS (+1) int by digestion with enzyme *XhoI* and sub-cloned into the plasmid pcDNA5/FRT_FLAG.mXBP1u.

pcDNA5/FRT_FS (+2) ex1

Plasmid pcDNA5/FRT_FS (+2) ex1 encodes the XBP1 mutant FS (+2) ex1. A *XhoI* restriction fragment obtained from pCMV2_FS (+2) ex1 was sub-cloned into plasmid pcDNA5/FRT_FLAG.mXBP1u.

pcDNA5/FRT_FS (+1) ex2

Plasmid pcDNA5/FRT_FS (+1) ex2 encodes mutant FS (+1) ex2, described above. A *HindIII* / *EcoRI* restriction fragment containing the FS (+1) ex2 mutation was obtained from plasmid pCMV2_FS (+1) ex2 and sub-cloned into the plasmid pcDNA5/FRT_FLAG.mXBP1u.

pcDNA5/FRT_FS repaired

Plasmid pcDNA5/FRT_FS repaired encodes the XBP1 mutant FS repaired, which is the combination of mutants FS (+2) ex1 and FS (+1) ex2 that produce a (+3) frameshift allowing the production of the HR2 peptide. To combine both mutations, a *SacI* / *PstI* restriction fragment derived from pCMV2_FS (+2) ex1 was sub-cloned into plasmid pcDNA5/FRT_FS (+1) ex2.

pcDNA5/FRT_FS (+1) int repaired

Plasmid pcDNA5/FRT_FS (+1) int repaired expresses XBP1 mutant FS (+1) int repaired. A *KpnI/EcoRV* restriction fragment obtained from pCMV2_FS (+1) int was subcloned into pcDNA5/FRT_FLAG.mXBP1u.

Table 1 Oligonucleotide primers

Primer number	Nucleotide sequence 5´-3´
1	CCGGGTCTGCAGAGTCCGCAGCACTCTGACTATGTGCACC
2	GGTGCACATAGTCAGAGTGCTGCGGACTCTGCAGACCCGG
3	GATCTACCATGGACTACAAAGACGATGACG
4	AATTCTGCAGAGGTGCACATTAGTCTGAGTGC
5	AATTCTGCAGAGGTGCACATTTAGTCTGAGTGC
6	CCAACTGCAGAGGTGCACATAGTCTGAGTGCTGCGGACTCAGCAGACCCG GCCACCAGCCTAGTACTCCACT
7	AAAGGATATCAGACTCAGAATCTGAAGAGGCAACAGTGTCAGAGTCCATTT GGGAAG
8	ACAGCTGCAGCAGGTGCAGGCCCAGTTGTCACCTCCCCAGAACATCTTCC CAATGGACTCTG
9	ACTCAGATCTGAAGAGGCAACAGTGTCAG
10	CCACCCACCTGGAGACACCGGTCAGAACGGCGAGCTCCT
11	AGGAGCTCGCCGTTCTGACCGGTGTCTCCAGGTGGGTGG
12	CGGGTCTGCTGAGTCCGCAGCAG
13	GCAGGTGCAGGCCCAGTTGTCAC
14	CAGGGTGATCATTCTCTGAGGGGCTG

Primer number	Nucleotide sequence 5´-3´
15	GATCTCTAAAACTAGAGGCTTGGTGTATACA
16	GAGCTGTGCAGAAACTCCGGCG
17	ACCAACTGCTGAATCTTTGGAATTCGAGT
18	AAAGCCGCTCGCAAGAGTGCG
19	ACTTGCCTCCTGCAAAGCAC
20	GCGTAAGTGATGTCCACCTCGATATGTG
21	CCGCTGGAAGATGGAACCGCTGG
22	CACTCAGACTACGTGCACCTC
23	CACTCAGACTATGTGCACCTC
24	CACTCTGACTATGTGCACCTC
25	CACTCAGACTAATGTGCACCTC
26	CACTCAGACTAAATGTGCACCTC

3.2. Cell culture

3.2.1. Cell lines and culture media

Human embryonic kidney 293 (HEK-293) and HeLa cells were grown in DMEM with 4.5 g/l Glucose supplemented with 10% fetal bovine serum, 2 mM L-Glutamine, 5 U/ml penicillin and 5 µg/ml streptomycin (Lonza) under standard growth conditions (37ºC, 5% CO2).

3.2.2. Transfection by calcium phosphate

Cells were transfected by the calcium phosphate technique at a confluence of 40-50%. Briefly, 16 hours prior to transfection, cells were splitted, counted and plated in the adequate plate volume. At the time of transfection, cells were washed once with serum-free DMEM and incubated in this medium before the addition of the transfection mix. For the preparation of the transfection mix, a mixture of plasmid DNA and 0.25 M $CaCl_2$ was added drop by drop while vortexing softly to an equal volume of 2X HEPES-buffered saline (pH 6.8-7.1) and incubated for 15 minutes at room temperature. Then, the calcium phosphate/DNA precipitate mix was added and cells were incubated for 2 hours under standard growth conditions (section 3.2.1). Finally, the transfection medium was discarded and replaced with standard growth medium as described above. Transfected cells were cultured for at least 24 hours before any treatment or harvesting.

3.2.3. Generation of stable cell lines

Stable cell lines were generated by Flp recombinase-mediated integration system (Invitrogen), according to the manufacturer´s instructions. This system allows the integration and expression of a gene of interest in mammalian cells at a specific genomic location. In the Flip-In T-REx-293 cell line, a Flp Recombination Target (FRT) site was introduced into its genome. An expression vector containing the gene of interest was integrated into the genome via Flp recombinase mediated DNA recombination at the FRT site (Fig.12) (O'Gorman et al., 1991).

Then, Flp-In T-REx-293 cells were seeded at 30% of confluence in a 100 mm-diameter tissue culture plate. 16 hours after plating, 1 µg of the pcDNA5/FRT plasmid encoding the gene of interest was co-transfected by the calcium phosphate method (see method in section 3.2.2) with 9 µg of the pOG44 plasmid, which constitutively expresses the Flp recombinase. Cells were cultured in growth medium and 24 hours post-transfection the medium were replaced with selection medium, (growth medium supplemented with 100 µg/ml Hygromicin B and 15 µg/ml blasticidin), in order to select those cells where integration had been successful. After 15 days of culture in selective medium (medium was

exchanged every two days during this period of time). Individual clones, which could be spotted by eye, were isolated by local trypsin treatment and transferred to12-well plate wells. Clones were amplified and transferred to 6-well plates. Expression of the gene of interest was analyzed at the RNA and protein levels by quantitative RT/PCR and by Western Blot, respectively.

3.2.4. Pharmacological induction of ER stress

To induce ER stress, cells were cultured in DMEM with serum and antibiotics (as described in section 3.2.1), supplemented with a final concentration of 1µM thapsigargin (Tg) (Applichem) or 5 ng/mL tunicamycin (Tm) (Applichem). Those drugs disrupt functionality of the ER provoking the ER protein misfolding. thapsigargin acts by blocking the ER calcium ATPase pump, leading to the depletion of ER calcium stores while tunicamycin inhibits N-linked glycosylation.

Typically, ER stress treatments were started 24-48 hours after transfection. Stressed cells were harvested and the extent of UPR signaling was monitored by RT-PCR and Western blot analysis.

3.3.. RNA manipulation methods.

3.3.1. RNA isolation

Total RNA was isolated from cells using the TRI reagent (Sigma) as specified by the manufacturer. Briefly, the adequate volume of TRI reagent (1 ml of TRI reagent per 10 cm^2 of culture plate surface area) was added directly to the cells previously washed with PBS buffer. Cell lysates were obtained by pipetting up and down several times. Then, lysates were transferred to 1.5 ml eppendorf tubes and mixed with 0.2 ml of chloroform per ml of TRI reagent used. After that, samples were shaken and incubated at room temperature for 5 minutes. The resulting mixtures were centrifuged at 12000 *xg* at 4°C for 15 minutes. The aqueous phase containing the RNA was carefully transferred to a fresh tube and mixed with 0.2 ml of isopropanol per ml of TRI reagent added. The RNA was then precipitated by centrifugation at 12000xg at 4°C for 15 minutes. The RNA pellet was washed with 1 ml of ethanol at 70% per ml of TRI reagent used (vortexing

was applied to the samples at this step) and then centrifuged at 12000xg at 4°C for 10 minutes. RNA pellets were dried for 5-10 minutes by air-drying at room temperature and then re-suspended in the appropriate volume of RNase free water. RNA concentration was measured by absorbance at 260nm in a ND 1000 Spectrophotometer (NanoDrop).

3.3.2. Reverse Transcription

Synthesis of cDNA from human or murine total RNA was performed by reverse transcription. First, 2 µg of total RNA was pre-treated with 2 units of DNAase I (Fermentas) in the presence of 32 units of Ribonuclease Inhibitor RNAseOut (Invitrogen) for 30 minutes at 37ºC followed by the inactivation of the DNAase by the incubation with EDTA 25 mM for 10 minutes at 65ºC. The M-MLV reverse transcriptase (Promega) catalyzed the reverse transcription. The reverse transcription reaction was incubated for 60 minutes at 37ºC and then reverse transcriptase was inactivated for 1 minute at 95ºC.

3.3.3. Quantitative RT/PCR

SYBR green PCR master mix (Bio-Rad) was used to set up the quantitative real-time PCR: The reaction (10 µL) contains 1.5 µM of forward and reverse primers (Table 2), 1µl of cDNA templates made from human or murine total RNA, and 1x·SYBR Green Supermix. The thermal cycling parameters were: step 1, 95ºC for 10 minutes; step 2, 95ºC for 15 seconds; step 3, 60ºC 15 seconds, step 4, 72ºC for 15 seconds. Steps 2-4 are repeated for 44 cycles. The data were analyzed with the iCycler iQ Real-time PCR detection system (BioRad) according to the manufacturer´s instructions.

Table 2 Pairs of oligonucleotide primers used in quantitative RT/PCR

Gene	Pair of primers for RT-PCR detection
human XBP1 spliced	12 + 14
murine XBP1 spliced	12 + 15
human XBP1 total	13 + 14
murine XBP1 total	13 + 15

Gene	Pair of primers for RT-PCR detection
human XBP1 unspliced	22 + 14
murine XBP1 unspliced	23 + 15
murine STOP1 XBP1 unspliced	24 + 15
murine FS (+1) int XBP1 unspliced	25 + 15
murine FS (+2) int XBP1 unspliced	26 +15
BiP	16 +17
Histone H3B3	18 + 19
Lucifarase	20 +21

3.3.4. Determination of splicing efficiency

XBP1 mRNA splicing efficiency was determined as the ratio between spliced and total amounts of the XBP1 mRNA, measured by quantitative RT/PCR (section 3.3.3). We used the forward primer (12) that specifically recognizes the sequence resulting from the junction of the exons after the splicing reaction, and one of the reverse primers (14) or (15) that can distinguish human or murine XBP1 mRNA, respectively (Table 1). Total XBP1 mRNA was detected using the forward primer (13), that recognized a sequence in the exon 1 that is contained in both the spliced and non-spliced XBP1 mRNA, in combination with the one of the reverse primers (14) or (15) (Table 1).

3.3.5. *In vitro* transcription

We used the *T7 RNA polymerase kit* (Promega). Briefly,1-3 µg of linearized pcDNA3.1(+) containing the gene of interest were incubated with the Optimization Buffer (40mM Tris pH 7.9, 6mM $MgCl_2$, 2mM spermidine and 10mM NaCl), 10mM DTT, 2.5mM each of rNTP mix, 100U of RNaseOut (Promega) and 40U of *T7 RNA polymerase*, in a final volume of 100 µl for 2 hours at 37°C. Then, 2 units of *DNase I RNase free* (Thermo Scientific) were added and incubated for 15 more minutes at 37ºC.

Transcripts were extracted by mixing with 1 volume of phenol-chloroform mix (1:1), incubated at room temperature for 5 minutes and centrifuged at 12000xg at 4°C for 15 minutes. Then, the aqueous phase was transferred to a fresh tube. *In vitro* transcribed RNA was precipitated by incubation with 2.5 volumes of absolute ethanol and 0.1 volumes of 3M NaOAc for 1 hour at -20°C and centrifugation at 12000xg at 4°C for 15 minutes. After washing the RNA pellet with 75% ethanol, RNA pellets were dried for 5-10 minutes by air-drying at room temperature and then re-suspended in the appropriate volume of RNase free water. RNA purity and size were monitored by electrophoresis in 1% agarose denaturing gels.

3.3.6. Selective 2′-hydroxyl acylation analyzed by primer extension (SHAPE)

For SHAPE analysis, an RNA fragment corresponding to nucleotides 1 to 568 of mXBP1u mRNA was *in vitro* synthetized, as described in section 3.3.5. This fragment contains the N-terminal coding sequence followed by the intron sequence of the mXBP1 mRNA. Transcription was performed using T7 RNA polymerase, and DNA template was removed by RQ1 DNase treatment (Promega), followed by phenol extraction and ethanol precipitation. For phenol extraction, one volume of a phenol-chloroform 1:1 mix was added to the reaction and, after centrifugation at 13000 rpm for 15 minutes, RNA in the aqueous phase was precipitated by addition of 2.5 volumes of absolute ethanol and 0.1 volume of 3M NaOAc. RNA was resuspended in RNAse-free water. Synthesis of full-length products and absence of contaminating DNA template was verified by agarose gel electrophoresis.

For SHAPE analysis, 2 pmol of RNA in a final volume of 18 µl of folding buffer (100 mM HEPES pH 8.0, 6 mM $MgCl_2$, 100 mM NaCl) were renatured *in vitro* by heating at 95°C for 2 minutes, snap cooling on ice for 2 minutes, and incubated at 37ºC for 20 minutes. Subsequently, folded RNAs were incubated either with DMSO (Sigma) as untreated RNAs or 6.5 mM of N-methylisotoic anhydride (NMIA) (Invitrogen) for 45 minutes at 37ºC, precipitated and resuspended in 10 µl of 0.5X TE.

For primer extension reactions, 10 µl of treated and untreated RNAs (2 pmol) were incubated with 2 pmol of the antisense 5'-end fluorescently-labeled primer 5'-TAGCCTTATGCAGTTGCTCTCC-3' (Applied Biosystems) (complementary to a sequence located in the luciferase gene, 72 nucleotides downstream of the XBP1 region) at 65ºC for 5 minutes; 35ºC for 5 minutes and snap cooling on ice for 2 minutes. Primer extension reactions were conducted in a final volume of 16 µl containing reverse transcriptase (RT) buffer (50mM Tris–HCl, pH 8.3, 3 mM $MgCl_2$, 75 mM KCl, 8 mM DTT) and 1 mM each dNTP. The mix was heated at 52ºC for 1 minute, prior to addition of 100 U of Superscript III RT (Invitrogen) and incubated at 52ºC for 30 minutes. The enzyme was inactivated by heating at 70ºC, 15 minutes. Di-deoxy sequencing reactions were performed using the same RNA transcript , 0.1 mM ddC and 0.5 mM each dNTP. NED fluorophore was used for both treated and untreated samples and FAM fluorophore was used for the sequencing ladder. cDNA products were resolved by capillary electrophoresis. Electropherograms were analyzed using QuSHAPE software (Karabiber et al 2012). The reactivity values obtained for the untreated RNA (DMSO) were subtracted from the NMIA treated sample to obtain the net reactivity for each nucleotide. Quantitative SHAPE reactivities for individual data sets were normalized to a scale spanning 0 to 2, in which 0 indicates an unreactive nucleotide and the average intensity at highly reactive nucleotides is set to 1.0. Data from three independent assays were used to calculate the mean (±SD) SHAPE reactivity.

RNA structure models incorporating the SHAPE reactivity values were predicted using RNAstructure software (Reuter & Mathews, 2010). SHAPE reactivity data was imposed as a pseudo-free energy change constraint together with nearest neighbor thermodynamic parameters using -0.8 kcal/mol and 2.6 for the intercept (b) and slope (m), respectively, as recommended (Deigan et al, 2009).

3.3.7. *In vitro* cleavage assay of XBP1 mRNA by IRE1α

Restriction-digested plasmids pcDNA3.1_mXBP1u and pcDNA3.1_FS (+1), encoding WT murine XBP1u mRNA and for mutant FS (+1) were used as templates for *in vitro* transcription in the presence of ^{32}P-UTP as described in

section 3.3.5. Illustra MicroSpin G-50 columns (GE Healthcare) were used to clean up the transcription reactions according to the manufacturer instructions. The size and integrity of the RNA products was confirmed by denaturing agarose gel electrophoresis.

RNA products were first folded in the IRE1α Cleavage Reaction Buffer (20mM HEPES pH 7, 70mM NaCl, 2mM ADP, 2mM $Mg(OAc)_2$, 5mM DTT, 5% glycerol) by incubation at 95°C for 2 minutes, chilled 2 minutes on ice, and then incubated at 37°C for 20 minutes and chilled again on ice.

RNA cleavage reactions were conducted at 30°C in IRE1α Cleavage Reaction Buffer, containing less than 1nM ^{32}P- labeled RNA substrate in the presence of 150nM or 400nM recombinant cytosolic domain of human IRE1α (hIRE1α). Reactions were prepared such that 1 µl of RNA was added to 9 µl of a pre-warmed reaction mixture containing all components except RNA. As the cleavage reaction was assembled, 1 ul samples were withdrawn every 15 seconds and mixed with 6 µl of Laemmli buffer (10 mM urea, 0.1% SDS, 0.1mM EDTA, 0.05 xylene cyanol and 0.05% of bromophenol blue). Samples were boiled and loaded in denaturing 6 % PAGE as described (Rio D.C. et al, 2014). After running, gels were dried and radiolabelled cleaved RNA fragments were detected using a Typhoon scanner (Amersham). Images were quantified using the ImageJ software (http://rsbweb.nih.gov/ij/).

Rate constants were estimated by fitting results to the following single exponential equation:

$$[(A - B).e^{-kt}] + B$$

where *k* is the rate constant and *t* (time) was the independent variable, *k* has units s^{-1} when the units for *t* are s. Best fits were estimated with the *MATLAB function fit ()* using the non-linear least squares method. In all cases, *A* (amplitude, y-intercept), *B* (baseline, and *k* were allowed to vary independently with not fixed values.

3.4. Protein manipulation

3.4.1. Harvesting of protein extracts

To obtain cell proteins extracts, cell cultures were washed with ice-cold phosphate buffer saline and then harvested with two different procedures according to the experiment performed.

Extraction with Laemmli buffer

Cells cultured in 6-well tissue culture wells were extracted with 200 µl per well of 1xLaemmli buffer (63mM Tris HCl, 10%Glycerol, 2%SDS, 0.0025% Bromophenol Blue pH 6.8) supplemented with DTT 0.1M (Sigma) PhosStop (Roche) and protease inhibitor Complete Mini (Roche). The resulting extract was transferred to a fresh tube. Before loading the samples in SDS-PAGE gels, extracts were boiled at 100ºC for 10 minutes.

Protein extraction with RIPA buffer

Cells were collected using a rubber policeman with an appropriate volume of PBS1x, transferred to a fresh tube and spun down by centrifugation at 3000 rpm for 3 minutes at 4°C. Then, cells pellet were re-suspended in the adequate volume (50-100µl) of RIPA buffer (150mM NaCl, 50mM TRIS pH 7.5, 1%Tritón X-100, 0.5%sodium deoxycolate) and lysed by pipetting up and down on ice. After lysis, cell extracts were sonicated for 30 seconds on ice in the Bioruptor (Diagenode) and centrifuged at maximum speed for 1 hour at 4°C. The supernatant was transferred to a fresh tube and protein concentration was quantified by BCA colorimetric assay (BioRad, see below). Before loading in SDS-PAGE gels, samples were mixed with Laemmli buffer, 1X final concentration, and boiled at 95ºC for 5 minutes.

3.4.2. Protein quantification

Protein samples obtained by cell lysis with RIPA buffer were quantified using the Bicinchoninic Acid Kit (Sigma), according to the recommendation of the manufacturer. Briefly, 25 µl of diluted samples and a set of Bovine Serum Albumin (BSA) dilutions with concentrations ranging from 200 to 1000 µg/ml were

assayed in 96-well plates. Triplicates of the dilutions of the BSA standard curve and duplicates for the samples were prepared. Then, 200 µl of BCA working reagent (1:8) were added to all the samples. The plate was sealed with a film and incubated for 15 minutes at 60°C. The absorbance of the samples was measured at 562 nm in a 680 XR microplate reader (Biorad). The protein concentration of the samples was determined by extrapolating their absorbance values from the standard curve of BSA protein.

3.4.3. Western Blot Assay

We followed the standard Western blot protocol. Proteins were resolved on SDS–polyacrylamide gels and transferred to nitrocellulose membranes (BioRad). The membranes were incubated in Blocking solution: 5% skimmed milk diluted in Tris Buffer Saline supplemented with 0.1% Tween20 (TBST) for 1 hour at room temperature. Once blocked, membranes were incubated with the corresponding primary antibody (see Table 3) diluted in blocking solution. Membranes were then washed 4 times with TBST to eliminate the excess of unbound antibody. Horseradish peroxidase-coupled secondary antibodies (Sigma) were incubated in blocking solution for 1 hour and washed as described for the primary antibodies (Table 3). Finally, proteins were detected by Amersham ECL Prime Western Blotting Detection Reagent (GE Healthcare). Proteins bands were quantified using the ImageJ software (http://rsbweb.nih.gov/ij/).

Table 3 Antibodies and reagents

Antibodies	Catalog Number	Company	Work dilution
anti-XBP1 (M186)	sc7160	Santa Cruz Biothecnology	1/1000
anti-Calnexin	NBP1-97485	Novus Biologicals	1/3000
anti-GAPDH	#3683	Cell Signalling	1/10000
Anti-Rabbit IgG-HRP	A0545	Sigma	1/10000
Anti-Vimentin	V6389	Sigma	1/200

anti-NMMHC-B	PRB-445P	Covance	1/200
anti-alpha-Tubulin	T6074	Sigma	1/200
Faloidin Alexa Fluor 658	A12380	Invitrogen	1/40
anti-GFP	ab6556	Abcam	1/200
anti_Mouse Alexa Fluor 488	A21202	Invitrogen	1/1000
anti_Rabbit Alexa Fluor 488	A21206	Invitrogen	1/1000
anti_Mouse-Cy3	C2181	Sigma	1/1500
anti_Rabbit-Cy3	C2306	Sigma	1/1500

3.4.4. Membrane flotation assay

To monitor RNA association to membranes we followed the method described by Mechler and Vassallli (Mechler & Vassalli 1975). Briefly, cells were seeded in four 150 mm-diameter culture plates and incubated at 37°C with 5% of CO_2. To avoid ribosomal run-off from mRNAs, we supplemented all buffers used with the translation elongation inhibitor cycloheximide (CHX) at 50 µg/ml (Sigma). As cells reached 60-70% of confluence, plates were chilled and washed twice with 10 ml of ice-cold PBS supplemented with CHX. Cells were collected, were scraped, collected and centrifuged at 3000 rpm at 4°C for 3 minutes. Cell pellets were re-suspended in 1 ml of ice-cold PBS1x-CHX and re-spun at 10 000 rpm at 4°C for 30 seconds. Then, cells were re-suspended in ice-cold hypotonic buffer medium RSB (0.01M KCl, 0.0015M $MgCl_2$, 0.01M Tris-HCl, pH 7.4, supplemented with 50 µg/ml CHX cycloheximide and 1X protease inhibitor cocktail Complete (Roche). Cells were allowed to swell by incubation on ice for 5 minutes and then were ruptured mechanically with 10 strokes with a Dounce tissue grinder (type b). The supernatant recovered after centrifugation at 1000g at 4°C for 2 minutes was used as the source for fractionation experiments, therefore, we refer to this

sample as “cell extract”. A small aliquote of the cell extract was stored at -20°C, while most of it was immediately fractionated (we noticed that freeze-thawing cell extracts compromised the quality of fractionations).

Membranes and cytosolic components were separated in discontinuous sucrose gradients (Fig.13). 0.2 ml aliquotes of cell extract were mixed with 1.65 ml of 2.5M sucrose made up in TKM buffer (0.05M Tris-HCl, pH 7.4, 0.150M KCl, 0.05M $MgCl_2$) supplemented with 50 µg/ml CHX and 1X protease inhibitor cocktail Complete (Roche), and incubated in constant agitation for 30 minutes at 4°C. The mixture was layered over 1.5 ml of 2.5 M sucrose-TKM in a polyallomer centrifuge tube (Beckman Coulter). On top of the cell extract-sucrose mix, we first layered 6 ml of 2.05 M sucrose-TKM and 2.5 ml of 1.25 M sucrose-TKM. The gradients were centrifuged for 10 hours at 25000 rpm 4°C in a SW40 Ti Beckman rotor. Membrane contents have a density range of 1.0-1.2 g/L and therefore will “float” in the gradient up to the interface between the 1.25M and the 2.05M sucrose layers. We collected 8 fractions of 1.5 ml from the top to the bottom of the tube (Fig.13).

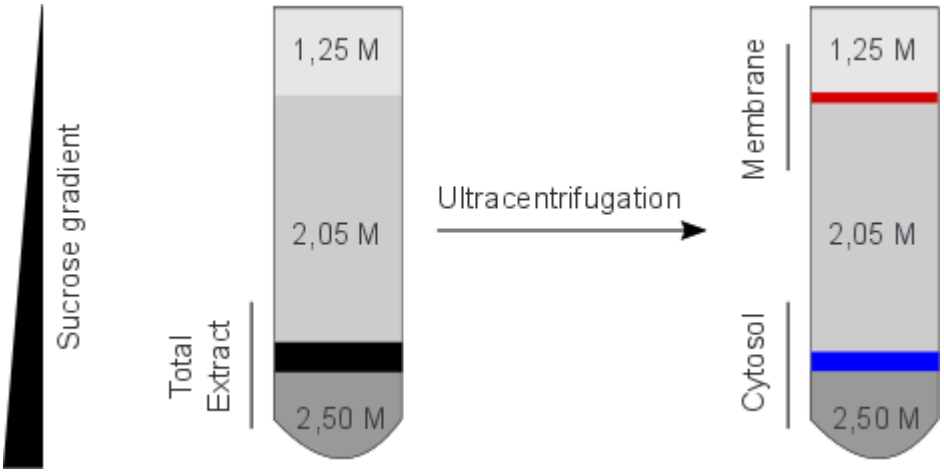

Figure 13. Schematic representation of the separation of membrane and cytosolic fractions by ultracentrifugation in a discontinuous sucrose gradient.

For protein analysis, 25 µl of each fraction were mixed with 6 µl of Laemmli buffer 5X (63mM Tris-HCl pH 6.8, 10%Glycerol, 2%SDS, 0.0025% Bromophenol Blue), boiled for 10 minutes and loaded in polyacrylamide gels for Western blot analysis.

For RNA analysis, 500 µl of each fraction were mixed with 500 µl of 0.2% SDS. Since RNA recovery from the different fractions could not be equeally efficient, we added to all fractions a "spike" *in vitro* transcribed luciferase synthetic RNA at this step, that would serve to normalize RNA recovery. Each fraction was then mixed with phenol-chloroform (1:1), the nucleic acid in the aqueous phase was precipitated with isopropanol and finally re-suspended in 10 µl of nuclease free-water. 2 µl of the purified RNA from each fraction was treated with RNAse-free DNase I and the remaining RNA was analyzed by quantitative RT-PCR, as described above (section 3.3.3).

3.5. Imaging Techniques

3.5.1. Live Cell Imaging

Visualization of IRE1α protein

To visualize IRE1α protein, HEK-293 stable cell lines expressing the tagged proteins IRE1α-eGFP or Ire-mCherry, encode in the plasmids pcDNA5_FRT-IRE1α-eGFP and pcDNA5_FRT-mCherry were used. To visualize, stable HEK-293 cells expressing IRE1α tagged proteins were seeded into glass-bottom microwell dishes (MatTek), at 3×10^5 cells/dish in selective growth media. The expression of IRE1α fused proteins was induced by incubation with 10 ng/ml of doxycycline (Sigma) for 16 hours, prior to visualization. Then, the activation of UPR was prompted by the addition of 1µM of thapsigargin (Applichem) in the culture media for 2 hours at 37ºC, 5% CO_2. IRE1α protein was then visualized before and after the induction of UPR on Cell Observer® SD Spinning disk (ZEISS) with the objective 63X C-Apochromat NA: 1.20 W Corr M27 (ZEISS). Images were analyzed with the ImageJ software (http://rsbweb.nih.gov/ij/).

3.5.2. Immunofluorescent assay

HeLa cells were grown on 18X18 mm round #1 collagen-coated coverglass in a 6-well tissue culture plate. Cells were washed once with 1 ml of PBS and then fixed by incubation with 1 ml of 4% paraformaldehyde methanol free (Thermo Scientific) for 10 minutes at room temperature. Then,

cells were washed three times with PBS and permeabilized with 1 ml of 0.01% Triton X-100 (Sigma) for 10 minutes at room temperature. Cells were washed three times with PBS. Primary antibodies were prepared in 3% BSA dissolved in PBS at the indicated dilutions (Table 3). A humidified chamber was assembled using a 150 mm tissue culture plate in which a single layer of parafilm was placed on the botton. Then, 40 µl of the primary antibody were dispensed onto the parafilm and the coverglass contained samples were gently transferred with the cells side down. The humidified chamber was closed with the tissue culture lid, covered with a flat water-saturated paper towel and incubated in the dark at 37°C for 30 minutes. After this time, coverglasses were gently transferred, cells-side up, to a fresh 6-well plate containing 1 ml of PBS and incubated for 5 minutes at room temperature. The PBS was removed and samples were washed two more time with PBS. Appropriate dilutions of secondary-labeled antibodies (Table 3) were dispensed in a cleaned parafilm into the humidified chamber and coverglass were carefully transferred, cells-side down, and incubated in the dark at 37°C for 30 minutes. After that, cells were washed three times with PBS as described above. Then, a small drop of vectashield (Vectors Laboratories) mounting medium with 4',6-diamidino-2-phenylindole (DAPI) was added onto a clean microscope slide, and coverglasses were mounted onto the slide, cells side down. The excess of mounting medium was removed and the coverglass perimeter was sealed with clear nail polish, allowed to dry in the dark. Samples were then visualized in a Zeiss LSM 510 META confocal microscopy with the EC Neufluar 100X oil objective and images were analyzed with ImageJ software (http://rsbweb.nih.gov/ij/).

3.5.3. Fluorescent *in situ* hybridization

We followed the FISH protocol developed by Stellaris Biosearch Technologies. Using the Stellaris Probe Designer, we designed 48 short oligonucleotide probes, each of which was labelled with the Quasar 570 fluorophores, which recognized either human XBP1 or GAPDH mRNAs. Each of these probes could bind the cognate mRNA, but would yield a poor labelling of the RNA molecule. However, the binding of multiple probes to their binding

site in the same mRNA molecule produce sufficient local fluorescence to detect single RNA molecules.

Briefly, HeLa cells were grown on 18X18 mm round #1 coverglass in a 6-well cell culture plate. Cells were washed once with 1 ml of nuclease-free PBS1x and then fixed by incubation with 1 ml of Fixation Buffer (3.7% Formaldehyde in PBS1x) for 10 minutes at room temperature. Then, cells were washed three times with PBS1x and permeabilized with 1 ml of ethanol 70% for at least 1 hour at 4°C. For the hybridization step, ethanol was removed and cells were pre-incubated for 5 minutes in Wash Buffer (10% formamide in 2X of Saline Sodium Citrate (SSC) at room temperature. After this step, 100 µl of the hybridization buffer (100 mg/ml Dextran Sulfate and 10% Formamide in 2X SSC), containing 0.5µM of probe mix labeled with Quasar 570 were added. A clean coverslip was carefully placed over the samples that were incubated in a dark humidified chamber at 37°C for 16 hours. Then, samples were washed with 1 ml of Wash Buffer, coverslips were removed carefully and samples were incubated again at 37°C for 30 minutes in the dark. Wash buffer was replaced by 1 ml of DAPI at 5 ng/ml dissolved in Wash Buffer, added to stain nuclei. After a 30 minutes incubation at 37°C in the dark, DAPI was aspirated and samples were washed once with 1 ml of 2xSSC.

Before imaging, samples were incubated with GLOX Buffer (0.4% glucose, 10mM Tris-HCl pH 8.0 in 2XSSC) without enzymes for 2 minutes at room temperature. Then, a small drop (approximately 15 µl) of GLOX Buffer with enzymes [1 µl Glucose oxidase solution (glucose oxidase from Aspergillus Niger, Sigma, diluted to 3.7 mg/ml in 50 mM sodium acetate, pH 5) and 1 µl of catalase from bovine liver, (Sigma)], were added onto a microscope slide, and coverglass was mounted onto the slide, cells side down. The excess of GLOX anti-fade medium was removed and the coverglass perimeter was sealed with nail polish. Samples were then visualized in the Zeiss Axio Imager M1 fluorescent microscope, using the EC Neufluar 63X oil objective.

To co-visualize XBP1 mRNA together with Vimentin fibers, we adapted the FISH Stellaris Protocol for Adherent Cells by combining it with

Immunofluorescence technique. For this purpose, the primary and secondary antibodies used to detect Vimentin fibers were included in the hybridization buffer and in the DAPI staining solution, respectively, at a 1/200 dilution. To visualize Vimentin fibers, a secondary antibody conjugated to Cy3 fluorophore was used. Except for these modifications, the rest of the FISH protocol was performed as described above. Both XBP1 RNA particles and Vimentin fibers were co-visualized in the Zeiss Axio Imager M1 the fluorescent microscopy using the EC Neufluar 63X oil objective.

To improve RNA visualization quality, we acquired stacks of images at different focal planes. These pictures were subjected to a deconvolution process, using the Huygens Software by Scientific Volume Imaging. The program first calculates a theoretical PSF (Point Spread Function) based on the microscope capture parameters and then performs the deconvolution process using a non-linear iterative method Classic Maximum Likelihood Estimation.

To analyze the colocalization between RNA particles and vimentin fibers we developed a specific script based on Java as a plugin of the open code ImageJ software (http://rsbweb.nih.gov/ij/). To detect the RNA particles, a Top-Hat filter was applied using a 3D filter plugin (Ollion et al. 2013). Otherwise, to detect the Vimentin fibers, a coherent filter developed in the *Coherence Enhancing Diffusion* plugin was used (Weickert 1999). The plugin carry out in our lab allows the determination of the co-localization grade by measuring the 3D distance between the XBP1 RNA particles and the Vimentin fibers segmented structures.

3.6. Yeast techniques

3.6.1. Yeast strains and plasmids.

Yeast mRNA visualization constructs as well as the Ire1Δ strain, containing a genomic U1A–GFP copy or not, have been described (Aragón et al. 2009). Ire1p variants in all assays were expressed under the control of the autologous promoter at near-endogenous levels either from centromeric pRS315 (Sikorski & Hieter 1989) derivatives or from a genomic copy

integrated from pRS305 (Sikorski & Hieter 1989) derivatives. All the Ire1 visualization constructs were cloned by Dr. Eelco van Anken at the group of Dr. Peter Walter (U. of California San Francisco and Howard Hughes Medical Institute).

All yeast strains used for this study were based on the W303a derived CRY1 strain (Aragón et al. 2009; Pincus et al. 2010), including the newly constructed strains IreE1Δ::KAN/SpR::HIS (used for all SpR splicing assays), Ire1Δ::KAN/Ire1ΔKR-mCherry::LEU, Ire1Δ::KAN/Ire1ΔKR/Δ[+]box-mCherry::LEU (used in Figure 3B), and Ire1Δ::KAN/hac1Δ::HIS (used in Figure 5C). The SpR copy was integrated into the genome of the Ire1Δ strain from a pRS304 (Sikorski & Hieter 1989) plasmid derivative of pDEP005 (Pincus et al. 2010). The mCherry-tagged Ire1 and Ire1 (ΔKR/Δ[+]-box) copies were integrated from pRS305 (Sikorski & Hieter 1989) based constructs.

3.6.2. Yeast culture techniques and stress induction.

Cells were grown in standard or 2X concentrated synthetic media containing glucose as carbon source at 30ºC. Stress was induced either with DTT or tunicamycin, using concentrations at which differences between (samples from) WT and UPR deficient yeast are best appreciated, as we empirically established before: 0.2 µg/ml tunicamycin for viability assays, 5 mM DTT for imaging of Ire1p clusters and mRNA recruitment (Aragón et al., 2009), and 2 mM DTT for the splicing reporter assay (Pincus et al. 2010).

3.6.3. Splicing reporter assay

Two days after transformation of splicing reporter (SpR) harboring Ire1Δ yeast (Ire1Δ::KAN/SpR::TRP) with plasmids bearing Ire1 variants, fresh colonies were resuspended in 500 µl of 2X synthetic media in 1ml deep 96-well plates and incubated for 8 hours at 30°C. Fluorescence of samples was then analyzed either before or after the addition of 2 mM DTT and a further 2 hours incubation at 30°C by flow cytometry using a BD LSR-II, as described (Pincus et al. 2010).

3.6.4. qRT-PCR assay

Total RNA was isolated by the hot phenol method and RT-PCR of spliced and total mRNA of *HAC1* and derivatives was performed, as described (Elizalde et al., 2014). The primers used to amplify spliced and total *HAC1* mRNA were (forward) CTTGACAATTGGCGTAATCCAGAA (for spliced) and (forward) CCACGAAGACGCGTTGACTTGCAG (for total) and (reverse) GCTATATCGTCGCAGAGTGGGTCTG (for both spliced and total).

3.6.5. Microscopy and image analysis

All imaging and quantitation of images were performed, as described (Aragón et al., 2009). In brief, samples for microscopy were taken from yeast that was kept in early log-phase for at least 16 hours in 2X Synthetic media before imaging. Microscopy of laser-excited mCherry or GFP was performed with a Yokogawa CSU-22 spinning disc confocal on a Nikon TE2000 microscope, controlled with μmanager and ImageJ. Images were captured with a 100X/1.4 NA Plan Apo objective on a Cascade II EMCCD and selected for analysis to contain significant signal above background but no saturated pixels. For display, images were processed in ImageJ and Adobe Photoshop such that the linear range of signals was comparable. Foci of Ire1 variants were determined and the co-localization index for U1A–GFP decorated SpRU1A, SL-PGK-3′ hac1U1A, or SpR Δ3′ BEU1A mRNA recruited to those foci was scored by using a customized MatLab script, as described (Aragón et al. 2009)

4. RESULTS

4.1. Challenging the co-translational XBP1 mRNA transport model

4.1.1. A short introduction to the XBP1 mRNA biology

In mammalian cells we can find two transcript variants of the XBP1 mRNA. The variant 1 named as unspliced XBP1 mRNA (XBP1u), which encodes for the Xbp1u protein. The XBP1u mRNA can be processed by IRE1 endoribonuclease on the cytosolic portion of the ER. IRE1 catalyzes the cleavage of a 26 nt-long intron inserted within the XBP1u open reading frame and after ligation of the exons by RctB ligase, emerges the second variant, the spliced XBP1 mRNA (XBP1s) (Fig.5).

The elimination of the XBP1 intron causes a (+1) frameshift, thereby resulting in a new open reading frame that encodes for the Xbp1s protein. The resulting Xbp1s isoform has the same N-terminus, but a longer C-terminus compared to the Xbp1u isoform. The Xbp1s isoform functions as one of the principal transcription factors that drive the transcriptional response to ER stress (UPR) (Fig.5).

Since XBP1 mRNA splicing catalyzed by IRE1 takes place at the cytosolic side of the ER membrane, the XBP1 mRNA has to travel from the nucleus to the ER, where IRE1 localizes. To explain the encounter of the XBP1 mRNA with IRE1 in mammalian cells, a co-translational model has been proposed (Yanagitani et al. 2009). According to this model, XBP1 mRNA is transported to the ER membrane via a co-translational targeting mechanism. As ribosomes are translating the unspliced XBP1 mRNA, from the nascent chain emerges a hydrophobic peptide (hydrophobic region 2, HR2), which promotes the association of the mRNA/ribosome/nascent chain complex to ER membranes. Once tethered to the ER, XBP1 mRNA becomes accessible to IRE1 to undergo splicing upon ER stress induction (Fig.6).

In the yeast *Saccharomyces cerevisiae*, ER stress caused by the accumulation of misfolded proteins in the lumen of the ER, promotes the oligomerization of the Ire1p molecules in the plane of the ER membrane. Such oligomerization leads to the activation of the Ire1p RNAse domain (Li et al. 2010). Unspliced *HAC1* mRNA, the yeast homologue of XBP1, is then recruited to the Ire1p clusters (Aragón et al. 2009). The efficient encounter between *HAC1* mRNA and Ire1p in these foci requires 1) the oligomerization of Ire1p 2) a conserved sequence element located in the 3´untraslated region of *HAC1* mRNA, named 3' bipartite element (3'BE), and 3), a mechanism to repress *HAC1* mRNA translation in cis,

imposed by its intron. One elegant hallmark of this mechanism is that it ensures the selective recruitment of unspliced, but not spliced *HAC1* mRNA to Ire1 splicing sites (Fig.4).

While some of the features discovered in yeast are conserved in higher eukaryotes, many of them don't seem to be maintained. In mammalian cells, the clustering of IRE1 in the presence of ER stress is conserved. However, the 3'BE could not be identified by homology in mammalian cells; also, unspliced XBP1 mRNA is translated because the short intron (26 nucleotides) cannot block translation as in the case of *HAC1*. The HR2 co-translational targeting model provides a distinct mechanism which, intriguingly, still explains the selective recruitment of unspliced XBP1 mRNA to ER membranes. Yet, this model cannot justify the directional transport of the XBP1u mRNA to IRE1 in cluster. Along with this caveat, some studies showed that mutants of XBP1u mRNA that do not contain the sequence encoding for the HR2 peptide could be efficiently spliced (Iwawaki & Akai 2006, Coelho et al. 2014). Given that the co-translational model cannot explain all the properties of the XBP1 mRNA splicing reaction, we decided to determine the contribution of the HR2 peptide to the splicing/transport of XBP1 mRNA.

4.1.2. Association of the XBP1 mRNA to cellular membranes

The co-translational model that described the transport of the XBP1 mRNA to the ER membrane is based on the association of XBP1u mRNA to ER membranes via the HR2 hydrophobic sequence. To determine the extent of this association, we first assessed the fraction of XBP1u mRNA associated to the ER membrane under physiological conditions. To that aim, we set up a membrane floatation assay based on the classical fractionation method developed by Mechler (Mechler & Vassalli 1975).

Briefly, total cell extracts from the mammalian Flp-in 293 cell line were obtained by hypotonic lysis, and post-nuclear supernatants were separated by ultracentrifugation in a discontinuous density gradient of sucrose (Fig.14A). After ultracentrifugation, cell membranes floated to reach their own density, which localized at the interface between 2.05M and 1.25M sucrose layers, while cytosolic components stayed at the bottom of the tube. Importantly, to avoid ribosomal run-off from the mRNAs, all the solutions were supplemented with the translation elongation

inhibitor cycloheximide. After ultracentrifugation, gradients were collected in 8 fractions, from the top (fraction 1) to the bottom (fraction 8) (Fig.14 A&B).

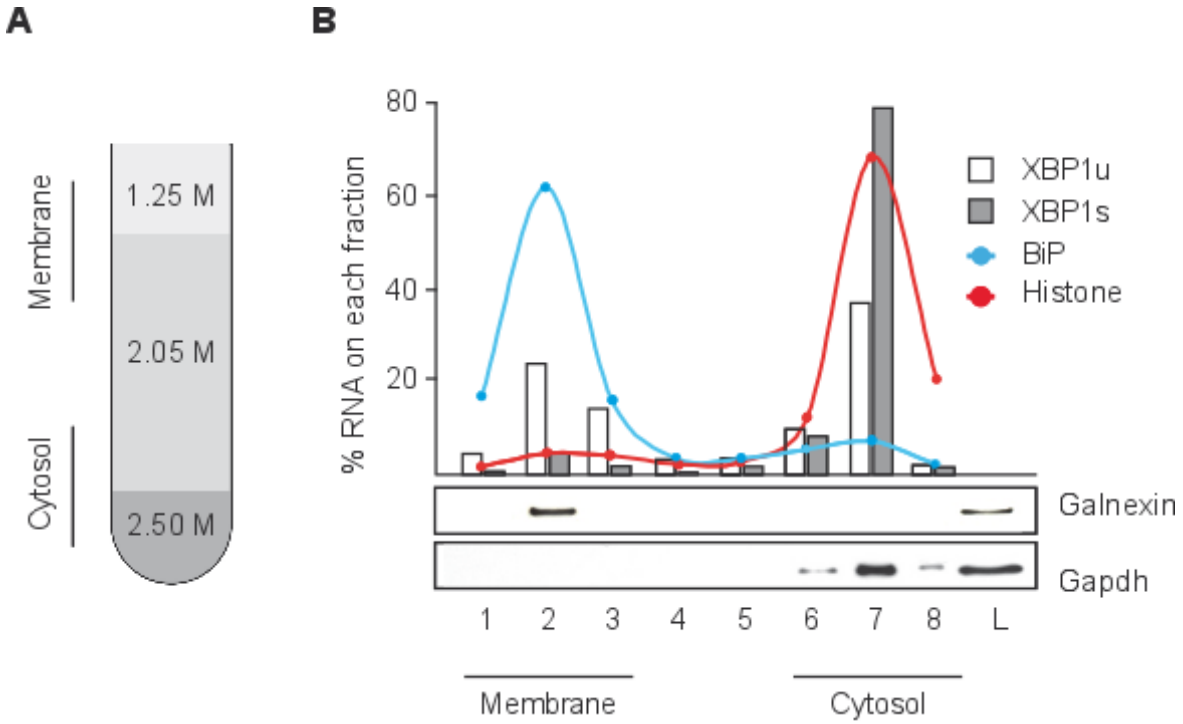

Figure 14. Scheme of the floatation assay used to monitor mRNA association to membranes. A) Flp-in 293 cells extracts were separated in discontinuous sucrose density gradient. Upon centrifugation, membrane components "float" to the interface between the 1.25M and 2.05M layers, while cytosolic components stay at the bottom of the tube. Membrane and cytosol fractions are marked. B) A representative experiment. Gradients where separated into eight fractions. The distribution of membrane (Calnexin) and cytosolic Glyceraldehyde 3-phosphate dehydrogenase (Gapdh) proteins within these fractions was determined by Western blot. Lane L, original extract. RNA was isolated from each fraction and the distribution of specific mRNAs was tested by quantitative RT-PCR. Histogram represents the percentage of mRNA on each fraction. As positive controls, we monitored the distribution of membrane-bound (BiP, blue line) and cytosolic (Histone H3B3, red line) mRNAs. XBP1u mRNA (white bars) is associated to membranes. XBP1s mRNA (grey bars) behaves as a cytosolic mRNA. Fractions 1-3 and fraction 6-8 were defined as membrane and cytosolic fractions, respectively.

We analyzed the distribution of cytosolic and membrane-bound proteins and RNAs in each fraction. As shown in Figure 14B, Calnexin, an ER resident protein, is recovered in fraction 2 while Gapdh – a soluble cytosolic protein – was detected in fractions 6 to 8. These markers identified Fractions 1 to 3 as the "membrane fractions", and Fractions 6 to 8 as the "cytosolic fractions". Consistent with the protein data BiP mRNA, which is delivered to the ER membrane by the SRP through its signal sequence, localized predominantly in fractions 1 to 3, while a cytosolic mRNA encoding for the Histone was found mainly in fractions 7-8 (Fig. 14B).

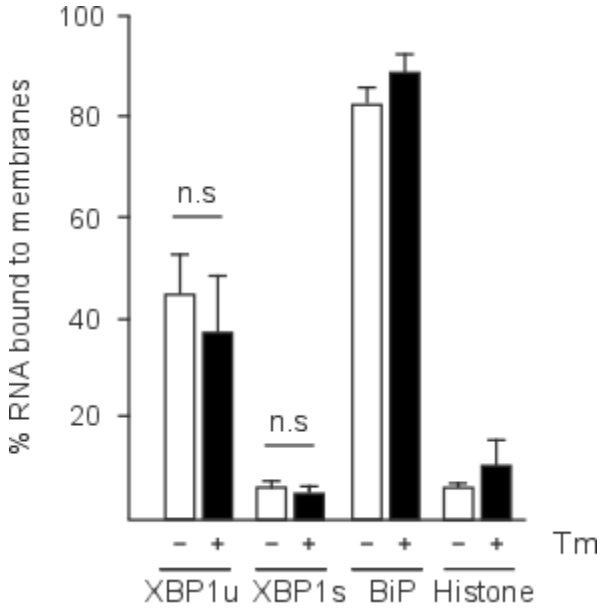

Figure 15. Quantification of membrane-associated mRNAs. Histograms represent the percentage of the indicated mRNAs, unspliced XBP1 (XBP1u), spliced XBP1 (XBP1s), BiP and Histone found in membrane fractions and referred to total amount of each mRNA in the whole gradient; in non-endoplasmic stress condition (white columns) and under acute endoplasmic stress (black columns) produced by incubation with 5ng/ml of tunicamycin (Tm) for 4 hours. Membranes association assay was performed as described in Figure 14. These results represent the media and the standard deviations of three independent experiments. Student's t-test was used to analyze differences in XBP1 mRNA membrane association percentage, between non and acute ER stress conditions, as indicated (significant p>0.5, n.s. not significant).

Once the cell fractionation assay was validated, we determined the association of XBP1u and XBP1s mRNAs to membranes. We quantified mRNA association to ER membranes as the percentage of mRNA detected in membrane fractions. To detect either XBP1 mRNA isoform, by RT-qPCR, we used specific primers that distinguish each transcript variant. In the absence of ER stress, 44% of the human XBP1u mRNA is associated to cellular membranes (Fig.15). This extent of association is lower than the one observed for SRP-targeted mRNAs (such as BiP mRNA, which shows an 81% of membrane association) (Fig.15). Still, XBP1u mRNA association was much higher than the one observed for cytosolic mRNA, such as the histone mRNA (7%) (Fig.15). These results confirm the selective association of XBP1u mRNA to ER membranes; the fraction of membrane-associated XBP1 mRNA in this study is similar to what had been reported in earlier studies (Diehn et al. 2000). In contrast, XBP1s mRNA was poorly associated to the ER (6% association),

behaving as the cytosolic Histone mRNA (Fig. 15). Together, these results are consistent with the results reported by Yanagitani et al. 2009 .

Since XBP1 mRNA splicing is relevant both under physiological and ER stress conditions, we performed the same analyzes in cells where ER stress was induced by incubation with tunicamycin, a chemical that blocks N-linked glycosylation thereby preventing protein folding within the ER. As shown in Figure 15, unspliced and spliced XBP1 mRNAs displayed a similar level of membrane association under ER stress conditions (Fig.15).

4.1.3. Characterization of XBP1 mRNA mutants lacking the HR2 peptide

The co-translational model states that the association of unspliced XBP1 mRNA to membranes and the ensuing splicing depend on the synthesis of the HR2 hydrophobic peptide. Using a N-terminally FLAG-tagged version of the murine XBP1 cDNA, reported previously by Calfon et al. 2002 as a WT construct, we generated a series of HR2-defective mutants. FLAG-tagged murine XBP1 is processed with similar efficiency in murine and human cells and therefore it is suitable to be used in human cell lines, where transfected, murine RNA variants can be distinguished from the human endogenous RNA (Calfon et al. 2002). First, we designed two XBP1 mutants unable to synthesize the HR2 peptides: 1) a mutant bearing a point mutation localized within the XBP1 intron that creates a premature termination codon inside the intron, in the frame of the unspliced form of XBP1 (STOP). Ribosomes translating the STOP mRNA would terminate translation before reaching the HR2 coding sequence; 2) a mutant with a 1 nucleotide insertion within the intron (FS (+1) int). FS (+1) int insertion produces a (+1) translational frameshift by which ribosomes translate XBP1 in a different open reading frame (Fig. 16A). The FS (+1) int mutant was originally designed by the group of Dr. Kenji Kohno to challenge the HR2 co-translational model (Ref Kohno). Both STOP and FS (+1) int mutations are located within the XBP1 intron, so the spliced forms of these mutant mRNAs are identical to WT spliced XBP1 mRNA.

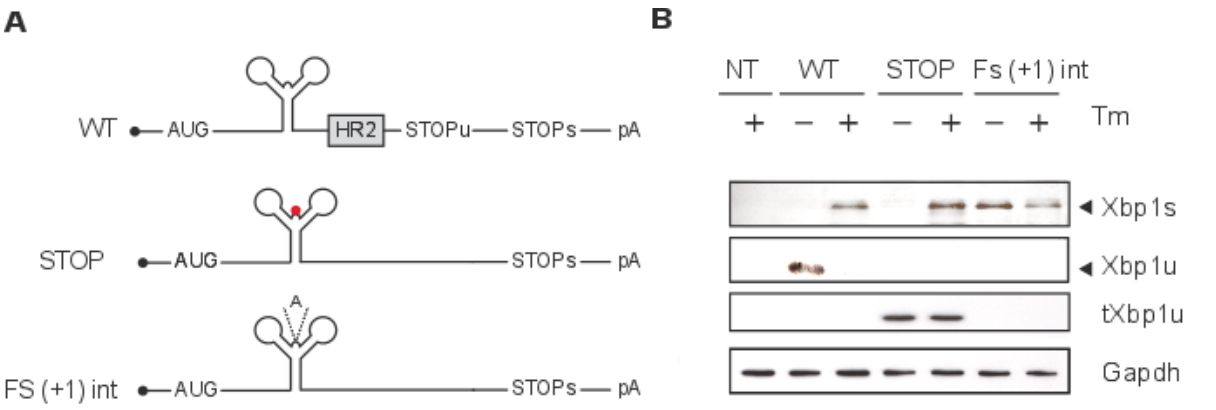

Figure 16 .Proteins produced by XBP1 mRNA mutants mRNA lacking the HR2 peptide. A) Scheme of the mutants used to challenge the co-translational model of XBP1 mRNA transport. STOP mutant bears a stop codon within the intron that interrupts unspliced ORF. A 1-nucleotide insertion within the intron of FS (+1) mutant produces a +1 frameshift thereby preventing the translation of the HR2 peptide. B) HEK-293 cells were transiently transfected with plasmid encoding for the WT version of XBP1 mRNA (WT) and the mutants STOP and FS (+1) int. 24 hours post-transfection, cells were treated (+) with tunicamycin (Tm) or mock untreated (-).Western blot analysis shows the expression of Xbp1u, Xbp1s,or tXbp1u (the truncated protein synthesized by the unspliced STOP mRNA).

We first verified the XBP1 mutant RNAs yielded the expected translation products. In the absence of ER stress WT XBP1u mRNA encodes a 33 kDa protein, Xbp1u. As described above, ER stress-induced splicing of the 26-nucleotide intron causes a translational frameshift downstream the intron position, which thereby encodes a different C-terminal half. The resulting protein, Xbp1s, is a larger 54 kDa protein (Fig.16B). Under non ER stress conditions, STOP XBP1 mRNA encodes a short, truncated Xbp1u protein (tXBP1u) of 19 kDa that could only be detected in high-percentage polyacrylamide gels, while its spliced form yields the WT Xbp1s protein band (Fig.16B). In the FS (+1) int mutant, the unspliced mRNA open reading frame is shifted such that the C-terminal half of the protein is identical to Xbp1s. Since the spliced version of FS (+1) int is identical to WT XBP1s mRNA, it also produces Xbp1s protein. Thus, FS (+1) int Xbp1u and Xbp1s proteins migrated as 54 kDa polypeptides (Fig.16B). Western blot analysis confirmed that the STOP and FS (+1) int mutants did not produce HR2-containing protein species.

4.1.4 HR2-deficient XBP1 mutant mRNAs cannot associate to membranes.

Next, we determined the membrane association of STOP and FS (+1) int mutants. To properly score membrane association, we first generated human Flp-in 293 stable cell lines expressing constitutively the murine WT allele of the XBP1 mRNA and the mutants STOP and FS (+1) int. Flp-in 293 cells have integrated a

stable FRT recombination site that ensures the efficient and directed integration of constructs at the same location of the genome, thereby making expression levels comparable. Cell extracts derived from these stable transformants were fractionated in membrane floatation experiments, as we described above (see section 4.1.2) (Fig.14). By quantitative RT-PCR we quantified the fraction of unspliced WT, STOP and FS (+1) int mRNAs bound to membranes (Fig.17A).

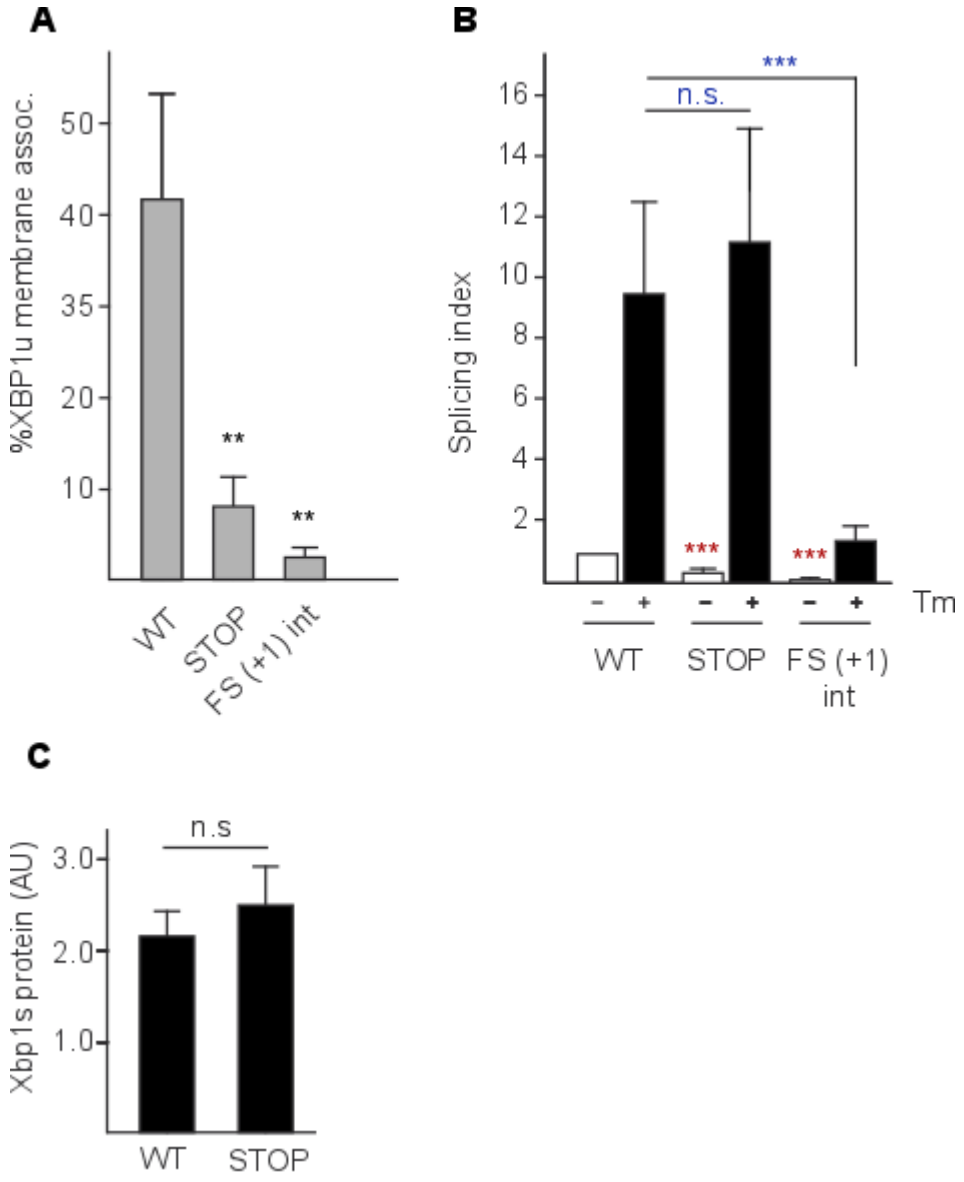

Figure 17. Membrane association, splicing efficiency and translation of XBP1 mRNA mutants lacking the HR2 peptide A) Histograms represent the percentage of the unspliced XBP1 mRNA from the WT version and the mutants STOP and FS (+1) int found in the membrane fraction, under non-ER stress conditions. Membrane association assay was performed as described in Figure 14. B) Histograms represent the splicing index of the XBP1 mRNA mutants STOP and FS (+1) int and the WT allele, under non-ER stress condition (white bars) and under acute ER stress condition (black bars) produced by incubation (+) or not (-) with 5ng/ml of tunicamycin (Tm) for 4 hours. To calculate the splicing efficiency of XBP1 mRNA, total RNA was isolated and the levels of total and spliced XBP1 mRNA were determined by quantitative RT-PCR. Splicing index = (Spliced/Total XBP1 mRNA) x100. The values were normalized relative to splicing of the WT mRNA under non-ER stress conditions C) Total

extracts from HEK-293 cells transfected with 4 µg of WT XBP1 and mutant STOP treated or not with 5ng/ml of tunicamycin for 4 hours were analyzed by western blot using anti-Xbp1 or anti-Gapdh antibodies (data not shown). Bands corresponding to Xbp1s and Gapdh proteins were quantified by ImageJ software and Xbp1s levels were represented as the ratio between the Xbp1s and Gapdh signals in arbitrary units (AU). Results represent the media and the standard deviations of three independent experiments. Student's t-test was used to analyze differences between mRNA splicing or proteins levels from the WT XBP1 and mutant STOP. (significant: ***($p \leq 0.001$), ** ($p \leq 0.01$) ; n.s.: not significant). In B) differences in splicing levels are indicated with color red and blue for physiological and acute ER stress conditions, respectively.

In these experiments, approximately 41% of WT murine XBP1 mRNA was associated to membrane fractions, a binding efficiency comparable to the one observed for endogenous human XBP1u mRNA (Fig.17A). Disruption of HR2 translation dramatically reduced the association of mutants STOP and FS (+1) int to membranes, to 8.35% and 2.69%, respectively (Fig. 17A). This low level of membrane association resembles the association rates of XBP1s or other cytosolic mRNAs (Fig.15). Thus, we concluded that in agreement with the current model (Yanagitani et. al., 2009), the association of XBP1 to membranes is HR2-dependent.

4.1.5 HR2-deficient mutants are efficiently spliced under acute stress.

Once the expression and membrane association of STOP and FS (+1) int mutants was confirmed, we evaluated their splicing capacity under normal and acute ER stress conditions. To this aim, HEK-293 cells were transiently transfected with plasmids encoding WT, STOP and FS (+1) int XBP1. Twenty-four hours after transfection, cells were either incubated with the ER stress inducer tunicamycin for 4 hours, or kept untreated. Total RNA was isolated and the relative amounts of spliced and total XBP1 mRNA (XBP1u+XBP1s) were quantified by RT/qPCR, using specific primers. Splicing efficiency was calculated as the ratio between spliced XBP1 mRNA over total XBP1 mRNA.

WT XBP1 mRNA displays a basal level of splicing, which is characteristic of the cell line analyzed and the culture conditions; typically, in HEK293 cells grown under standard conditions approximately 8-10% of the RNA is spliced. We observed that tunicamycin treatment increased about ten-fold the splicing levels of transfected WT murine XBP1. STOP and FS (+1) int RNAs displayed an altered splicing capacity, but not in the same way the HR2 model anticipated. Under non-stress conditions, the splicing levels of both STOP and FS (+1) int mutants were lower (31% and 15% relative to WT XBP1, respectively) (Fig.17B). However, under acute ER

stress STOP mutant splicing efficiency was similar, while the FS (+1) int displayed a dramatic reduction in splicing efficiency (15% relative to WT) (Fig.17B). As expected from the RNA splicing data, mutant STOP mRNA produced WT levels of Xbp1s transcription factor under ER stress, confirming that HR2 synthesis was not needed to support high levels of splicing (Fig.17C).

These results were surprising because the two HR2 mutants behaved as expected under non-stress conditions, but their behavior under acute stress was divergent. Since both STOP and FS (+1) int mutants were unable to promote HR2-dependent association to membranes, we concluded that the different splicing observed among them should not be caused by the HR2 deficiency. Therefore, we decided to confirm an HR2-independent effect of the FS (+1) mutation.

4.1.6 New frameshift mutants designed to confirm the HR2 model.

Insertion of one nucleotide in mutant FS (+1) int could disrupt splicing 1) because this mutation creates a translational frameshift or 2) because it may affect XBP1 mRNA transport or splicing catalysis by other means. To distinguish between these two possibilities, we designed new frameshift mutants containing insertions either upstream (exon1) or downstream (exon2) the UPR intron. In the case of mutant FS (+2) exon1, HR2 translation was avoided by insertion of two nucleotides in the first exon of XBP1u mRNA, causing a (+2) frameshifting. Mutant FS (+1) exon2 produced a (+1) frameshift by the insertion of one nucleotide, just before the sequence encoding HR2 peptide (Fig.18). When both mutations were combined, we obtained the FS repaired mutant that recovered the HR2 (+3) open reading frame, allowing HR2 peptide synthesis (Fig.18).

To determine if FS (+1) int deficient splicing was associated to the loss of HR2 synthesis, two adenines were inserted in exon 2 of the FS (+1) int sequence such that the resulting mutant could produce the HR2 peptide while bearing the intronic mutation. We named this mutant FS (+1) int repaired (Fig.18).

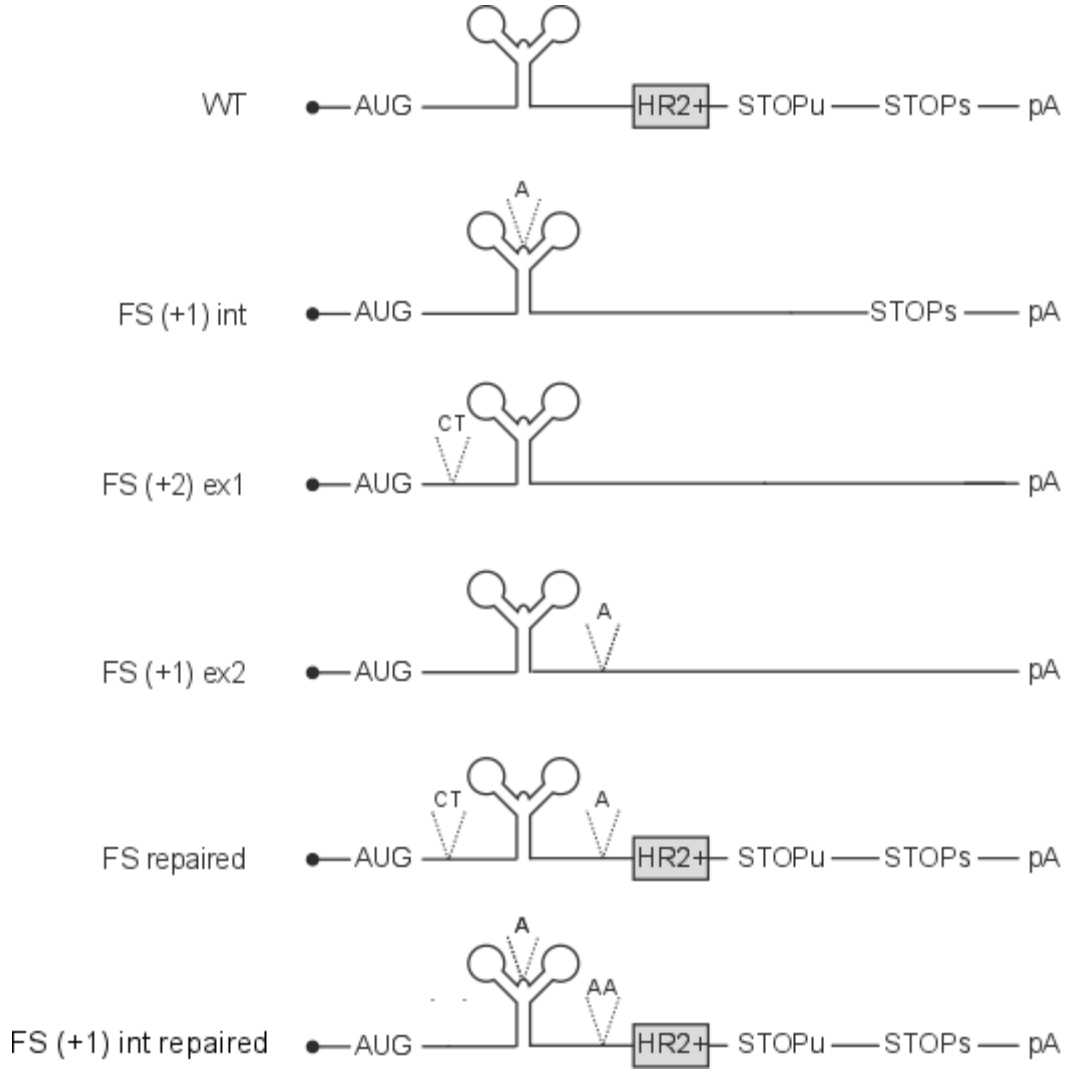

Figure 18. Schematic representation of XBP1 mRNA frameshift mutants. Scheme of frameshift (FS) insertion mutants localized outside the intron sequence. Insertions within exon 1 (ex1), exon 2 (ex2) and intron (int) yielded +1 or +2 frameshifts as indicated. FS repaired was created by combining FS (+1) ex2 and FS (+2) ex1, while FS repaired (int) contains the (+1) int mutation and (+2) in the exon 2. Both FS repaired mutants restore the HR2 open reading frame

4.1.7 The HR2 co-translational model explains the association of XBP1 mRNA to membranes

Stable Flp-in HEK 293 cell lines expressing the new frameshift mutants were generated and their association to membranes was determined as described above in Figures 14 and 15. As shown in Figure 19C, only those mutants encoding the HR2 peptide in the unspliced open reading frame were associated to membranes, while HR2 synthesis-defective mutants displayed comparable low levels of membrane association. These results confirm again the importance of HR2 peptide for the stable association of XBP1 mRNA to membranes.

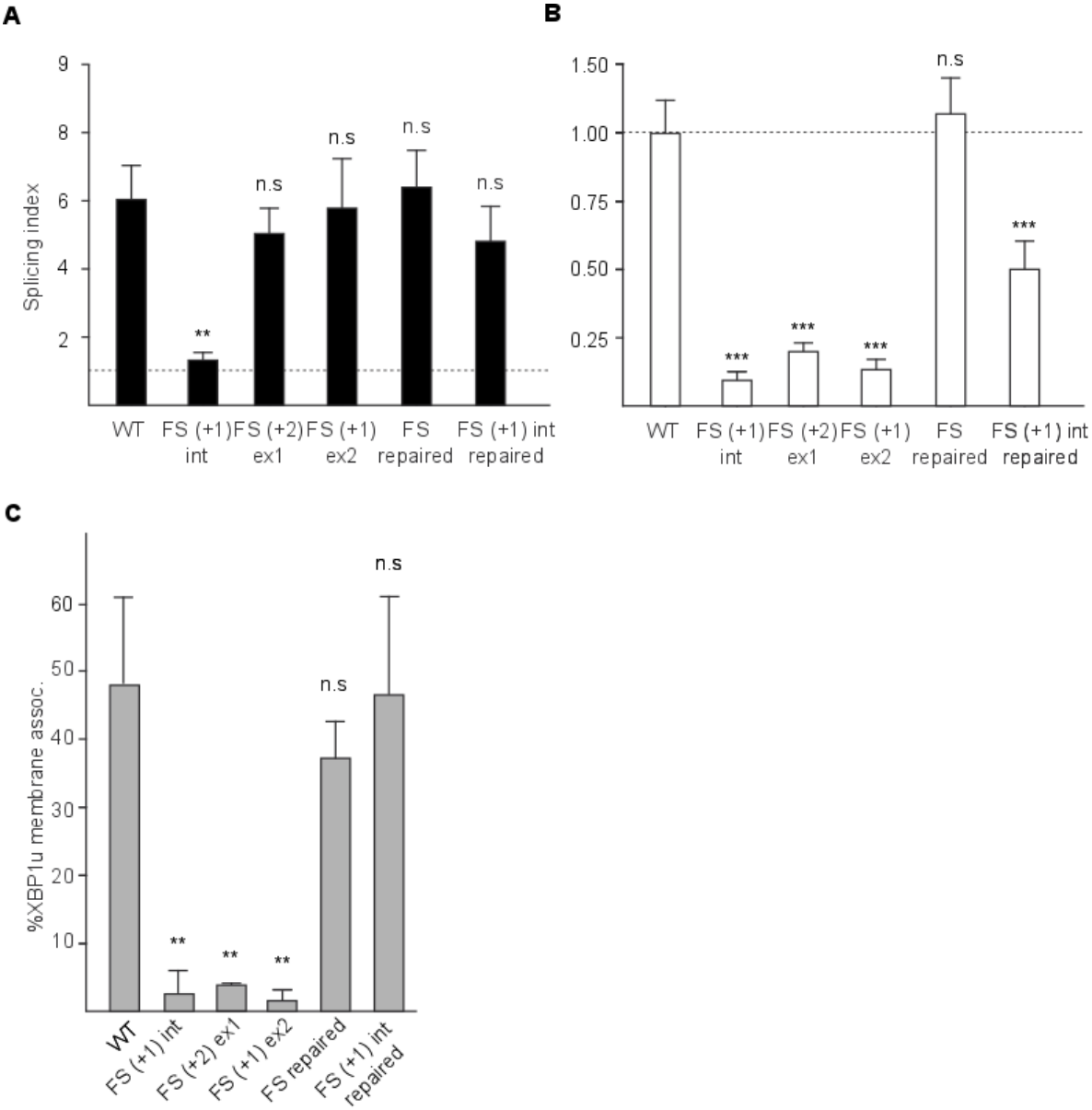

Figure 19. XBP1 mRNA frameshift mutants lacking the HR2 peptide A) Histogram represents the splicing efficiency of the XBP1 mRNA frameshift mutants (described in Figure 18) and the WT allele under acute endoplasmic stress conditions, induced by treatment with 5 ng/ml of tunicamycin for 4 hours, and expressed as fold change versus the splicing mean value of WT under physiological conditions. The splicing index was calculated as described in Figure 17. B) Histogram represents the splicing index of the XBP1 mRNA frameshift mutants and the WT allele under physiological conditions expressed as in A). C) Histograms represent the percentage of the unspliced XBP1 mRNA found in membrane fraction, from the WT version and the frameshift mutants, under non-ER stress conditions. Membranes association assay was performed as described in Figure 14. All results represent the media and the standard deviations of three independent experiments. Student's t-test was used to analyze differences between the WT XBP1 mRNA and frame shift mutants (significant: ** ($p \leq 0.01$), *** ($p \leq 0.001$; n.s: not significant).

4.1.8 Splicing efficiency of the frameshift mutants

To evaluate the splicing efficiency of the frameshift mutants under control and ER stress conditions, HEK-293 cells were transiently transfected with WT XBP1 mRNA or mutants FS (+1) int, FS (+2) exon1 and FS (+1) exon2, FS repaired and FS (+1) int repaired. Twenty-four hours after transfection cells were kept untreated or incubated with tunicamycin for 4 hours. XBP1 splicing efficiency was measured at basal and acute ER stress as described above (Figure 19A&B).

The analysis of splicing revealed three main findings: 1) Under acute ER stress, frameshift mutants FS (+2) exon1 and FS (+1) exon2 displayed splicing levels comparable to the WT mRNA, while FS (+1) int mutant underwent less efficient splicing (Fig.19A & Fig.17B). Thus, the reduction of splicing efficiency of this mutant cannot be ascribed to a defect in HR2-dependent targeting. 2) Interestingly, in basal conditions splicing of all HR2-defective mutants was significantly lower when compared to WT (Fig.19B), suggesting that basal splicing strictly relies on HR2 synthesis. In line with this notion, FS repaired was able to recover WT basal splicing levels. 3) Intriguingly, mutant FS (+1) int repaired displayed a low basal splicing but under acute ER stress splicing levels were almost completely recovered (Fig. 19A & 17B).

Altogether, these results demonstrate that co-translational targeting of XBP1 to the ER membrane is necessary for splicing under physiological, non-ER stress conditions, but is dispensable under acute ER stress conditions. The low splicing efficiency of mutant FS (+1) int owes to the disruption of the intron sequence/structure and not to the disruption of HR2 peptide production, because other frameshifting mutants were efficiently spliced under ER stress. Along with this idea, the intron sequence/structure may play an important role in the transport/splicing catalysis of XBP1.

4.1.9 HR2-defective XBP1 mRNAs respond to ER stress as quickly as WT.

Given that HR2-defective mutants display low levels of splicing in basal conditions, but are efficiently processed under stress, we analyzed the build-up of the splicing reaction in time course experiments. To that aim, HEK-293 cells were transiently transfected with plasmids encoding WT XBP1 or mutant STOP, as a

representative HR2-defective allele. ER stress was induced by incubation with tunicamycin and splicing rate was measured every 45 minutes for a total period of 320 minutes.

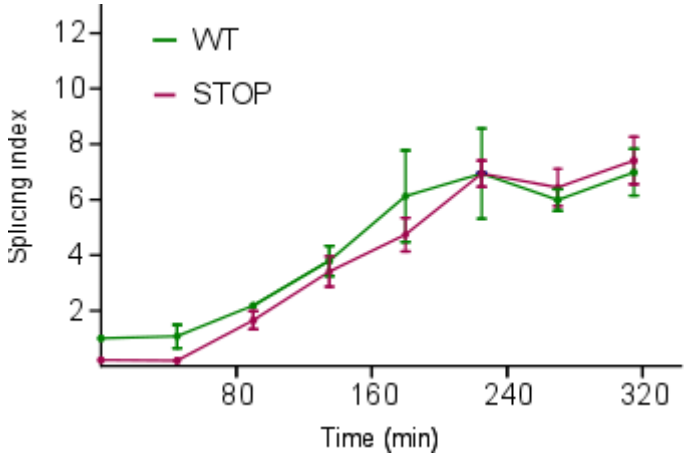

Figure 20. Splicing reaction kinetics of the XBP1 mRNA WT allele and mutant STOP. HEK-293 cells were transiently transfected with 1 µg of WT and STOP version of XBP1 mRNA. Cells were treated with 5ng/mL of tunicamycin for the indicated times Splicing index was calculated as described in Fig.17 . These results represent the mean plus standard deviation of three independent experiments.

Splicing of both XBP1 mRNA variants reached similar splicing levels, but at early time points splicing efficiency of the STOP mutant was lower (Fig.20). The results indicate that ER stress promotes a targeting program that could overrule HR2-dependent targeting.

4.2 Identification of the elements required to sustain XBP1 splicing under ER stress.

Taken together, our results indicated that the co-translational targeting of XBP1 mRNA is required to sustain basal splicing, and may be complemented or replaced by other targeting mechanisms under acute ER stress conditions. To explore this new mechanism, we performed a systematic study of the *cis*-acting elements in XBP1 mRNA needed to support splicing in an HR2-independent manner.

4.2.1 The FS (+1) int mutation does not affect hIRE1α binding or cleavage *in vitro*.

The XBP1 intron itself could be a targeting determinant because insertion of one nucleotide was enough to disrupt splicing in an HR2-independent manner. It is unlikely that this mutation affects the capacity of IRE1α to recognize or cleave the splice sites within the intron, because restoration of HR2 synthesis in the FS (+1) int variant recovered splicing capacity. Still, we decided to examine the possibility that FS (+1) int may reduce IRE1α binding or catalytic activity. To address this question, two fragments including nucleotides 1-581 or 1-582 from the WT XBP1u mRNA and the FS (+1) int mutant, respectively, were *in vitro* transcribed by T7 polymerase in the presence of a ^{32}P- labeled CTP. The XBP1 sequence used for these assay corresponded to the minimum fragment of XBP1 mRNA that showed an efficient cleavage *in vitro* (Korennykh A.V., et. al., 2009). Pre-folded RNA fragments from WT and mutant FS (+1) int were incubated with two concentrations (150nM and 400nM) of recombinant human IRE1α cytosolic domain at 30°C for 0, 15, 30, 60, 120 and 240 seconds. RNA products were then separated in a denaturing PAGE and the relative abundance of this substrate or the cleavage fragments was detected by autoradiography. Cleavage rates were calculated after quantifying substrate RNA disappearance over time (Fig. 21A&B).

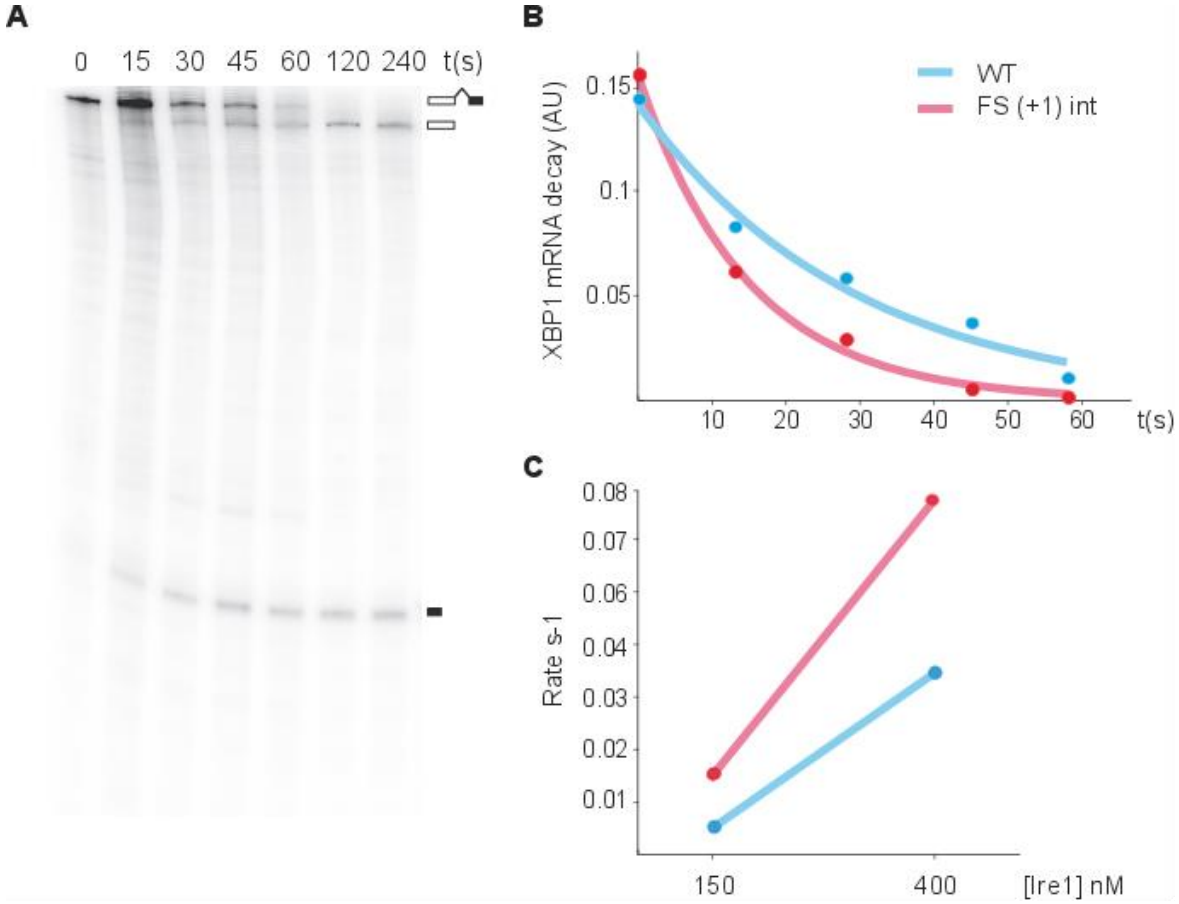

Figure 21. *In vitro* cleavage of XBP1 RNA fragments by recombinant IRE1α. A) Autoradiography shows a representative cleavage experiment of WT XBP1 mRNA fragment of 581 nucleotides by recombinant human IRE1α cytosolic domain. The migration of full-length and cleavage products are indicated. B) Quantitation of the disappearance of cleavable substrates of two XBP1 RNA fragments of 581 and 582 from the WT allele (blue) and the frame shift mutant FS (+1) int (red), respectively, at 140 nM IRE1α concentration are represents. C) Representation of the cleavage rates constant k observed (kobs) for WT and mutant FS (+1) int RNAs at a concentration of IRE1α 150nM and 400 nM.

Our results indicate that, at least in this assay, the rates of cleavage calculated for mutant FS (+1) int RNA were similar – if not higher – than those observed for the WT RNA. Thus, mutant FS (+1) int was as good substrate for IRE1α endonucleolytic cleavage as the WT XBP1 mRNA. Together with the notion that the splicing defect of this mutant *in vivo* can be partially rescued by HR2 peptide, these findings suggest that XBP1 intron may contribute to XBP1 targeting *in vivo*.

4.2.2 SHAPE analysis reveals two possible conformations for XBP1 intron.

Whithin the XBP1 mRNA sequence, the XBP1 intron and its exonic boundaries are the best conserved element. From yeast to human cells, IRE1 protein

recognizes and cleaves the 5' and 3' splice sites. The non-canonical intron can appear in two different ways: as a long (>80 nt) version found in *S. cerevisiae* and related yeast species and a short one (<30 nt) found in metazoans and in some ascomycete fungi. A study based in multiple sequence alignment and Infernal package (infernal.janelia.org) identified conserved features in the secondary structures of the sequences flanking the *HAC1*/XBP1 intron in eukaryotic cells from different species (Hooks & Griffiths-Jones 2011) (Fig.22). The species containing the long intron maintain the short stem 1 and stem 2 (found in the vicinity of long and short introns), but in the long introns these structures are separated by 70 to 360 nucleotides.

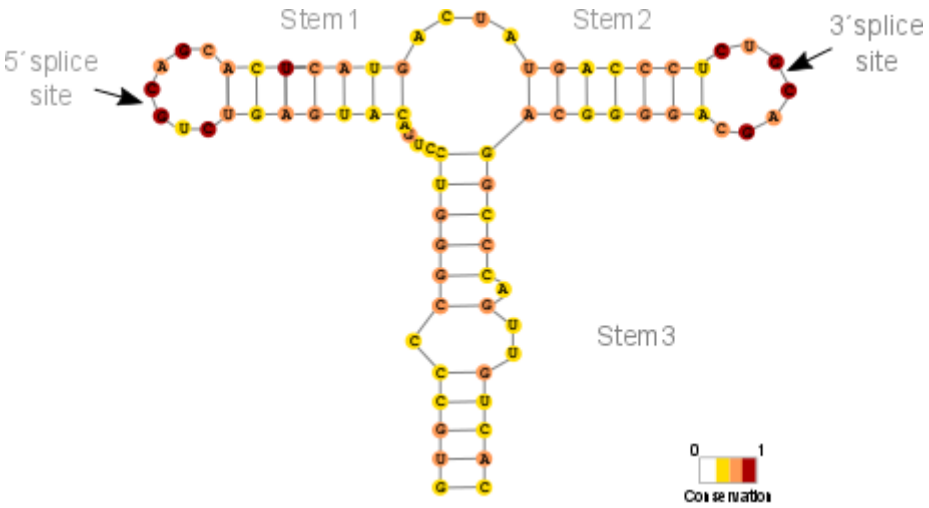

Figure 22. Consensus structure of HAC1/XBP1 mRNA. Sequence conservation at each position is shown by color scale, where white and red colors indicate the lowest and highest conservation grades, respectively.

Source: Adapted from Hooks & Griffiths-Jones 2011

In the predicted *HAC1*/XBP1 intron structure the 5´ and 3´ splice sites conform an heptanucleotide loop that contains the highly conserved sequences CNG/CNGN (Yoshida et al. 2001; Hooks & Griffiths-Jones 2011; Sidrauski & Walter 1997) at the end of the stem 1 and stem 2, respectively. Upstream and downstream of the 5´and 3´splices sites is a third stem (stem 3), that keeps the stem 1 and 2 in proximity.

The RNA folding predictions and biochemical evidence indicate that both hairpin structures (stems 1 and 2) are necessary for IRE1-mediated cleavage (Gonzalez 1999). Interestingly, in all the analyzed sequences of metazoans both

stem loop structures (stem1 and stem 2) are also conserved, even when the primary sequence is not conserved (Fig.23A).

In order to understand the structure of XBP1 intron we performed a selective 2′-hydroxyl acylation analyzed by primer extension (SHAPE) experiment. To this aim, we transcribed in vitro a fragment of WT XBP1 mRNA, spanning nucleotides 450 to 524 of FLAG-tagged murine XBP1 cDNA containing the intron sequence. After *in vitro* refolding, the RNA fragment was treated with N-methylisatoic anhydride (NMIA), which preferentially reacts with the 2´-OH group of the ribose whenever the nucleotide is available. The nucleotides that are in a primarily single-stranded structure are strongly reactive to NMIA, while nucleotides involved in base pairs are not. NMIA-modified nucleotides can stall the reverse transcriptase, thereby providing the basis for the structural probing of the RNA. After the incubation with NMIA, reverse transcription was performed and the cDNA products derived from the untreated and NMIA treated were resolved by capillary electrophoresis in denaturing conditions in parallel with a sequence ladder obtained using the same primer.

Results in Figure 23A showed the SHAPE reactivity profile of three independent assays. Globally, the resulting profiles revealed that most of the intron nucleotides showed low levels of reactivity to NMIA, suggesting that most of this RNA domain is structured. We next predicted the secondary structure of the XBP1 RNA fragment using the RNAstructure software (Reuter & Mathews, 2010) taking into account the SHAPE data.

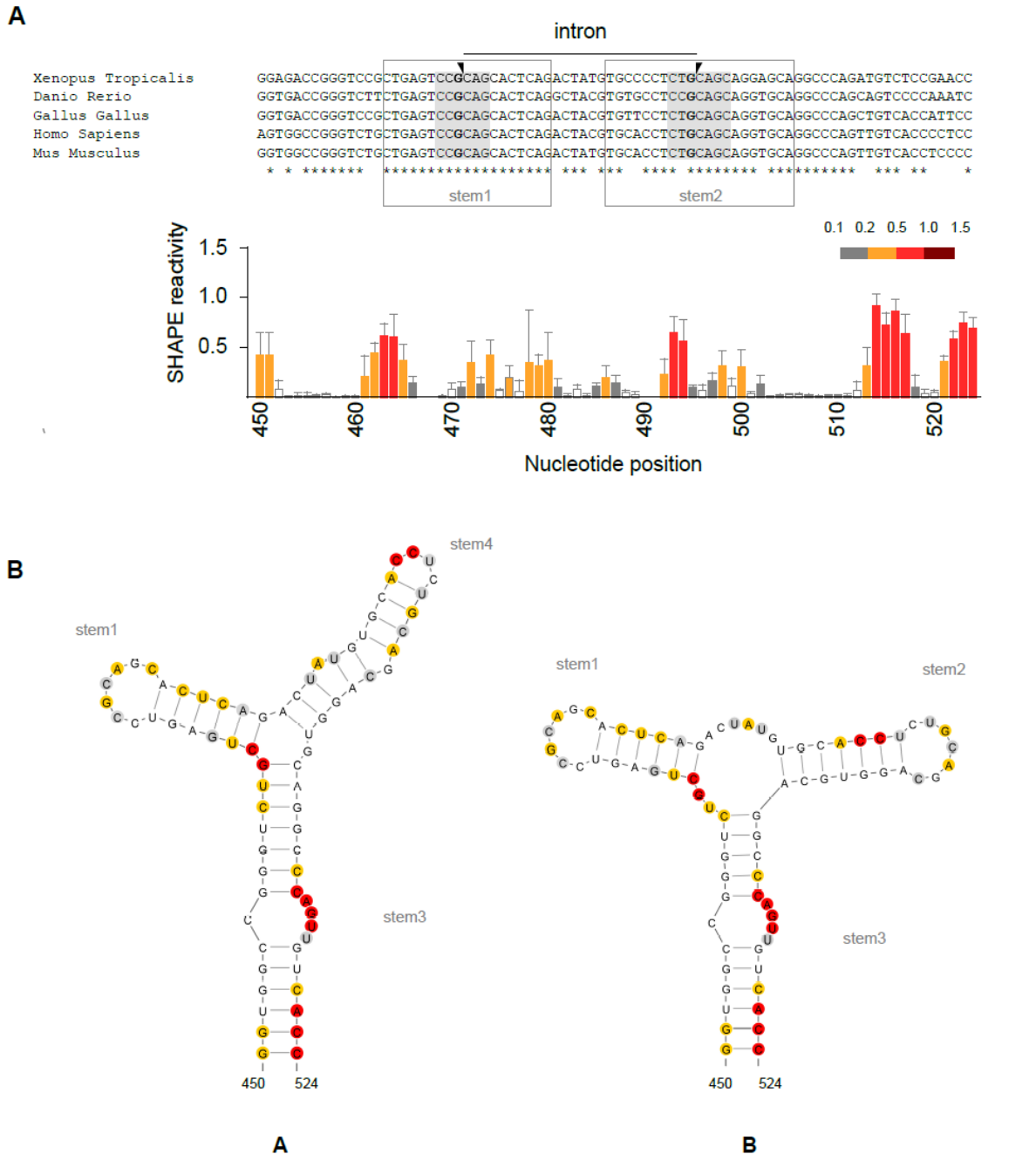

Figure 23. Structure of XBP1 intron sequence by SHAPE analysis. A) Conservation sequence alignment of XBP1 cDNA fragments containing the intron sequence from indicated species. The intron sequences are indicated and delimitated with black triangles. The sequences of 5´and 3´splice sites are highlighted in gray. SHAPE reactivity profiles for each nucleotide are shown. Values correspond to the mean SHAPE reactivity and the Standard Deviation for three independent assays. Quantitative SHAPE reactivities for individual data sets were normalized to a scale spanning 0 to 2, in which 0 indicates an unreactive nucleotide and the average intensity for highly reactive nucleotides is set to 1.0. B) Predicted secondary structures of XBP1 sequences containing the intron. Representation of the XBP1 intron structures A (-61.4 kcal/mol) and B (-58.4 kcal/mol), predicted by RNAStructure software, given the SHAPE values.

Two alternative RNA conformations fit best with the SHAPE reactivity data. In both structures, the XBP1 intron appears at the top of a stem-loop structure with an inserted bulge stem 3, which could stabilize the structure of the intron sequence and allow the association with proteins factors. Interestingly, the conformation of the intron was very different in the lowest free minimal energy structure (A) and the alternative conformation (B) (Fig.23B). In the (A) conformation, the predicted 3' splice site stem loop (stem 2) did not fold as the predicted structure (Fig. 22), and an alternative stem loop (stem4) was assembled instead, imposed mostly by the high reactivity shown by a pair of Cs to NMIA. On the contrary, the B structure showed the canonical secondary structure (Fig.22) with both 5´and 3´splicing sites (stem 1 and stem 2) exposed and suitable for cleavage by IRE1 (Fig.23). The A and B structures suggest that the intron sequence could possess two interchangeable conformations that could play a role in the targeting reaction (Fig.23).

4.2.3 Mutational analysis on the XBP1 mRNA sequence

Aragón et al. 2009 found a conserved bipartite targeting element in the 3´ untranslated region of the *HAC1* mRNA that is required for its proper transport to the IRE1 clusters under ER stress. By analogy, we wondered if the XBP1 mRNA contains elements in its own sequence that contribute to its transport/splicing in a HR2 independent manner under ER stress. To this aim, systematic deletions were performed from 5´and 3´ extremes of the N-terminal flag tagged murine XBP1 mRNA and in a sensitized XBP1 mRNA allele that contained the STOP mutation. All mutants start their translation using the same reading frame as WT XBP1u. Then, HEK-293 cells were transiently transfected with plasmids encoding for XBP1 mRNA deletion mutants, represented in Figure 24, and their splicing rate was measured at 0 or 4 hours after the induction of ER stress by treatment with tunicamycin.

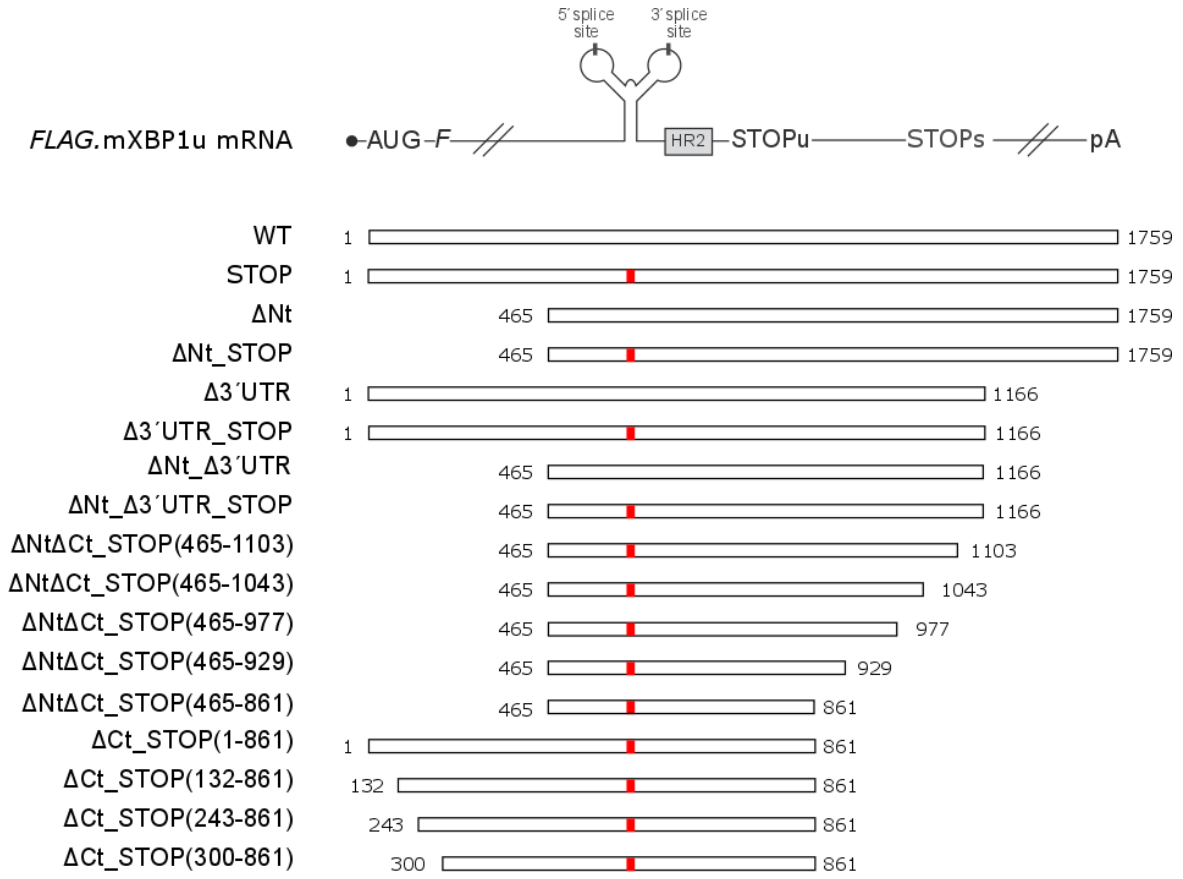

Figure 24. Schematic representation of XBP1 mRNA deletion mutants. A Flag tagged murine unspliced XBP1 mRNA (FLAG.mXBP1u) construct reported by Calfon et al. 2002 was named WT. Start codon (AUG) indicates the start of the coding sequence and it is followed by the sequence encoding FLAG peptide (*F*). The sequence coding for the unspliced form of Xbp1 protein (frame 1) starts at the first codon after the end of FLAG peptide and ends at stop codon UAA (STOPu), while the spliced form (frame 3) ends at the stop codon UGA (STOPs), 355 bp downstream. The intron of 26 nucleotides was flanked by the 5´ and 3´ splice sites and followed by the coding sequence for the hydrophobic region 2 (HR2). Mutation in the intron sequence from the STOP mutation in the intron is indicated by a red box. Initial and final nucleotide within the FLAG.mXBP1 mRNA sequence is indicated for each mutant, where 1 is the nucleotide A of the AUG initial codon.

Figure 25 represents the splicing efficiency for each exogenous XBP1 mRNA mutant compared with the WT construct. As we showed before, the XBP1 mRNA STOP mutant, unable to produce HR2 peptide, supports a splicing efficiency similar to the WT version of XBP1 mRNA under ER stress (Fig.25). However, when we evaluated the ΔNt mutant, which lacks the first 465 nucleotides of the N-terminal coding sequence, we observed a significant reduction of the splicing efficiency under ER stress (Fig.25), and this phenotype was accentuated when we abolished the HR2 peptide production by the insertion of the STOP mutation (Fig.25).

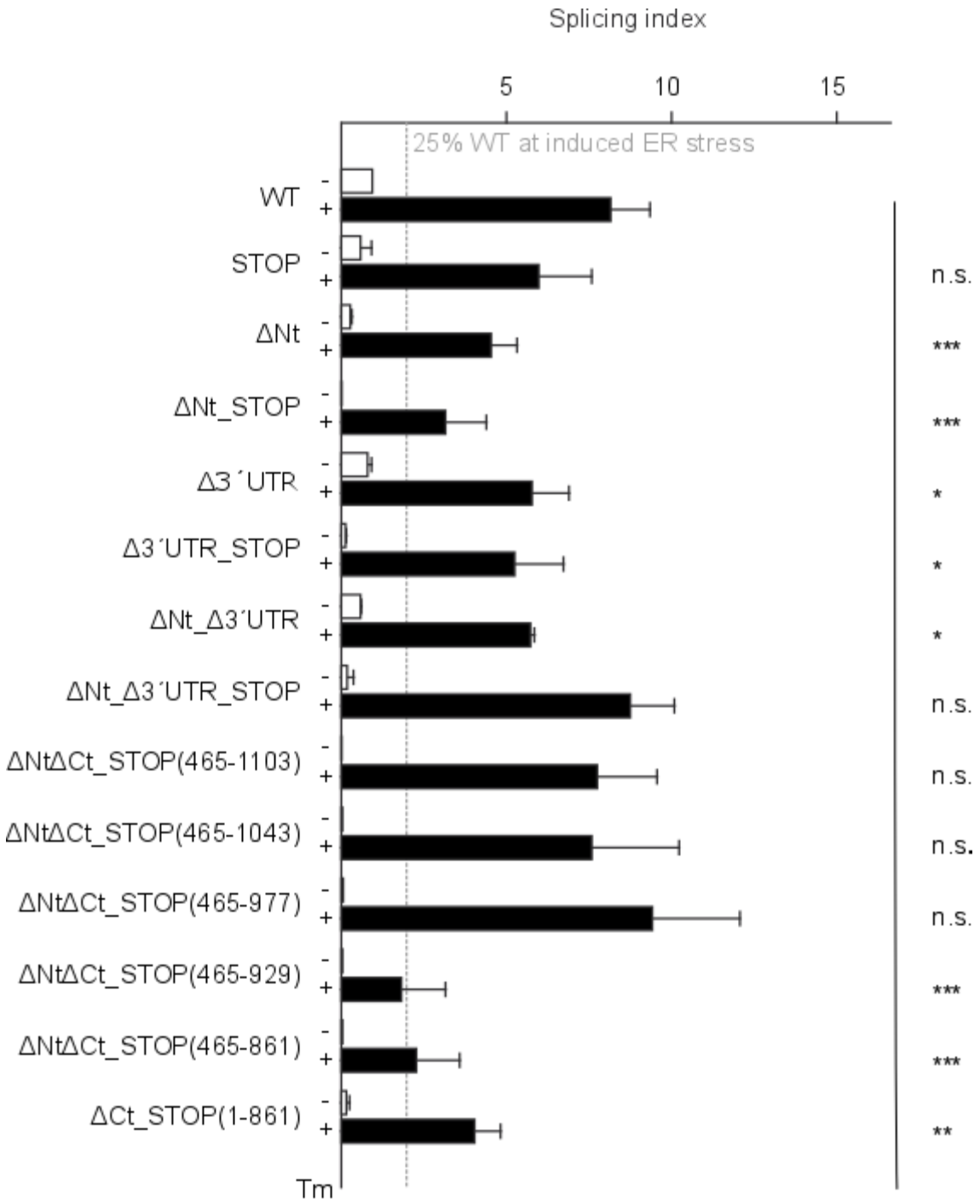

Figure 25 Splicing efficiency of XBP1 mRNA deletion mutants. Histograms show the splicing efficiency expressed in arbitrary units (AU) of the XBP1 mRNA deletion mutants under non ER stress condition (-, white bars) and acute ER stress induced by treatment (+) with 5ng/ml of tunicamycin for 4 hours (black bars). The splicing index was calculated as described in Figure 17. The columns and bars represent the means and standard deviations, respectively, of three independent experiments. All the data were normalized against the value from the WT splicing index under non ER stress conditions. Statistical significance in a Student's t-test of differences in splicing levels as compared with WT is indicated (*$p \leq 0.05$; **$p \leq 0.01$, ***$p \leq 0.001$, n.s.: not significant).

Therefore, these results suggest the existence of an HR2-independent transport determinant on the N-terminal coding sequence, responsible of loss in the splicing efficiency when the N-terminal coding sequence was eliminated. Next, we removed the 3´untranslated region of the XBP1 mRNA and we observed a significant reduction on the splicing efficiency compared to the WT construct. The splicing efficiency did not decrease when we combined the 3´UTR deletion with the STOP or ΔNt mutations (Fig. 25), which indicates possible presence of an independent splicing regulation element on the XBP1 3´UTR. The 3´UTRs constitute a platform for RNA binding proteins (RNPs) association which can regulate the localization and stability of target mRNAs. Recently, Sugimoto et al. 2015 reported that Staufen 1, a RBP able to bind double strand RNA RBP enrolled in the localization and stability of mRNAs, binds to a duplex spanning 858 nucleotides in the 3´UTR of the human XBP1 mRNA and regulates its splicing and stability. The secondary structure that allows the binding of Staufen is formed by the pairing of a sequence located at the 3´UTR with nucleotides located on the coding sequence of the human XBP1 mRNA (Sugimoto et al. 2015). Unfortunately, the 3´UTR sequence of the murine Flag-tagged XBP1u mRNA construct reported by Calfon et al. 2002 and used in this mutational analysis is incomplete and does not contain the sequence responsible for the formation of the duplex recognized by Staufen 1. However, restoration of the 3´UTR on the Flag.mXBP1u mRNA by members of our lab did not produce an increase of the splicing efficiency compared to the original construct under ER stress. Therefore, our mutational analysis results suggest that the 3´UTR may contain other elements that contribute to the transport/splicing of XBP1 mRNA.

Surprisingly, the mutant ΔNt_Δ3´UTR_STOP, which contain a combination of previous mutations which showed a reduction in the splicing rate, was spliced with the same efficiency that the WT construct under ER stress (Fig.25). This unexpected result could mean that the ΔNt_Δ3´UTR_STOP mutant of 700 nucleotides in length may contain a splicing element belonging to an HR2-independent mechanism that could be enhanced in the absent of others splicing determinants.

Note that all the mutants where the STOP mutation was inserted showed a decrease in the physiological splicing efficiency compared with their parental mutant, which confirms our first remarks that the co-translational model based in the HR2 peptide is important for the basal splicing, but is not required for the one induced by

acute ER stress. Therefore, from this point we continue the mutational analysis using the sensitive the STOP mutant as the XBP1 mRNA starting construct (Fig.25).

In order to discover new splicing determinants contained in the sequence of the ΔNT_Δ3´UTR_STOP mutant we performed serial deletions of approximately 60 nucleotides each one starting from the C-terminus coding sequence, as indicated in Figure 24. We obtained a drop of 75% of the splicing efficiency with respect to the WT when we deleted a fragment of 48 nucleotides located from nucleotide 465 to 977 of the Flag.mXBP1u mRNA (Fig.25), suggesting that this sequence is important to support an efficient transport/splicing of the XBP1 mRNA.

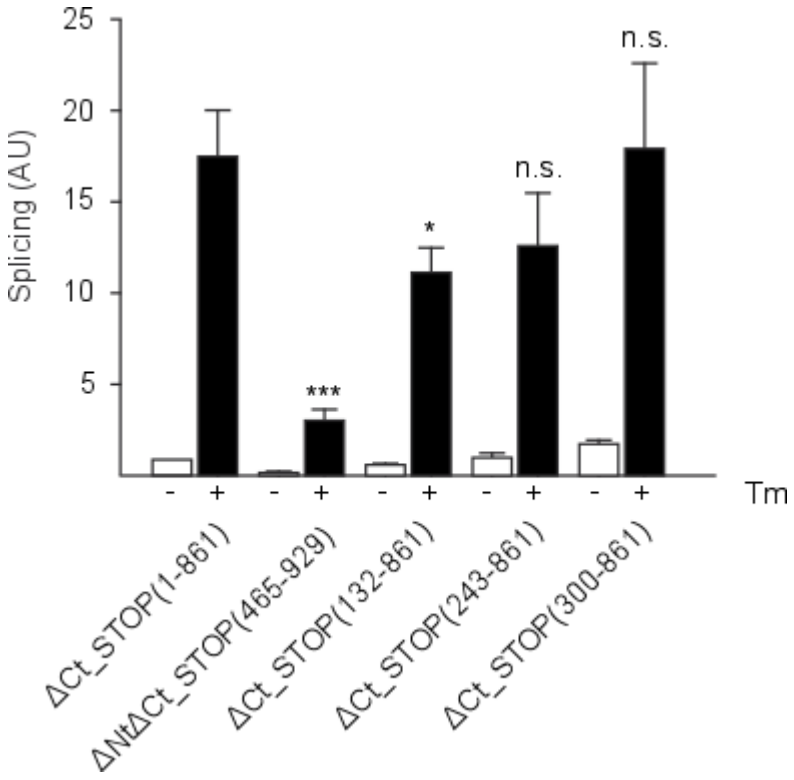

Figure 26. Splicing efficiency of mutants of XBP1 mRNA with N-terminal sequential deletions. Histograms represent the splicing efficiency expressed as splicing index for the indicated XBP1 mRNA mutants under non ER stress condition (white bars) and acute ER stress condition induced by treatment (+) or not (-) with 5ng/ml of Tunycamycin for 4 hours (black bars). The splicing efficiency was calculated as described above in Figure 17. The columns and bars represent the means and standard deviations, respectively, of three independent transfection experiments. All mutants were normalized against the value from the ΔNT_ΔCt_STOP(1-861) splicing efficiency under non ER stress condition Statistical significance in a Student's t-test of differences in splicing levels as compared with WT is indicated (,*p ≤ 0.05; **p ≤ 0.01, ***p≤0.001, n.s.: not significant).

Interestingly, when we added the sequence encoding for the entire N-terminal region to the ΔNT_ΔCt_STOP(465-861) mutant (ΔCt_STOP(1-861)) we observed a

partial recovery of the splicing efficiency comparing with the WT (Fig.24 & Fig.25). The partial rescue of the ΔNT_ΔCt_STOP(465-861) splicing defect suggests the existence of an splicing element that works in an additive way with the element lost when the sequence from nucleotides 977 to 929 was deleted. We then performed serial deletions in the N-terminal coding sequences, starting from the 5´-extreme (Fig.25), in order to define better the region responsible for the partial recovery of the ΔNT_ΔCt_STOP (465-861) splicing efficiency. Figure 26 shows that when we added the fragment of the N-terminal coding sequence that starts in the nucleotide 243 of the Flag.mXBP1u we were able to reproduce the recovery obtained when the entire N-terminal coding sequence was inserted.

Together, all the results from the sequential deletions starting from both the N-terminal and the C-terminal coding sequence allow us to determine the minimum core sequence of the murine XBP1 mRNA that can support an efficient splicing. The core sequence has 557 base pairs, starting in the nucleotide 243 and ending in the nucleotide 929 of the Flag.mXBP1u mRNA construct.

4.3 Role of the cellular cytoskeleton in the splicing reaction of the XBP1 mRNA

4.3.1 Analysis of XBP1 mRNA splicing after disruption of cytoskeleton components

As described in section 1.2.3 of the Introduction chapter, the active transport of RNA within the cell is mediated by cellular cytoskeleton. The proposed molecular mechanism states that the RNA binds to a motor protein, through the interaction of an RBP that promotes its transport along the cytoskeletal fibers.

Interestingly, a recent study reported that the non-muscle myosin heavy chain IIB (NMMHC IIB), a subunit of non-muscle myosin IIB (NMMIIB), interacts specifically with IRE1α under ER stress (He et al. 2012). NMMIIB belongs to the myosin II motor family, that forms contractile structures with actin filaments (Vicente-Manzanares et al. 2009), which are regulated by the phosphorylation of the Regulatory Light Chain (RLC) of the NMMIIB. These authors showed that upon ER stress the Ser19 residue of RLC is phosphorylated deriving in its activation, which is required for the correct

oligomerization and activation of IRE1α and the production of the Xbp1s transcription factor (He et al. 2012). Taking into account this observation we wondered whether the cytoskeleton may also be involved in the XBP1 mRNA transport to the IRE1α foci. Furthermore, we also wanted to evaluate the contribution of others cytoskeleton components to the splicing/transport of XBP1 mRNA. Therefore, we proceeded to evaluate if the XBP1 splicing efficiency could be affected by disruption of different cytoskeleton components.

To this end, we pre-treated HeLa cells with drugs that disrupt different components of the cellular cytoskeleton (Table 4) and measured the splicing efficiency of the human XBP1 mRNA after induction of ER stress.

Table 4 Drugs to disrupt cytoskeleton components.

Drug	Target	Mechanism of action	Reference
Blebbistatin	Myosin II	Inhibits the ATPase activity of myosin II proteins	Kovács et al. 2004
Nocodazole	Tubulin	Depolymerizes microtubules	Samson et al. 1979
Cytochalasin D	Actin	Inhibits the polymerization of actin monomers (G-actin)	Wakatsuki et al. 2001
Latrunculin B	Actin	Inhibits the polymerization of actin filaments	Wakatsuki et al. 2001
Withaferin A	Vimentin	Alters the vimentin filaments distribution	Bargagna-Mohan et al. 2007

Figure 27 shows the XBP1 mRNA splicing efficiency after destabilization of cytoskeleton components like Myosin II, tubulin, actin and vimentin. In the absent of ER stress, the disruption of any of the cytoskeleton components analyzed does not reduce the XBP1 mRNA splicing efficient when is compared to the untreated cells. But we observed a different behavior under acute ER stress.

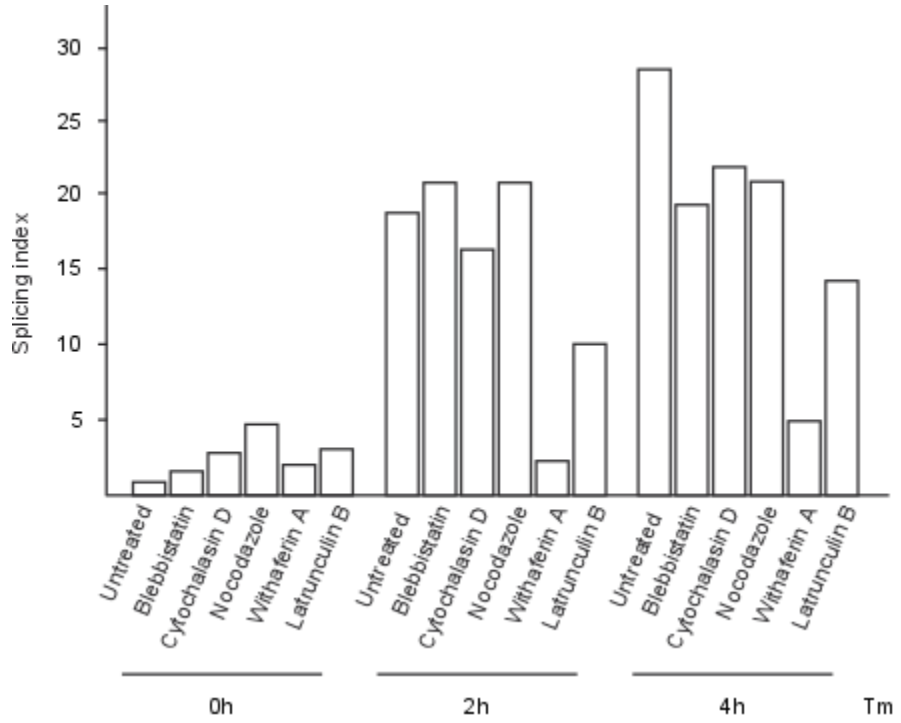

Figure 27. Contribution of cytoskeleton components on the XBP1 mRNA splicing efficiency. HeLa cells were pre-treated or not (untreated) for 3 hours with drugs that disrupt the different cytoskeleton components: Blebbistatin (50µM) inhibits the motor protein Non Muscle Myosin II; Cytochalasin D (1µM) inhibits the polymerization of actin fibers; Nocodazole (8µM) inhibits the polymerization of the microtubules fibers; Withaferin A (2µM) inhibits the secondary filaments of Vimentin; Latrunculin B (20µM) inhibits the polymerization of actin fibers. Then, the ER stress was induced by incubation with 5ng/µl of tunicamycin (Tm) for 0, 2, and 4 hours (h). Then, total RNA was isolated and the splicing efficiency of the human XBP1 mRNA was measured as described in figure 17 by quantitative PCR.

First, we found that the inhibition of the NMMIIB by incubation with Blebbistatin, which inhibited the ATPase activity of myosin II proteins (Kovács et al. 2004), did not affect the splicing efficiency (Fig.27). This result was unexpected, because previous studies showed a reduction of the Xbp1s protein expression levels in ER stressed cells after treatment with Blebbistatin (He et al. 2012).

Another work performed in yeast reported that IRE1α clusters are on or near to F-actin filaments (Ishiwata-Kimata et al. 2013). In our hands, when we disrupted the actin fibers with two different drugs we obtained divergent results. Cell treated with Latrunculin B, which inhibits the polymerization of actin monomers, reduces splicing efficiency to approximately 50% at 2 and 4 hours of induced ER stress (Fig.27). On the other hand, the incubation with Cytochalasin D, which also inhibits the polymerization of actin fibers, but by blocking the actin filament (F-filament) elongation, did not reduce the splicing efficiency (Fig.27). This different effect could

be due to the fact that Latrunculin B is 10-100 times more effective than Cytochalasin D (Wakatsuki et al. 2001).

We observed that the XBP1 mRNA splicing slightly increased in physiological ER stress conditions when the Tubulin cytoskeleton was disturbed by treatment with Nocodazol, whereas no effect was observed at later times of ER stress (Fig.27).

Interestingly, when we inhibited the intermediate filaments of vimentin by incubation with Whitaferin A, which altered the vimentin filaments distribution (Bargagna-Mohan et al. 2007) the splicing efficiency of the XBP1 mRNA was dramatically reduced by more than 80%, compared to the untreated cells (Fig.27). This result was very surprising, because vimentin has not been related before with UPR and XBP1 splicing. These results suggest that actin and vimentin fibers could be involved on the splicing/transport of the XBP1 mRNA upon ER stress.

4.3.2 Co-visualization of IRE1α protein and cytoskeleton fibers

The observation that the intact actin vimentin cytoskeletal networks were necessary to sustain XBP1 splicing under acute ER stress suggested that these cytoskeletal components could participate in the formation of IRE1α splicing center or in the recruitment of XBP1 mRNA transport to them. If that was the case, IRE1 α foci should be spatially related to these fibers. To assess this point, we visualized IRE1α and the cytoskeletal components under normal and stress conditions.

To visualize human IRE1 α, we cloned a recombinant version of the protein bearing an internal monomeric eGFP tag. The design of the IRE1α-eGFP fusion protein was based in the previous work published by Li et al. 2010. Specifically, the coding sequence for the eGFP fluorescent protein was inserted between the sequences encoding for the transmembrane and the kinase domain (Fig.28A). We demonstrated that the IRE1α-eGFP undergos XBP1 splicing similarly to the WT construct (data not shown). Under non ER stress conditions IRE1α-eGFP was evenly distributed diffusely throughout the ER; however, upon thapsigargin treatment, a strong inducer of ER stress, IRE1α-eGFP foci were detected (Fig.28B). As shown before, in a time course experiment where cells were treated with tunicamycin, the splicing of XBP1 mRNA nicely paralleled the formation of IRE1α -GFP foci (data not shown).

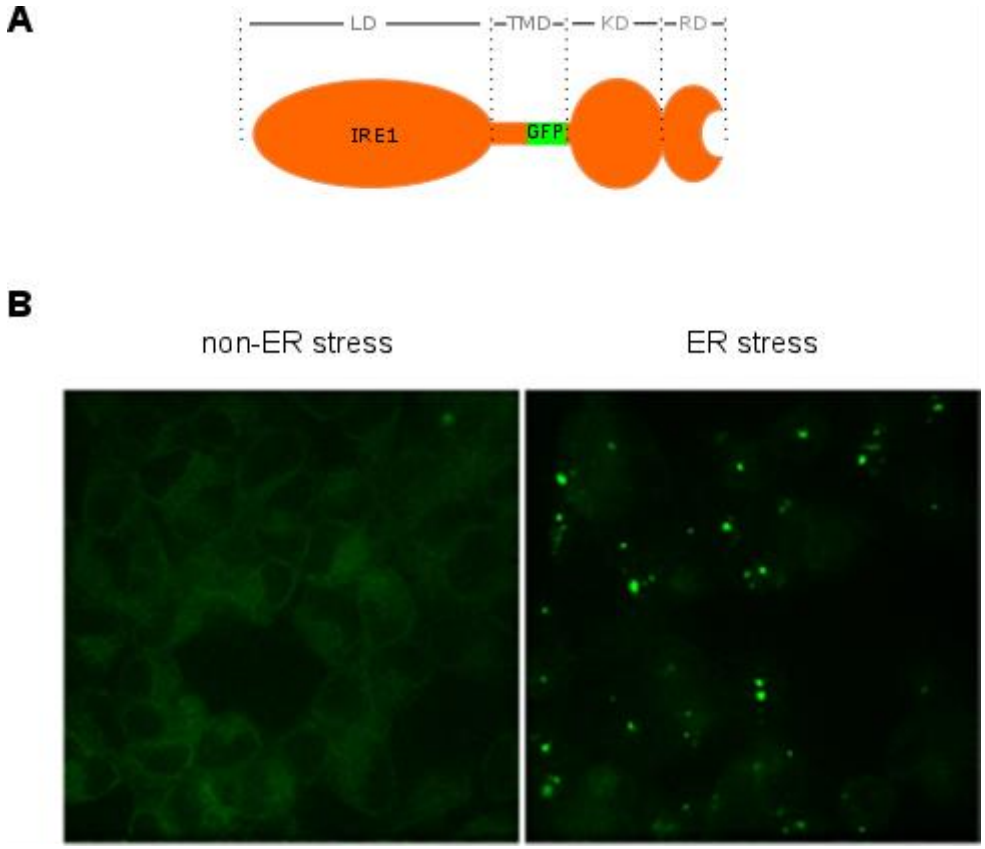

Figure 28. Fluorescent IRE1α-eGFP fusion protein. A) Schematic representation of the human IRE1α fused with the fluorescent protein eGFP. The Luminal Domain (LD), Transmembrane Domain (TMD), Kinase Domain (KD) and RNAse Domain (RD) are indicated. B) Confocal images of Flp-in HEK-293 cells stable expressing the IRE1α_eGFP construct in the absence and presence of ER stress induced by incubation with thapsigargim (Tg) for 0 and 4 hours, respectively.

To co-visualize IRE1α foci and cytoskeletal fibers, HeLa cells were transiently transfected with IRE1α-eGFP. 24 hours after transfection ER stress was induced by incubation with thapsigargin for 2 hours. Then, cells were fixed with paraformaldehyde and IRE1α-eGFP fusion protein and the cytoskeleton fibers were detected by immunofluorescence.

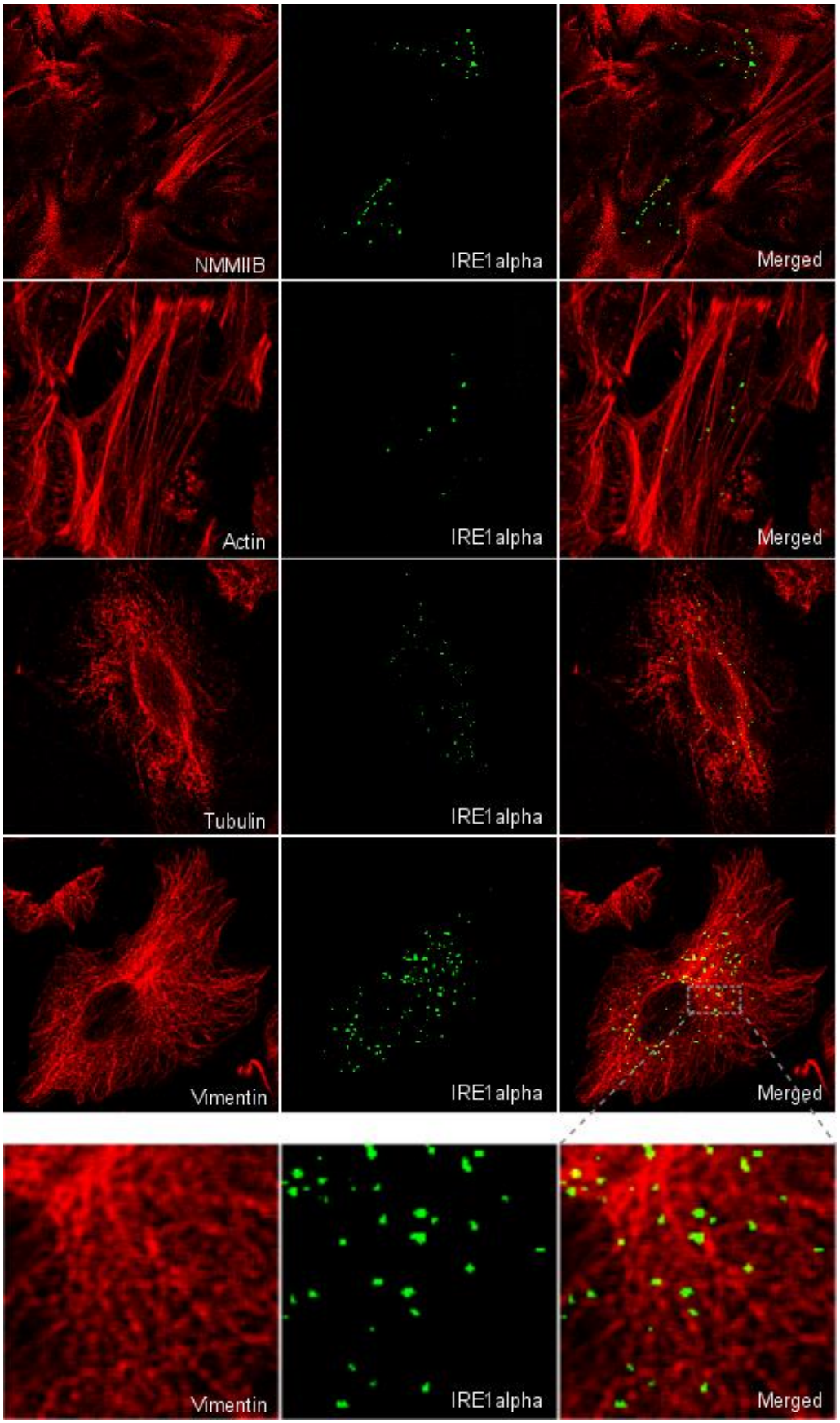

Figure 29. Co-visualization of IRE1α clusters and cytoskeletal fibers. Confocal stack images of cytoskeleton fibers of actin, tubulin, non-muscle myosin IIB (NMMIIB), and vimentin together with

IRE1α-eGFP fusion protein upon ER stress induced with 1μM of thapsigargin for 2 hours. The expression of IRE1α-eGFP fusion protein was induced by incubation with 10 ng/ml of doxycycline (Sigma) for 16 hours.

The visualization of IRE1α clusters together with different cytoskeletal fibers by confocal microscopy is shown in Fig. 29. Immunofluorescence analysis of non-muscle myosin and actin showed that both components were detected almost exclusively in stress fibers, which are bundles of actin filaments anchored at sites of cell attachment to the culture dish surface, and constitute the same actin structure that participates in focal adhesions. To our surprise, IRE1α foci were observed predominantly in focal planes where actin or NMMIIB could not be visualized.

When co-visualized with tubulin or vimentin fibers, IRE1α clusters seem to assemble in close vicinity to vimentin fibers or, to a lower extent, to microtubules. The co-localization of IRE1α and vimentin/tubulin fibers is apparent after ER stress is induced, while a weak co-localization was observed under non-ER stress conditions (Fig.30).These observations, together with the effect of Withaferin A in XBP1 splicing suggest that vimentin fibers could provide a path for the XBP1 mRNA to reach IRE1α foci. Still, these evidences are preliminary and a more detailed, quantitative analysis of this co-localization would be necessary to draw solid conclusions.

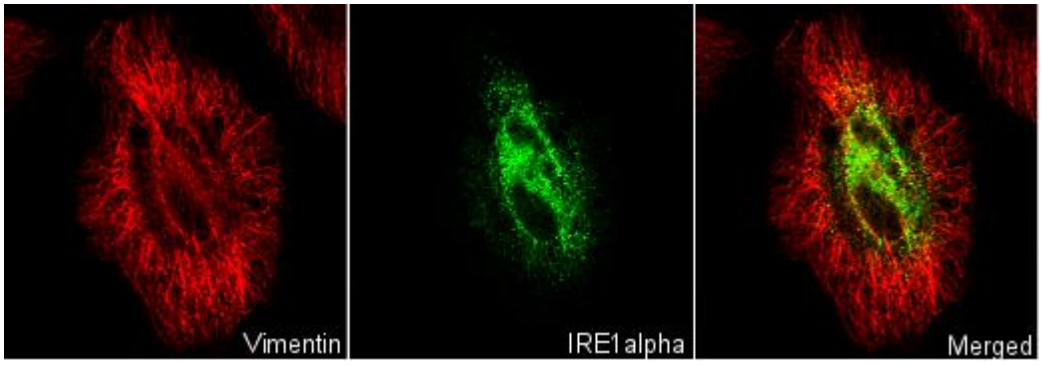

Figure 30. IRE1α and vimentin do not colocalize under non-stress conditions. Confocal stack images of Vimentin together with IRE1α_eGFP fusion protein upon non-ER stress conditions.

4.3.3 Co-visualization of XBP1 mRNA and cytoskeleton fibers

When confirmed, the co-localization between IRE1α and vimentin fibers would support a working hypothesis, whereby vimentin filaments could function as a path

through which unspliced XBP1 mRNA could be transported directly to splicing centers under ER stress conditions. This is a surprising concept because there is very limited evidence documenting the transport of mRNAs through intermediate filaments. Still, recent work from the Stefanovic group has established the importance of vimentin fibers in the regulation of collagen mRNA stability and translation (Challa & Stefanovic 2011).

To test if unspliced XBP1 mRNA molecules could be transported through vimentin fibers, we combined the Fluorescent in Situ Hybridization (FISH) and immunofluorescence techniques. To this end, HeLa cells treated with thapsigargin for 2 hours were fixed. XBP1 mRNA particles were labeled using Quasar570-conjugated specific primers against human XBP1 mRNA. Simultaneously, the vimentin filaments were immunodetected and labeled with Cy3 fluorescent-conjugated antibodies. As a control cytosolic mRNA we visualized GAPDH mRNA.

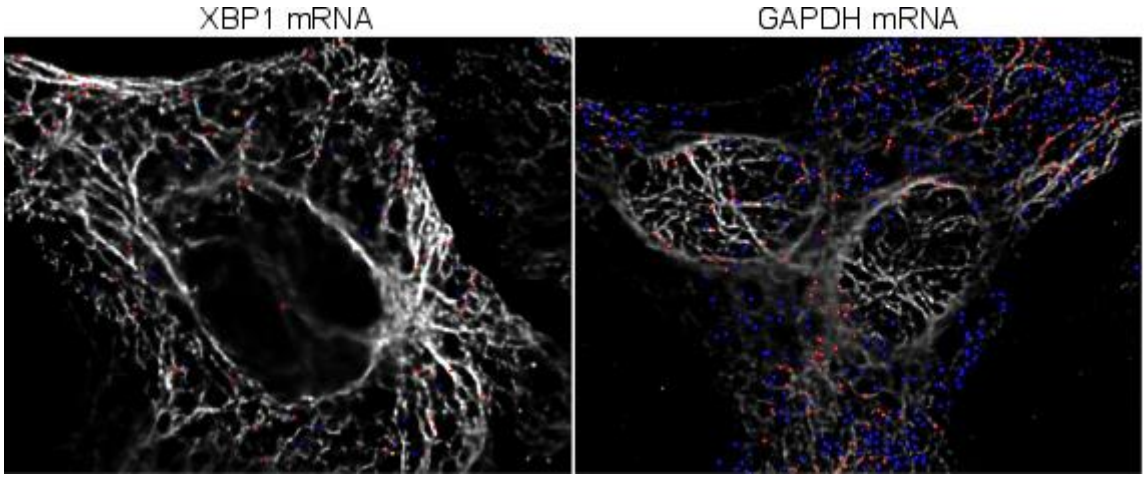

Figure 31. Co-visualization of XBP1 mRNA with vimentin filaments. Hela cells treated with 1μM of thapsigargin for 2 hours to induce ER stress were used for detection of XBP1/GAPDH mRNA together with vimentin filaments. RNAs particles that co-localized with vimentin fibers are shown in red colour, while non-colocalized RNAs are represented in blue colour.

In figure 31, XBP1 mRNA particles co-localizing with vimentin fibers are represented in red color, while non-colocalizing RNA particles are shown in blue. We observed that although not all RNA particles co-localized with the vimentin filaments, the fraction of XBP1 mRNA particles co-localizing with vimentin on the vimentin filaments was much higher than the one observed in the control, GAPDH mRNA (Fig.31). Because the oligonucleotide probes used cannot distinguish between the

unspliced and spliced XBP1 mRNA, we cannot rule out the possibility that vimentin filaments interact specifically with either the spliced or unspliced XBP1 mRNA. As the methodology to co-visualize endogenous XBP1 mRNA and cytoskeletal fibers has been established we will explore in greater detail the importance of this preliminary finding.

4.4 Studying the molecular mechanism of the *HAC1* mRNA recruitment by Ire1p

The *HAC*1/XBP1 splicing reaction mediated by Ire1p is conserved in all eukaryotic cells. Although different models of *HAC1*/XBP1 mRNA transport have been proposed for yeast and mammalian cells, they share some common features. Deepening in the molecular mechanism that governs the unconventional splicing of *HAC1*/XBP1 mRNA helps to understand this regulatory mechanism of the UPR and its evolution from yeast to mammalian cells.

In *Saccharomyces cerevisiae*, ER stress triggers the clustering of Ire1p molecules into a discrete number of foci. From these sites, Ire1p recruits *HAC1* mRNA through a conserved element located at the 3' untranslated region of *HAC1* mRNA, known as 3' bipartite element (3'BE) (Aragón et al. 2009). As shown in Figure 32A, deletion of *HAC1* 3'BE results in the disruption of the co-localization between *HAC1* mRNA and Ire1p in foci.

Our collaborators from the group of Dr. Eelco van Anken (San Raffaele Scientific Institute, Italy) recently identified by mutational analysis, a domain within Ire1p that is necessary and sufficient to recruit *HAC1* mRNA to Ire1p foci. The recruiting moiety consists of a conserved aminoacid stretch at the Ire1p linker domain, the part of Ire1p connecting the transmembrane and the kinase domains, that is highly enriched in positively charged aminoacids; therefore, it was named the [+]-box domain. At its core, the[+]-box domain contains an RGG domain (RGNRGG) flanked by acidic aminoacids. Point mutations in these glycine and arginine residues disrupts RNA recruitment but do not affect Ire1p clustering (van Anken et al. 2014). Along the same lines, the [+]-box sequence is required for the *HAC1* mRNA recruitment to Ire1p foci (Fig.32B).

Interestingly, an Ire1p mutant only containing the [+]-box domain at its cytosolic side (lacking the Kinase and RNAse domains (ΔKR)), could efficiently recruit a recombinant *PGK1* mRNA variant, bearing only the 3'BE element from *HAC1*. Thus, the [+]-box domain/3'BE element pair are the minimal components that completely determine *HAC1* mRNA targeting to Ire1p foci. Our immediate goal is to identify how such recruitment works.

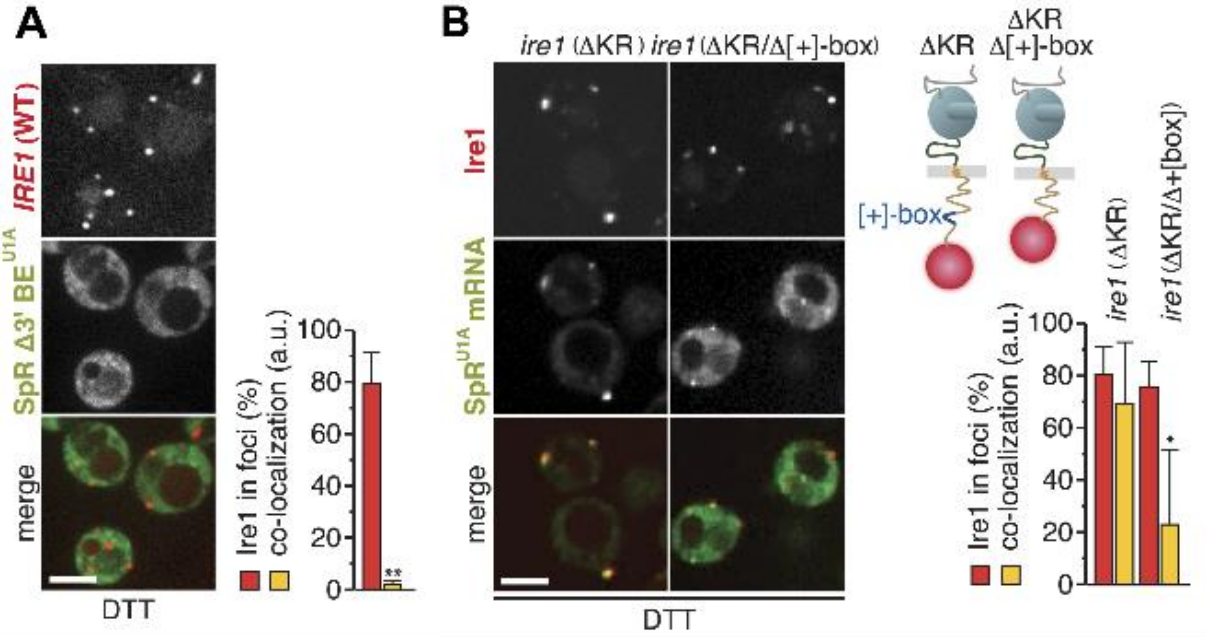

Figure 32. Ire1p /*HAC1* mRNA *cis*-elements that mediate their encounter. A) Localization of Ire1p and *HAC1* mCherry-tagged Ire1p and splicing reporter (SpR) Δ3′ BE^{U1A} mRNA decorated with U1A–GFP. ER-stress was induced with 10mM DTT for 45 minutes. Scale bar represents 5 µm. Co-localization index for mRNA recruitment into foci (mean and s.e.m., n = 10) (right). Statistical significance of the difference in mRNA recruitment of SpR Δ3′ BE^{U1A} was tested using a Student's t-test (**p ≤ 0.01). B) Localization of Ire1–GFP or Ire1–mCherry and of U1A–GFP decorated SpRU1A mRNA. Imaging was performed in Ire1 Δ yeast complemented with a genomic copy of C-terminally mCherry-tagged (ΔKR) or (ΔKR/Δ[+]-box) Ire1 mutant alleles, as schematically shown (B top right), or with plasmids encoding Ire1 WT. Scale bars represent 5 µm. Bar diagrams depict the percentage of Ire1 signal in foci (red bars) and the co-localization index for mRNA recruitment into foci of Ire1 variants (mean and s.e.m., n = 5–10).

The accumulation of positively charged aminoacids in the [+]-box domain could serve as an RNA binding domain, and therefore contribute to the docking of incoming *HAC1* mRNA molecules. Alternatively, the [+]-box domain may not only provide the RNA affinity to dock Ire1 substrate mRNA, but also could engage in the transport itself. To elucidate at which level the [+]-box domain is working, we designed a synthetic tethering mechanism to test if this artificial mechanism overrules the requirement of a functional 3'BE.

We reasoned that if the [+]-box is a docking determinant, it could be functionally bypassed by the artificial tethering of *HAC1* mRNA to Ire1p. To implement an artificial tethering, we inserted 16 repeats of a U1A binding site in the 3´UTR of *HAC1* mRNA (*HAC1*^{U1A} mRNA) and a U1A-RNA binding module into Ire1 kinase domain (Ire1-U1A), which docks to the U1A binding site (Brodsky & Silver 2000) (Fig.33).

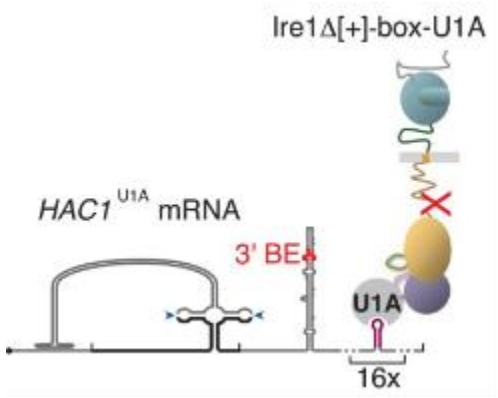

Figure 33. Schematic representation of mRNA docking 'bypass'. The U1A module placed in the αF–αEF loop of Δ[+]-box mutant Ire1 facilitates binding of *HAC1*^{U1A} mRNA via its 16 (16X) repeats of U1A motifs.

As shown in Figure 34 the insertion of the U1A-RNA binding module reduces *HAC1* splicing, but still maintains high splicing rates that support the growth of cells under stress (Fig. 34). The fusion protein Ire1-U1A can then associate to *HAC1*^{U1A} mRNA.

As previously demonstrated, deletion of the [+]-box domain blocks *HAC1*^{U1A} mRNA splicing and thereby cells could not survive in the presence of tunicamycin. However, *HAC1*^{U1A} splicing was partially rescued by the insertion of the U1A module in Ire1p, demonstrating that the artificial tethering was able to functionally compensate the [+]-box deletion (Fig.34). This evidence support a docking mechanism as proposed above.

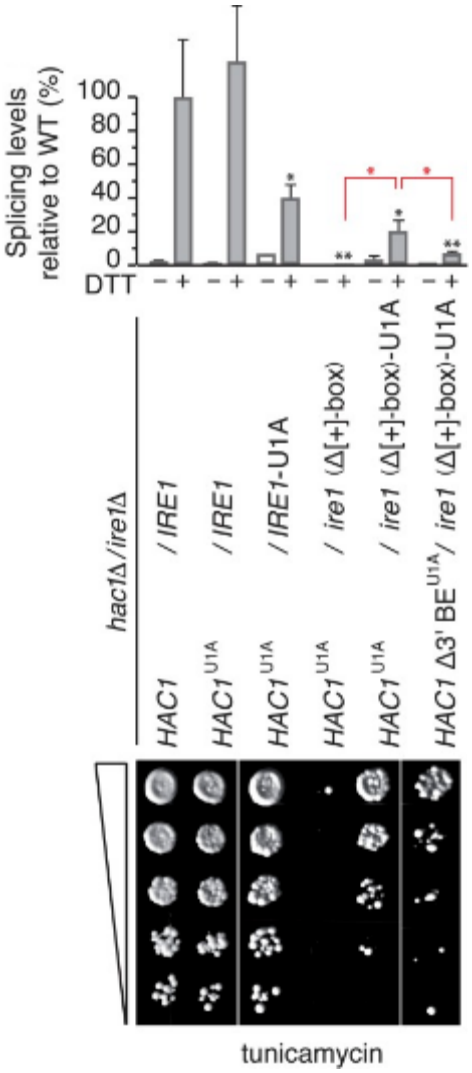

Figure 34. Step-wise docking of mRNA is a pre-requisite for activating Ire1p. **Top**, Splicing was measured by quantitative RT-PCR before or after ER-stress induction with 2mM DTT for 30 minutes. For display of RT-PCR results, the signal for *HAC1*Δ/Ire1Δ yeast complemented with WT *HAC1* and Ire1 under ER-stress conditions was set at 100%; mean and s.d. (n = 2) are shown. Statistical significance in a Student's t-test of differences in splicing levels as compared with WT is indicated in black and of differences in splicing levels compared with the 'bypass' (*HAC1*^{U1A}+ Ire1 Δ[+]-box-U1A) is indicated in red (*p ≤ 0.05; **p ≤ 0.01). **Bottom**, viability assay under ER-stress conditions (0.2 µg ml^{-1} tunicamycin) of *HAC1*Δ/Ire1Δ yeast complemented with centromeric plasmids bearing WT Ire1p or Δ[+]-box mutant Ire1 either untagged or tagged with the U1A module in the αF–αEF loop, as well as with centromeric plasmids bearing WT *HAC1*, *HAC1*^{U1A}, or *HAC1 Δ3' BE*^{U1A} . Serial dilutions of yeast cultures were spotted on YPD plates supplemented with tunicamycin and grown for at least 48 hours at 30ºC.

If the sole role of the [+]-box domain is to dock the 3'BE element, the double [+]-box/3'BE mutant should be rescued by U1A tethering as efficiently as the single [+]-box deletion mutant, while rescue should be less efficient if the 3'BE element contributes to RNA recruitment by other targeting mechanism. The results in Figure

34 suggest that beyond the docking of *HAC1* mRNA to foci, the 3'BE may constitute a targeting element that functions at earlier steps than docking.

5. DISCUSSION

XBP1 mRNA associates with the ER membrane.

The non-conventional XBP1 mRNA splicing reaction performed by the endonuclease IRE1 is a key step in the activation of the Unfolded Protein Response. Since IRE1 is an ER-resident protein, XBP1 mRNA splicing must initiate on the cytosolic surface of the ER. Previously, (Yanagitani et al. 2009) had shown that unspliced XBP1 (XBP1u) mRNA is pre-associated to the ER membrane under non-ER stress conditions. However, the biochemical definition of such association was not clear/quantitative enough: By employing a detergent extraction method and velocity sedimentation the authors found that the majority of the XBP1u mRNA was bound to the membrane fraction, but they could not quantify the extent of XBP1u mRNA membrane association, because they obtained an imperfect separation of the cytosolic and membrane fractions (Yanagitani et al. 2009). In this study, we aimed to quantify the percentage of XBP1u mRNA associated to membranes by using a different biochemical approach based on the work published by Mechler & Vassalli in 1975, where membrane components were efficiently separated from cytosolic contents by "floatation" in a discontinuous sucrose density gradient. Our results show that approximately 40% of the unspliced XBP1 mRNA (XBP1u) is associated to membranes under physiological conditions. In contrast, the spliced XBP1 (XBP1s) mRNA displays a low (10%) extent of association to membranes, similar to histone mRNA or other typically cytosolic transcripts (Fig. 15). This result is consistent with independent studies where the association of XBP1 mRNA to membranes was found significantly increased in the membrane-bound transcriptome (Diehn et al. 2000). Additionally, we found that after induction of acute ER stress, membrane association of XBP1 mRNA is not significantly reduced. This evidence suggests that the delivery of XBP1u mRNA to the ER membrane may be constantly maintained under stress conditions. An alternative explanation is that the fraction of XBP1u mRNA associated to membranes under ER stress conditions could represent a pool of unspliced mRNA molecules that fails to be spliced. In line with this possibility, data from the group of Dr. Peter Walter demonstrated in yeast that a fraction of unspliced *HAC1* mRNA is not processed under ER stress conditions.

HR2-dependent targeting mechanism promotes physiological tethering of XBP1 mRNA to the ER and splicing.

Current models propose that XBP1u mRNA associates to ER membranes in a co-translational manner. The hydrophobic peptide encoded by the XBP1u mRNA open reading frame promotes the delivery of the XBP1u mRNA/ribosome/protein nascent chain ternary complex to the ER surface (Yanagitani et al. 2009). Pausing of ribosomes at the vicinity of the XBP1u stop codon – caused by the translation of a C-terminal peptide (CTR) – is necessary to stall ribosomes on the XBP1 mRNA after the HR2 peptide has been produced, thereby providing the stability to the mRNA/ribosome/nascent chain complex that supports mRNA docking to membranes (Yanagitani et al. 2011). We generated different XBP1 mutants unable to produce the HR2 peptide by inserting either premature STOP codons upstream the HR2 coding sequence or by nucleotide insertions in different positions before the HR2 coding sequence. These mutants efficiently disrupted XBP1u mRNA membrane association (Fig.17&19). Furthermore, the strong correlation between membrane association and XBP1 splicing indicates that at least under non-ER stress conditions HR2 mediated membrane association allows the efficient XBP1 mRNA/IRE1 encounter.

Among all the mutants used to challenge the co-translational targeting model, there was a single XBP1 mutant where the positive correlation between basal splicing and membrane association was lost. The FS (+1) int repaired mutant bears a one-nucleotide insertion within the XBP1 intron and compensatory mutations downstream the intron to restore the HR2 open reading frame (Fig.16). While this mutant was efficiently associated to membranes, its basal splicing was strongly inhibited (Fig. 17). One possibility is that the mutation affects the recognition and/or the catalysis of cleavage by IRE1. However, this mutant RNA was cleaved as efficiently as the WT substrate *in vitro* by recombinant purified RNA (Fig.21). Also, under acute ER stress conditions it was well spliced (Fig.19). These evidences suggest that under basal splicing conditions the requirement for splicing are different than under ER stress, and that alterations in the intron structure/conformation could differently affect splicing under normal and stress situations.

The FS (+1) int mutation may interfere with either the transport of XBP1 mRNA to IRE1, in an HR2-independent mode, or with the ligation of the resulting

exons after cleavage. This latter hypothesis seems counterintuitive, because the frameshifting mutation is within the intron, which should be released after splicing, and therefore should not affect exon ligation. However, a recent report demonstrated that after excision of the XBP1 intron, an RNA-intrinsic conformation change occurs, causing the release of the intron and the pairing of the exons to form an extended stem that facilitates ligation (Peschek et al. 2015). One formal possibility is that the FS (+1) int mutation could interfere with the structural re-arrangements of XBP1 intron after cleavage and thereby impede the completion of XBP1 splicing.

A recent work from Plumb and colleagues (Plumb et al. 2015) proposes that HR2-mediated XBP1 mRNA membrane targeting is facilitated by the Signal Recognition Particle (SRP) complex. A peptide domain located in the luminal portion of IRE1 interacts with the Sec61α subunit of the translocon under basal and ER stress conditions. According to these observations, SRP components are needed to bring XBP1 mRNA to the translocon thereby facilitating the splicing of XBP1 mRNA, but also the processing of IRE1 RIDD substrates (Plumb et al. 2015). Most RIDD targets encode proteins with a signal sequence at their N-terminus, which is necessary for their degradation by the RIDD pathway (Hollien & Weissman 2006); thus, IRE1 could stay linked to the translocon as a sentinel to check the load and folding of polypeptides as they are translocated in the ER, and the SRP targeting complex could be the vehicle to deliver these mRNA to the translocon.

Interestingly, the yeast ortholog of XBP1, *HAC1* mRNA, is also bound by SRP54 (del Alamo et al. 2011) suggesting that SRP54 may play a conserved role in XBP1/*HAC1* processing. However, unpublished data from our group indicate that deletion of yeast SRP54 does not affect *HAC1* mRNA splicing. Also in opposition to the idea that SRP54 transports XBP1 mRNA to the ER, SRP54 knock-down in human cells induces an increase in XBP1 splicing. These observations are surprising and suggest that redundant mechanisms may operate to warrant UPR splicing.

HR2 translation is dispensable for splicing under acute ER stress conditions.

Under acute ER stress, XBP1u mutants unable to produce the HR2 peptide, were spliced with comparable efficiencies to the WT mRNA (Fig.19), indicating that HR2-independent mRNA targeting mechanisms must operate under acute stress. This observation is supported by earlier findings from other groups: **1)** A luciferase

ER stress reporter where the luciferase coding sequence was under the control of the XBP1 intron (only the spliced form of the XBP1-LUC mRNA would be translated into luciferase protein) was constructed with a minimal XBP1 sequence lacking the HR2 peptide. Even when the quantitative data were not comprehensive, this construct seemed to be efficiently spliced (Iwawaki & Akai 2006). This reporter system was adapted to generate a transgenic mouse model that documents ER stress *in vivo* (Iwawaki et al. 2004). **2)** Using a similar logic, a XBP1u mRNA reporter construct without the HR2 coding sequence was used in a synthetic biological approach to identify RtcB ligase as the enzyme responsible of the junction of the XBP1 exons after the splicing reaction in mammalian cells (Lu et al. 2014). The fact that UPR catalytic components could be identified by means of an HR2-deficient RNA construct demonstrates that this minimal XBP1u mRNA element was sufficient to be recruited by IRE1. **3)** In the fruit fly *Drosophila melanogaster,* elimination of the 3′ exon of XBP1u encoding the C-terminal half of XBP1u protein (that includes the HR2 peptide) did not affect splicing rates of a mutant mRNA (Coelho et al. 2014). **4)** While most IRE1 substrate RNAs encode proteins, IRE1 is also capable of recruiting and processing a subset of miRNA precursors (Upton et al. 2012). Under ER stress, IRE1 processes a subset of miRNAs that specifically repress the translation of caspase-2 mRNA, thereby triggering their rapid decay (Upton et al. 2012). The selective decay of these non-coding RNAs demonstrates that there must be a mechanism to recruit RNAs to IRE1 in a translation-independent manner. Together with the results presented here, this body of evidence supports the notion that while the transport of XBP1 to the ER membrane can occur through the HR2 sequence, HR2-independent targeting modes account for efficient splicing rates.

From an evolutionary perspective, the targeting principles that operate in yeast could be conserved in higher eukaryotes. As described in this work, yeast IRE1 recruits the *HAC1* mRNA by means of a conserved targeting element at the 3′ untranslated region of the mRNA, requiring also the translational repression of its translation imposed in *cis* by the intron-5′UTR pairing (Aragón et al. 2009). It is tempting to speculate that the targeting mechanism could be conserved from yeast to human, where the translational repression could be enforced *in trans* by PERK, which reduces overal translation. Even when we observe significant differences

between yeast and metazoan UPR mechanisms, we will explore in the future if the main mechanistic principles are conserved.

A new conformation for XBP1 intron?

Along these lines, our structural studies predicted the existence of two different intron conformations (Fig.23) that could be involved in regulating the splicing reaction. The *in vitro* SHAPE data are consistent with a structural model where splice sites are not folded as expected. In order to test this prediction, we have generated intron mutants that forced either the canonical or non-canonical conformation of XBP1 intron (data not shown). Since the non-canonical conformation cannot be recognized by IRE1 to be cleaved, we could only monitor the splicing of the canonical "forced" mutant; this mutant underwent efficient splicing, so in principle our alternative conformation may not occur *in vivo* or be functionally relevant. Unfortunately, these mutants were generated in a XBP1 construct able to produce the HR2 peptide and therefore cannot exclude the possibility that this alternative conformation could contribute to targeting in an HR2-independent mode.

We postulate that the FS (+1) int mutation disrupts XBP1 mRNA transport to IRE1 foci *in vivo*, a step that *in vitro* cleavage experiments (in solution) could not recapitulate. In support to this idea, restoration of HR2 synthesis in mutants bearing the FS (+1) int mutation rescued the splicing efficiency of these mutants, demonstrating that this mutation participates in processes other than catalysis. A structural analysis of this mutant, and the identification of possible targeting factors bound to WT XBP1 intron will help to establish its role in the encounter with IRE1.

Why two different/redundant targeting mechanisms?

XBP1 mRNA splicing and IRE1 protein clustering are dramatically different under normal and stress conditions, indicating that UPR signaling may be wired differently to produce responses of different amplitude and properties. In line with this notion, it was first described that IRE1 becomes competent to process *HAC1*/XBP1 mRNA only after assembly in high order structure oligomers (Korennykh et al. 2009). However, a recent report demonstrated that the organization into multimers is not necessary for RIDD RNA turnover (Tam et al. 2014). This observation is in agreement with reports describing that RIDD is constitutively active and its intensity

increases progressively until the cell dies due to excessive stress, while the XBP1u mRNA splicing is only transiently activated upon ER stress induction (Maurel et al. 2014).

Our results show clearly that the co-translational targeting model is key to ensure basal splicing and dispensable under ER stress. These observations fit with the dramatic re-localization of IRE1 under the experimental conditions used in our study (Li et al. 2010). Putting together our results and the observations from the above studies, we propose that the transport of XBP1u mRNA in the physiological state, when IRE1 is dispersed through the ER membrane, occurs in a co-translational manner and requires SRP-mediated targeting to the ER. This transport mechanism could also apply to RIDD substrates under ER stress. In contrast, under acute ER stress, IRE1 dissociates from the translocons to assemble into high-order foci at specific sites in the ER. This re-localization would have two functional consequences: **1)** IRE1 would not be in the vicinity of translocons and therefore SRP-mediated targeting of RNA would not serve to feed IRE1 protein with substrates as rapidly as needed **2)** IRE1 would polarize in sites that could recruit RNA by a mechanism different from the co-translational / SRP model.

To date, there is no evidence that HR2-mediated RNA transport could determine targeting to specific sites within the cell. This transport could be specially relevant in polarized cells, such as neurons. An increasing body of evidence demonstrated that XBP1 is stimulated by synaptic inputs (Martínez et al. 2016) where XBP1 may be localize at ER subdomains located in dendrites (Cui-Wang et al. 2012). The delivery of mRNAs to distal domains of the neuron is generally organized by cytoskeletal transport. It is tempting to speculate that HR2-independent targeting could facilitate XBP1 distribution in synaptic terminals.

In other cell types, like immune cells, activation by cytokines induces a strong acute UPR. In some cases, i.e. in the formation of the immune synapse, immune responses drive the reorganization of cytoplasmic contents into a highly polarized state (Ritter et al. 2013). Again, an HR2-independent transport could allow splicing under these conditions.

XBP1 mRNA splicing and cytoskeletal fibers.

The polarization of IRE1 molecules into a discrete number of ER foci under stress poses a targeting problem: How can unspliced XBP1 mRNA molecules find the location where IRE1α concentrates. A number of studies have identified cytoskeletal relays to direct the transport of mRNAs to polarized sites inside the cell (Bullock 2007, Bookwalter et al. 2009, Chao et al. 2010). In the case of IRE, there are several evidences linking IRE1 to cytoskeletal components under ER stress conditions. **1)** ER stress induces phosphorylation of the regulatory light chain of non-muscle myosin II (NMMII). The phosphorylation of the RLC enables the interaction of the non-muscle myosin heavy chain IIB (NMMIIB) with IRE1 only under acute ER stress, which is required for IRE1 oligomerization and for the production of proportional levels of the Xbp1s transcription factor (He et al. 2012). The interaction of IRE1α with NMMIIB is essential to ensure the stability of IRE1 foci. **2)** In yeast, deletion of MYO1, a gene that encodes the class-II myosin heavy chain, impairs IRE1 clustering under ER stress conditions (Ishiwata-Kimata et al. 2013); however this deletion does not seem to reduce *HAC1* splicing. Furthermore, a recent study performed in *S. cerevisiae* found that the (He, Beatty, Han, Ji, Ma, Robert S. Adelstein, et al. 2012)paralogue kinases Kin1 and Kind2 promote *HAC1* mRNA targeting, splicing, and translation via the 3´BE (Anshu et al. 2015), suggesting that the 3´BE could recruit RBPs that promote *HAC1* mRNA targeting and splicing. Kin kinases share identical domain organization with the microtubule affinity-regulating kinase (MARK) in mammals, which participates in the regulation of tubulin cytoskeleton (Tassan & Le Goff 2004). These observations indicate that ER stress activates cytoskeletal components in order to warrant the polarization of IRE1 and the recruitment of mRNA to build robust responses to ER insults. We postulate that cytoskeletal fibers participate in the active transport of XBP1u mRNA directly to the IRE1 clusters.

Our preliminary observations from the co-visualization of IRE1 / XBP1mRNA with some cytoskeletal fibers indicate that vimentin filaments could be spatially related with both IRE1 clusters and XBP1 mRNA under ER stress conditions, but additional biochemical evidence would be necessary to confirm this observation. Intriguingly, vimentin protein was classified as a candidate RNA binding protein in a proteome-wide, high-throughput study that identified proteins interacting with

polyadenylated RNA in human cells (Castello et al. 2012). However, intermediate filaments have not been related to mRNA transport as actin or tubulin fibers, and it is not clear how vimentin could participate in the transport/splicing of the XBP1 mRNA.

The best evidence linking vimentin cytoskeleton and RNA regulation is the role of intermediate filaments in collagen mRNA stability. Type I collagen proteins are folded co-translationally in the ER lumen, as their nascent chains are co-translationally threaded through the translocon pore. The assembly of these fibers requires that mRNAs encoding the fiber components are delivered to the ER in a coordinated manner, and therefore these mRNAs seem to be co-regulated. A 5'UTR stem loop structure in collagen mRNAs recruits the RNA binding protein LARP6, which in turn associates to non-muscle myosin and vimentin (Challa & Stefanovic 2011) (Challa & Stefanovic 2011; Zhang & Stefanovic 2016). The experimental evidence published indicates that such association accounts for the stability of collagen mRNAs and, possibly, for the partitioning of these mRNA at the ER. Taking into account this precedent, we consider it possible that vimentin is also involved in the stabilization of the XBP1 mRNA. In fact, another study done in fibroblast cells reported that spliced XBP1 mRNA is stabilized within the first 3 hours after induction of ER stress in a process that depends on IRE1α splicing and the block in translation produced by eIF2α phosphorylation (Majumder et al. 2012). Among the future directions we will examine the stability of either HR2-deficient XBP1 mutants or our deletion nonfunctional mutants.

HAC1 mRNA transport. Targeting or Anchoring?

In collaboration with Dr. Eelco van Anken we found and characterized the domain of yeast Ire1p protein required to recruit *HAC1* mRNA to Ire1p foci. This domain motif enriched in positively charged amino acids, called the [+]-box sequence, is within the linker cytosolic domain of Ire1p. In particular, the [+]-box sequence contains a conserved arginine-glycine-glycine (RGG) motif, repeats of which can be found in several RNA binding protein families, including snRNPs, hnRNPs, and snoRNPs (Godin & Varani 2007; Thandapani et al. 2013). Thus, it seems likely that the [+]-box sequence interacts directly with *HAC1* mRNA. Our results demonstrate that the [+]-box sequence docks the *HAC1* mRNA to the Ire1p clusters mRNA under ER stress, presumably through a direct interaction between the

RGG motif and *HAC1* mRNA. RGG motifs typically have a low affinity for RNA, which is why they are normally repeated in the RBP domains (Godin & Varani 2007). Therefore, monomeric Ire1p may not display sufficient affinity to recruit *HAC1* mRNA, while ER stress-induced Ire1p oligomerization could cluster RGG motifs from multiple monomers, thereby increasing the avidity for *HAC1* mRNA and explaining the selective recruitment of *HAC1* mRNA to the Ire1p only under ER stress (Aragón et al. 2009). The RGG motif is conserved in Ire1 linker domain from different yeast species, but it could not be identified in metazoans such as *Drosophila melanogaster*, *Caenorhabditis elegans* and *Homo sapiens* (van Anken et al. 2014), suggesting that alternative recruitment/docking mechanisms may exist in higher eukaryotes.

In yeast, a *cis*-acting sequence called the 3´-bipartite element (3´BE) mediates the recruitment of the *HAC1* mRNA to the Ire1p clusters under ER stress conditions (Aragón et al. 2009). The [+]-box is sufficient to recruit an heterologous mRNA containing the 3′BE, indicating that these two minimal components determine UPR mRNA targeting. Now, the question is to understand the mechanism of engagement.

The easiest model is that the *HAC1* mRNA could diffuse through the cytosol and specifically associates to [+]-box assemblies whenever Ire1p was clustered. Then the [+]-box domain may only facilitate RNA docking. We have not performed *in vitro* or *in vivo* experiments to determine the RNA binding capacity of the [+]-box element or its specificity for the *HAC1* mRNA. Unpublished experiments from the group of Dr. Peter Walter suggest that the [+]-box domain could bind RNA in a non-specific manner and that such association could enhance Ire1 RNAse activity. Still, if recruitment was only dependent on docking, we would expect that the artificial docking of *HAC1* mRNA to Ire1p could bypass such recruitment.

However, the U1A-mediated synthetic tethering of *HAC1* mRNA and Ire1p demonstrated that the 3′ BE contributes to *HAC1* mRNA splicing efficiency even when an artificial tether has been provided (Fig.34), indicating that 3′ BE could be needed for targeting steps preceeding docking.

We propose a model where *HAC1* mRNA transport to foci could be staged in steps. Firstly, the 3´BE sequence located on the *HAC1* 3'UTR could be recognized by an RBP and direct, either by itself or by promoting the binding of other RBPs, the transport of *HAC1* mRNA through the cytoplasm to the ER membrane subdomains

where Ire1p is located. Indeed, similar mechanism principles have been described for the targeting of the *ASH1* mRNA to the bud tip in yeast (ASH could be the paradigm for most cytoskeleton-driven transport) (Beach & Bloom 2001). Secondly, once there, the RGG motifs of the active Ire1p cluster may induce the anchoring of the *HAC1* mRNA in place, as a previous step of the splicing reaction.

In mammalian cells, the RGG motif is not present on the cytosolic Ire1p domain and no *cis*-acting elements have been identified in XBP1u mRNA. However, a systematic mutational analysis allowed us to identify of a minimal XBP1u mRNA sequence sufficient for efficient splicing (Fig.25). Additionally, we identified two RNA regions located 5´ and 3´ of the intron sequence that are necessary to support efficient splicing (Fig. 25&26). Thus, it would be conceivable that these elements could match up with the mammalian linker domain to provide the targeting specificity through non-conserved components, but still following the same principles found in yeast.

The coexistence of HR2-dependent targeting and a new transport mechanism.

Taking into account the main findings of this thesis work, we hypothesize that in physiological conditions, where IRE1 is mostly in a monomeric state, the co-translational model proposed by Yanagitani et al. (2009) could allow the pre-association of ~~the~~ unprocessed XBP1u mRNA/ribosomes to the ER membrane, possibly in an SRP-dependent manner. The anchoring of XBP1 mRNA to the ER membrane could allow a fast adaptation to fluctuations in the protein folding status at the ER lumen. We speculate that the co-translational XBP1 mRNA transport could use the same mechanism as RIDD substrate mRNAs. In contrast, during acute ER stress, the HR2 peptide is dispensable to undergo an efficient splicing, revealing the existence of a different transport mechanism. We reason that, given the polarization of IRE1 molecules into ER foci, this alternative mechanism promotes XBP1 mRNA transport directly to IRE1α clusters. The rearrangement of IRE1α molecules into foci is possible made in coordination with specific cytoskeletal fibers. The sequences identified in the sequence of XBP1 mRNA needed to support splicing could be recognized by RNA Binding Proteins (RBP) that engage XBP1 mRNA to cytoskeletal fibers, like vimentin (Fig.35). The existence of more than one mechanism of transport for a particular RNA has been observed previously. *In vivo* mRNA visualization

studies have shown that different transport mechanism are used for the proper localization of an mRNA, the prevalence of one of which depends on the timing and transport efficiency required (Eliscovich et al. 2013).

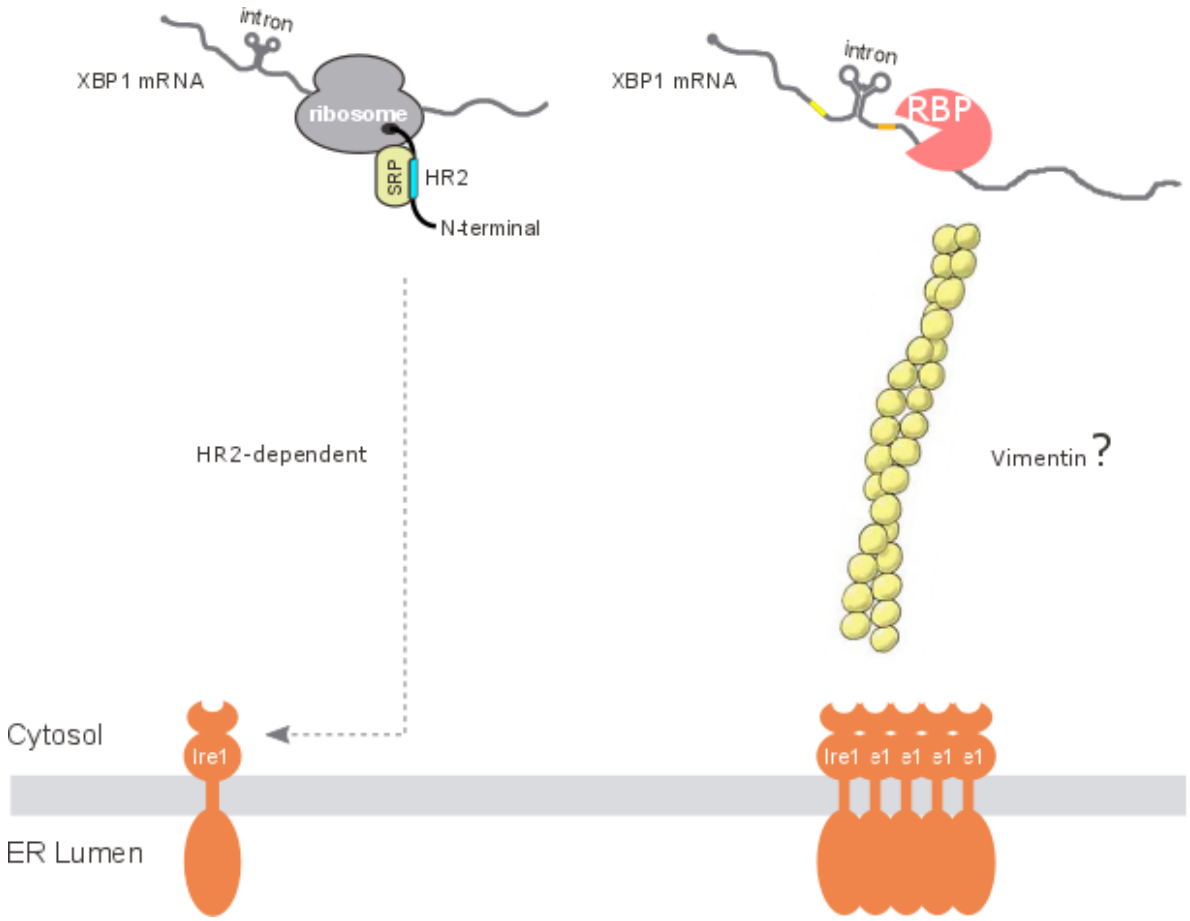

Figure 35. Proposed model for XBP1 mRNA transport to IRE1 foci.

6. CONCLUSIONS

1. Membrane floatation assays have shown that around 40% of the unspliced XBP1 mRNA is pre-associated to intracellular membranes. This association is significantly higher than that shown for the spliced XBP1 mRNA, and lower than the association observed for mRNAs transported to the ER through the signal peptide sequence. The association of the XBP1 mRNA to the ER is unaffected by ER stress.

2. XBP1 mRNA association to membranes depends on the translation of the hydrophobic peptide HR2 under non-stress conditions, which is encoded by the unspliced XBP1 mRNA.

3. In agreement with the HR2 co-translational targeting model, under non-ER stress conditions there is a strong correlation between XBP1 mRNA membrane association and XBP1 mRNA splicing.

4. The synthesis of the hydrophobic peptide HR2 is dispensable to support an efficient XBP1 splicing under acute ER stress.

5. Mutational analysis performed on the XBP1 mRNA sequence has demonstrated the existence of two additional elements, nucleotides 360 to 420 and 861 to 977 are necessary for the efficient processing of the XBP1 mRNA under acute ER stress.

6. The XBP1 mRNA splicing is sensitive to the disruption of the vimentin filaments by treatment of the drug Withaferin A. Additionally, upon ER stress conditions, the vimentin filaments seem to be spatially related with the IRE1 clusters and with the XBP1 mRNA particles. We propose that vimentin fibers could be involved in XBP1 mRNA transport to the reticulum stress response centers organized by IRE1.

7. In *Saccharomyces cerevisiae*, a 3´-untranslated region element in the *HAC1* mRNA (known as the 3´BE element,) and a stretch of positively charged aminoacids located at the liker domain of Ire1p ([+]-box sequence) are

sufficient to recapitulate the recruitment of RNA to ER stress-induced Ire1p foci.

8. The [+]-box sequence could serve as a docking site for the *HAC1* mRNA to IRE1 clusters, through the 3'BE element. Besides the docking function, tethering experiments suggest that the 3'BE is involved in targeting steps that precede docking.

7. REFERENCES

Acosta-alvear, D. et al., 2007. Article XBP1 Controls Diverse Transcriptional Regulatory Networks. , pp.53–66.

Akopian, D. et al., 2013. Signal Recognition Particle: An Essential Protein-Targeting Machine. *Annual Review of Biochemistry*, 82(1), pp.693–721. Available at: http://www.annualreviews.org/doi/abs/10.1146/annurev-biochem-072711-164732.

del Alamo, M. et al., 2011. Defining the specificity of cotranslationally acting chaperones by systematic analysis of mRNAs associated with ribosome-nascent chain complexes. *PLoS biology*, 9(7), p.e1001100. Available at: http://dx.plos.org/10.1371/journal.pbio.1001100.

An, J.J. et al., 2008. Distinct Role of Long 3´UTR BDNF mRNA in Spine Morphology and Synaptic Plasticity in Hippocampal Neurons. *Cell*, 134(1), pp.175–187.

van Anken, E. et al., 2014. Specificity in endoplasmic reticulum-stress signaling in yeast entails a step-wise engagement of HAC1 mRNA to clusters of the stress sensor Ire1. *eLife*, 3, p.e05031. Available at: http://elifesciences.org/lookup/doi/10.7554/eLife.05031.

Anshu, A. et al., 2015. A Novel Role for Protein Kinase Kin2 in Regulating HAC1 mRNA Translocation, Splicing, and Translation. *Molecular and Cellular Biology*, 35(October), pp.199–210. Available at: http://mcb.asm.org/lookup/doi/10.1128/MCB.00981-14.

Aragón, T. et al., 2009. Messenger RNA targeting to endoplasmic reticulum stress signalling sites. *Nature*, 457(7230), pp.736–740.

Aronov, S. et al., 2007. mRNAs encoding polarity and exocytosis factors are cotransported with the cortical endoplasmic reticulum to the incipient bud in Saccharomyces cerevisiae. *Molecular and cellular biology*, 27(9), pp.3441–3455. Available at: http://mcb.asm.org/content/27/9/3441.full.

Bargagna-Mohan, P. et al., 2007. The Tumor Inhibitor and Antiangiogenic Agent Withaferin A Targets the Intermediate Filament Protein Vimentin. *Chemistry and Biology*, 14(6), pp.623–634.

Barlowe, C. et al., 1994. COPII: A membrane coat formed by sec proteins that drive vesicle budding from the endoplasmic reticulum. *Cell*, 77(6), pp.895–907.

Beach, D.L. & Bloom, K., 2001. ASH1 mRNA localization in three acts. *Mol Biol Cell*, 12(9), pp.2567–77. Available at:

http://www.pubmedcentral.nih.gov/articlerender.fcgi?artid=59695&tool=pmcentrez&rendertype=abstract.

Bergsten, S.E. & Gavis, E.R., 1999. Role for mRNA localization in translational activation but not spatial restriction of nanos RNA. *Development (Cambridge, England)*, 126(4), pp.659–669.

Bernales, S., McDonald, K.L. & Walter, P., 2006. Autophagy counterbalances endoplasmic reticulum expansion during the unfolded protein response. *PLoS Biology*, 4(12), pp.2311–2324.

Bernales, S., Papa, F.R. & Walter, P., 2006. Intracellular signaling by the unfolded protein response. *Annual review of cell and developmental biology*, 22, pp.487–508.

Bertolotti, a et al., 2000. Dynamic interaction of BiP and ER stress transducers in the unfolded-protein response. *Nature cell biology*, 2(6), pp.326–332.

Bertrand, E. et al., 1998. Localization of ASH1 mRNA particles in living yeast. *Molecular cell*, 2(4), pp.437–445.

Blower, M.D. et al., 2007. Genome-wide analysis demonstrates conserved localization of messenger RNAs to mitotic microtubules. *Journal of Cell Biology*, 179(7), pp.1365–1373.

Bonifacino, J.S. & Glick, B.S., 2004. The Mechanisms of Vesicle Budding and Fusion. *Cell*, 116(2), pp.153–166.

Bookwalter, C.S., Lord, M. & Trybus, K.M., 2009. Essential features of the class V myosin from budding yeast for ASH1 mRNA transport. *Molecular biology of the cell*, 20(14), pp.3414–3421.

Brodsky, a S. & Silver, P. a, 2000. Pre-mRNA processing factors are required for nuclear export. *RNA (New York, N.Y.)*, 6(12), pp.1737–1749.

Bullock, S.L., 2007. Translocation of mRNAs by molecular motors: Think complex? *Seminars in Cell and Developmental Biology*, 18(2), pp.194–201.

Calfon, M. et al., 2002. IRE1 couples endoplasmic reticulum load to secretory capacity by processing the XBP-1 mRNA. *Nature*, 415(6867), pp.92–96.

CARO, L.G. & PALADE, G.E., 1964. PROTEIN SYNTHESIS, STORAGE, AND DISCHARGE IN THE PANCREATIC EXOCRINE CELL. AN AUTORADIOGRAPHIC STUDY. *The Journal of cell biology*, 20(9), pp.473–95. Available at: http://www.ncbi.nlm.nih.gov/pubmed/14128049.

Carrara, A.M. et al., 2014. Title : Unconventional binding of BiP ATPase domain to Ire1 and Perk is dissociated by unfolded protein C H 1 to initiate stress signaling. , pp.1–16.

Carrasco, D.R. et al., 2007. The Differentiation and Stress Response Factor XBP-1 Drives Multiple Myeloma Pathogenesis. *Cancer Cell*, 11(4), pp.349–360. Available at: http://dx.doi.org/10.1016/j.ccr.2007.02.015.

Casas-Tinto, S. et al., 2011. The ER stress factor XBP1s prevents amyloid-beta neurotoxicity. *Human molecular genetics*, 20(11), pp.2144–60. Available at: http://www.ncbi.nlm.nih.gov/pubmed/21389082.

Castello, A. et al., 2012. Insights into RNA Biology from an Atlas of Mammalian mRNA-Binding Proteins. *Cell*, 149(6), pp.1393–1406.

Cha, B.J., Koppetsch, B.S. & Theurkauf, W.E., 2001. In vivo analysis of drosophila bicoid mRNA localization reveals a novel microtubule-dependent axis specification pathway. *Cell*, 106(1), pp.35–46.

Challa, A. a & Stefanovic, B., 2011. A Novel Role of Vimentin Filaments: Binding and Stabilization of Collagen mRNAs. *Molecular and cellular biology*, 31(18), pp.3773–3789.

Chao, J. a. et al., 2010. ZBP1 recognition of β-actin zipcode induces RNA looping. *Genes and Development*, 24(2), pp.148–158.

Chartrand, P. et al., 1999. Structural elements required for the localization of ASH1 mRNA and of a green fluorescent protein reporter particle in vivo. *Current Biology*, 9(6), pp.333–336.

Chen, D. et al., 2008. Multiple pathways differentially regulate global oxidative stress responses in fission yeast. *Molecular biology of the cell*, 19(1), pp.308–317.

Chen, Q. et al., 2011. Hierarchical regulation of mRNA partitioning between the cytoplasm and the endoplasmic reticulum of mammalian cells. *Molecular biology of the cell*, 22(14), pp.2646–58. Available at: http://www.molbiolcell.org/cgi/doi/10.1091/mbc.E11-03-0239.

Chen, X. et al., 2014. XBP1 promotes triple-negative breast cancer by controlling the HIF1α pathway. *Nature*, 508(7494), pp.103–7. Available at: http://www.nature.com/doifinder/10.1038/nature13119.

Choi, S.B. et al., 2000. Messenger RNA targeting of rice seed storage proteins to specific ER subdomains. *Nature*, 407(6805), pp.765–767.

Coelho, D.S., Gaspar, C.J. & Domingos, P.M., 2014. Ire1 mediated mRNA splicing in a C-terminus deletion mutant of Drosophila Xbp1. *PloS one*, 9(8), p.e105588. Available at: http://www.pubmedcentral.nih.gov/articlerender.fcgi?artid=4138184&tool=pmcentrez&rendertype=abstract.

Condeelis, J. & Singer, R.H., 2005. How and why does beta-actin mRNA target? *Biology of the cell / under the auspices of the European Cell Biology Organization*, 97(1), pp.97–110.

Connor, J.H. et al., 2001. Growth Arrest and DNA Damage-Inducible Protein GADD34 Assembles a Novel Signaling Complex Containing Protein Phosphatase 1 and Inhibitor 1 Growth Arrest and DNA Damage-Inducible Protein GADD34 Assembles a Novel Signaling Complex Containing Protein Phospha. , 21(20), pp.6841–6850.

Cox, J.S., Shamu, C.E. & Walter, P., 1993. Transcriptional Induction of Genes Encoding Endoplasmic-Reticulum Resident Proteins Requires a Transmembrane Protein-Kinase. *Cell*, 73(6), pp.1197–1206. Available at: <Go to ISI>://WOS:A1993LH54800015.

Cox, J.S. & Walter, P., 1996. A novel mechanism for regulating activity of a transcription factor that controls the unfolded protein response. *Cell*, 87, pp.391–404.

Credle, J.J. et al., 2005. On the mechanism of sensing unfolded protein in the endoplasmic reticulum. *Proceedings of the National Academy of Sciences of the United States of America*, 102(52), pp.18773–18784.

Cretenet, G., Le Clech, M. & Gachon, F., 2010. Circadian Clock-Coordinated 12 Hr Period Rhythmic Activation of the IRE1α Pathway Controls Lipid Metabolism in Mouse Liver. *Cell Metabolism*, 11(1), pp.47–57.

Crofts, A.J. et al., 2010. Isolation and identification of cytoskeleton-associated prolamine mRNA binding proteins from developing rice seeds. *Planta*, 231(6), pp.1261–1276.

Cui, X. a, Zhang, H. & Palazzo, A.F., 2012. p180 promotes the ribosome-independent localization of a subset of mRNA to the endoplasmic reticulum. *PLoS biology*, 10(5), p.e1001336. Available at: http://www.pubmedcentral.nih.gov/articlerender.fcgi?artid=3362647&tool=pmcen

trez&rendertype=abstract.

Cui, X. a. et al., 2013. Identification of a region within the placental alkaline phosphatase mRNA that mediates p180-dependent targeting to the endoplasmic reticulum. *Journal of Biological Chemistry*, 288(41), pp.29633–29641.

Cui-Wang, T. et al., 2012. Local zones of endoplasmic reticulum complexity confine cargo in neuronal dendrites. *Cell*, 148(1-2), pp.309–321. Available at: http://dx.doi.org/10.1016/j.cell.2011.11.056.

Davies, M.P. a et al., 2008. Expression and splicing of the unfolded protein response gene XBP-1 are significantly associated with clinical outcome of endocrine-treated breast cancer. *International Journal of Cancer*, 123(1), pp.85–88.

Delanoue, R. et al., 2007. Drosophila Squid/hnRNP Helps Dynein Switch from a gurken mRNA Transport Motor to an Ultrastructural Static Anchor in Sponge Bodies. *Developmental Cell*, 13(4), pp.523–538.

Deshler, J.O., Highett, M.I. & Schnapp, B.J., 1997. Localization of Xenopus Vg1 mRNA by Vera protein and the endoplasmic reticulum. *Science (New York, N.Y.)*, 276(5315), pp.1128–1131.

Diehn, M. et al., 2000. Large-scale identification of secreted and membrane-associated gene products using DNA microarrays. *Nature genetics*, 25(1), pp.58–62.

Dienstbier, M. et al., 2009. Egalitarian is a selective RNA-binding protein linking mRNA localization signals to the dynein motor. *Genes and Development*, 23(13), pp.1546–1558.

Doyle, M. & Kiebler, M. a, 2011. Mechanisms of dendritic mRNA transport and its role in synaptic tagging. *The EMBO journal*, 30(17), pp.3540–3552. Available at: http://dx.doi.org/10.1038/emboj.2011.278.

Egea, P.F. et al., 2004. Substrate twinning activates the signal recognition particle and its receptor. *Nature*, 427(6971), pp.215–221.

Eliscovich, C. et al., 2013. mRNA on the move: The road to its biological destiny. *Journal of Biological Chemistry*, 288(28), pp.20361–20368.

Filigheddu, N. et al., 2007. Ghrelin and Des-Acyl Ghrelin Promote Differentiation and Fusion of C2C12 Skeletal Muscle Cells. *Molecular biology of the cell*, 18(July), pp.986–994.

Forrest, K.M. & Gavis, E.R., 2003. Live imaging of endogenous RNA reveals a

diffusion and entrapment mechanism for nanos mRNA localization in Drosophila. *Current Biology*, 13(14), pp.1159–1168.

Friedlander, R. et al., 2000. A regulatory link between ER-associated protein degradation and the unfolded-protein response. *Nature cell biology*, 2(7), pp.379–384. Available at: papers3://publication/doi/10.1038/35017001\nfile:///Users/SAHARA/Library/Mobile Documents/com~apple~CloudDocs/Papers/Library.papers3/Articles/2000/Friedlander/2000 Friedlander\npapers3://publication/uuid/6D4B6AA7-CCC3-40BA-8A66-B787E638C761\nhttp://eutils.

Fundakowski, J., Hermesh, O. & Jansen, R.P., 2012. Localization of a subset of yeast mRNAs depends on inheritance of endoplasmic reticulum. *Traffic*, 13(12), pp.1642–1652.

Fusco, D. et al., 2003. Single mRNA molecules demonstrate probabilistic movement in living mammalian cells. *Current Biology*, 13(2), pp.161–167.

Gardner, B.M. & Walter, P., 2011. Unfolded Proteins Are Ire1-Activating Ligands That Directly Induce the Unfolded Protein Response. *Science*, 333(6051), pp.1891–1894.

Godin, K.S. & Varani, G., 2007. How arginine-rich domains coordinate mRNA maturation events. *RNA biology*, 4(2), pp.69–75. Available at: http://www.ncbi.nlm.nih.gov/pubmed/17873524.

Gonzalez, I. et al., 1999. ASH1 mRNA localization in yeast involves multiple secondary structural elements and ASH1 protein translation. *Current Biology*, 9(6), pp.337–340.

Gonzalez, T.N., 1999. Mechanism of non-spliceosomal mRNA splicing in the unfolded protein response pathway. *The EMBO Journal*, 18(11), pp.3119–3132. Available at: http://www.pubmedcentral.nih.gov/articlerender.fcgi?artid=1171393&tool=pmcentrez&rendertype=abstract.

Hachet, O. & Ephrussi, A., 2004. Splicing of oskar RNA in the nucleus is coupled to its cytoplasmic localization. *Nature*, 428(6986), pp.959–963.

Halic, M. et al., 2004. Structure of the signal recognition particle interacting with the elongation-arrested ribosome. *Nature*, 427(6977), pp.808–14. Available at:

http://dx.doi.org/10.1038/nature02342.

Hamada, S. et al., 2003. The transport of prolamine RNAs to prolamine protein bodies in living rice endosperm cells. *The Plant cell*, 15(10), pp.2253–2264.

Harding, H.P. et al., 2003. An Integrated Stress Response Regulates Amino Acid Metabolism and Resistance to Oxidative Stress National Institute of Environmental Health Sciences. , 11, pp.619–633.

Harding, H.P. et al., 2000. Regulated translation initiation controls stress-induced gene expression in mammalian cells. *Molecular cell*, 6(5), pp.1099–1108.

Harding, H.P., Zhang, Y. & Ron, D., 1999. Protein translation and folding are coupled by an endoplasmic-reticulum-resident kinase. *Nature*, 397(6716), pp.271–274.

Haze, K. et al., 1999. Mammalian transcription factor ATF6 is synthesized as a transmembrane protein and activated by proteolysis in response to endoplasmic reticulum stress. *Molecular biology of the cell*, 10(11), pp.3787–3799.

He, Y., Beatty, A., Han, X., Ji, Y., Ma, X., Adelstein, R.S., et al., 2012. Nonmuscle Myosin IIB Links Cytoskeleton to IRE1α Signaling during ER Stress. *Developmental Cell*, 23(6), pp.1141–1152. Available at: http://dx.doi.org/10.1016/j.devcel.2012.11.006.

He, Y., Beatty, A., Han, X., Ji, Y., Ma, X., Adelstein, R.S., et al., 2012. Nonmuscle myosin IIB links cytoskeleton to IRE1α signaling during ER stress. *Developmental cell*, 23(6), pp.1141–52. Available at: http://www.ncbi.nlm.nih.gov/pubmed/23237951.

Hermesh, O. & Jansen, R.P., 2013. Take the (RN)A-train: Localization of mRNA to the endoplasmic reticulum. *Biochimica et Biophysica Acta - Molecular Cell Research*, 1833(11), pp.2519–2525. Available at: http://dx.doi.org/10.1016/j.bbamcr.2013.01.013.

Hetz, C. et al., 2009. XBP-1 deficiency in the nervous system protects against amyotrophic lateral sclerosis by increasing autophagy. *Genes and Development*, 23(19), pp.2294–2306.

Heuck, A. et al., 2010. The structure of the Myo4p globular tail and its function in ASH1 mRNA localization. *Journal of Cell Biology*, 189(3), pp.497–510.

Hocine, S., Singer, R.H. & Grünwald, D., 2010. RNA processing and export. *Cold Spring Harbor perspectives in biology*, 2(12), pp.565–566.

Hollien, J. et al., 2009. Regulated Ire1-dependent decay of messenger RNAs in

mammalian cells. *Journal of Cell Biology*, 186(3), pp.323–331.

Hollien, J. & Weissman, J.S., 2006. Decay of endoplasmic reticulum-localized mRNAs during the unfolded protein response. *Science (New York, N.Y.)*, 313(5783), pp.104–107.

Hooks, K.B. & Griffiths-Jones, S., 2011. Conserved RNA structures in the non-canonical Hac1/Xbp1 intron. *RNA biology*, 8(4), pp.552–556.

Hoozemans, J.J.M. et al., 2007. Activation of the unfolded protein response in Parkinson's disease. *Biochemical and Biophysical Research Communications*, 354(3), pp.707–711.

Hoozemans, J.J.M. et al., 2005. The unfolded protein response is activated in Alzheimer's disease. *Acta Neuropathologica*, 110(2), pp.165–172.

Huh, W.J. et al., 2010. XBP1 controls maturation of gastric zymogenic cells by induction of MIST1 and expansion of the rough endoplasmic reticulum. *Gastroenterology*, 139(6), pp.2038–49. Available at: http://www.ncbi.nlm.nih.gov/pubmed/20816838.

Ishiwata-Kimata, Y. et al., 2013. F-actin and a Type-II Myosin Are Required for Efficient Clustering of the ER Stress Sensor Ire1. *Cell structure and function*, 38(2), pp.135–43. Available at: http://www.ncbi.nlm.nih.gov/pubmed/23666407.

Iwakoshi, N.N. et al., 2003. Plasma cell differentiation and the unfolded protein response intersect at the transcription factor XBP-1. *Nature immunology*, 4(4), pp.321–329.

Iwawaki, T. et al., 2004. A transgenic mouse model for monitoring endoplasmic reticulum stress. *Nature medicine*, 10(1), pp.98–102.

Iwawaki, T. & Akai, R., 2006. Analysis of the XBP1 splicing mechanism using endoplasmic reticulum stress-indicators. *Biochemical and Biophysical Research Communications*, 350(3), pp.709–715.

Jagannathan, S. et al., 2014. De novo translation initiation on membrane-bound ribosomes as a mechanism for localization of cytosolic protein mRNAs to the endoplasmic reticulum. *RNA (New York, N.Y.)*, 20(10), pp.1489–98. Available at: http://www.ncbi.nlm.nih.gov/pubmed/25142066.

Jambhekar, A. & Derisi, J.L., 2007. Cis-acting determinants of asymmetric, cytoplasmic RNA transport. *RNA (New York, N.Y.)*, 13(5), pp.625–642.

Johnstone, O. & Lasko, P., 2001. T Ranslational R Egulation and Rna L Ocalization

in D Rosophila. , pp.365–406.

Jonikas, M.C. et al., 2009. Comprehensive characterization of genes required for protein folding in the endoplasmic reticulum. *Science (New York, N.Y.)*, 323(5922), pp.1693–7. Available at: http://www.ncbi.nlm.nih.gov/pubmed/19325107.

Keenan, R.J. et al., 1998. Crystal structure of the signal sequence binding subunit of the signal recognition particle. *Cell*, 94(2), pp.181–191.

Keenan, R.J. et al., 2001. The signal recognition particle. *Annual review of biochemistry*, 70, pp.755–775.

Kertesz, M. et al., 2010. Genome-wide measurement of RNA secondary structure in yeast. *Nature*, 467(7311), pp.103–107. Available at: http://dx.doi.org/10.1038/nature09322.

Khaminets, A. et al., 2015. Regulation of endoplasmic reticulum turnover by FAM134B-mediated selective autophagy. *Nature*, 522(7556), pp.359–62. Available at: http://www.ncbi.nlm.nih.gov/pubmed/26040717.

King, M. Lou, Messitt, T.J. & Mowry, K.L., 2005. Putting RNAs in the right place at the right time: RNA localization in the frog oocyte. *Biology of the cell / under the auspices of the European Cell Biology Organization*, 97(1), pp.19–33.

Kislauskis, E.H., Zhu, X. & Singer, R.H., 1994. Sequences responsible for intracellular localization of beta-actin messenger RNA also affect cell phenotype. *The Journal of cell biology*, 127(2), pp.441–451.

Korennykh, A. V et al., 2009. The unfolded protein response signals through high-order assembly of Ire1. *Nature*, 457(7230), pp.687–693. Available at: http://dx.doi.org/10.1038/nature07661.

Kovács, M. et al., 2004. Mechanism of blebbistatin inhibition of myosin II. *Journal of Biological Chemistry*, 279(34), pp.35557–35563.

Lakkaraju, A.K.K. et al., 2008. SRP Keeps Polypeptides Translocation-Competent by Slowing Translation to Match Limiting ER-Targeting Sites. *Cell*, 133(3), pp.440–451.

Latham, V.M. et al., 2001. A Rho-dependent signaling pathway operating through myosin localizes β-actin mRNA in fibroblasts. *Current Biology*, 11(13), pp.1010–1016.

Lécuyer, E. et al., 2007. Global Analysis of mRNA Localization Reveals a Prominent

Role in Organizing Cellular Architecture and Function. *Cell*, 131(1), pp.174–187.

Lee, A.-H. et al., 2011. Dual and opposing roles of the unfolded protein response regulated by IRE1alpha and XBP1 in proinsulin processing and insulin secretion. *Proceedings of the National Academy of Sciences of the United States of America*, 108(21), pp.8885–90. Available at: http://www.pnas.org/content/108/21/8885.long.

Lee, A.-H. et al., 2005. XBP-1 is required for biogenesis of cellular secretory machinery of exocrine glands. *The EMBO journal*, 24(24), pp.4368–80. Available at: http://emboj.embopress.org/content/24/24/4368.abstract.

Lee, K.P.K. et al., 2008. Structure of the Dual Enzyme Ire1 Reveals the Basis for Catalysis and Regulation in Nonconventional RNA Splicing. *Cell*, 132(1), pp.89–100.

Leung, E. & Brown, J.D., 2010. Biogenesis of the signal recognition particle. *Biochemical Society transactions*, 38(4), pp.1093–1098.

Li, H. et al., 2010. Mammalian endoplasmic reticulum stress sensor IRE1 signals by dynamic clustering. *Proceedings of the National Academy of Sciences of the United States of America*, 107(37), pp.16113–16118.

Li, X., Franceschi, V.R. & Okita, T.W., 1993. Segregation of storage protein mRNAs on the rough endoplasmic reticulum membranes of rice endosperm cells. *Cell*, 72(6), pp.869–879.

Lin, A.C. & Holt, C.E., 2007. Local translation and directional steering in axons. *The EMBO journal*, 26(16), pp.3729–3736.

Ling, S.C.W. et al., 2012. Response of myeloma to the proteasome inhibitor bortezomib is correlated with the unfolded protein response regulator XBP-1. *Haematologica*, 97(1), pp.64–72.

Lipatova, Z. & Segev, N., 2015. A Role for Macro-ER-Phagy in ER Quality Control. *PLOS Genetics*, 11(7), p.e1005390. Available at: http://dx.plos.org/10.1371/journal.pgen.1005390.

Long, R.M. et al., 2000. She2p is a novel RNA-binding protein that recruits the Myo4p-She3p complex to ASH1 mRNA. *The EMBO journal*, 19(23), pp.6592–6601.

Loya, A. et al., 2008. The 3'-UTR mediates the cellular localization of an mRNA encoding a short plasma membrane protein. *RNA (New York, N.Y.)*, 14(7),

pp.1352–65. Available at: http://www.ncbi.nlm.nih.gov/pubmed/18492794.

Lu, P.D., Harding, H.P. & Ron, D., 2004. Translation reinitiation at alternative open reading frames regulates gene expression in an integrated stress response. *Journal of Cell Biology*, 167(1), pp.27–33.

Lu, Y., Liang, F.X. & Wang, X., 2014. A Synthetic Biology Approach Identifies the Mammalian UPR RNA Ligase RtcB. *Molecular Cell*, pp.1–13.

Macdonald, P.M. & Kerr, K., 1998. Mutational analysis of an RNA recognition element that mediates localization of bicoid mRNA. *Molecular and cellular biology*, 18(7), pp.3788–3795.

MacDougall, N. et al., 2003. Drosophila gurken (TGFα) mRNA localizes as particles that move within the oocyte in two dynein-dependent steps. *Developmental Cell*, 4(3), pp.307–319.

Majumder, M. et al., 2012. A Novel Feedback Loop Regulates the Response to Endoplasmic Reticulum Stress via the Cooperation of Cytoplasmic Splicing and mRNA Translation. *Molecular and Cellular Biology*, 32(5), pp.992–1003.

Martin, K.C. & Ephrussi, A., 2009. mRNA Localization: Gene Expression in the Spatial Dimension. *Cell*, 136(4), pp.719–730. Available at: http://dx.doi.org/10.1016/j.cell.2009.01.044.

Martin, K.C. & Zukin, R.S., 2006. RNA trafficking and local protein synthesis in dendrites: an overview. *The Journal of neuroscience : the official journal of the Society for Neuroscience*, 26(27), pp.7131–7134.

Martínez, G. et al., 2016. Regulation of Memory Formation by the Transcription Factor XBP1. *Cell reports*, 14(6), pp.1382–94. Available at: http://www.ncbi.nlm.nih.gov/pubmed/26854229.

Mary, C. et al., 2010. Residues in SRP9/14 essential for elongation arrest activity of the signal recognition particle define a positively charged functional domain on one side of the protein. *RNA (New York, N.Y.)*, 16(5), pp.969–979.

Maurel, M. et al., 2014. Getting RIDD of RNA: IRE1 in cell fate regulation. *Trends in Biochemical Sciences*, 39(5), pp.245–254. Available at: http://dx.doi.org/10.1016/j.tibs.2014.02.008.

Mccullough, K.D. et al., 2001. Gadd153 Sensitizes Cells to Endoplasmic Reticulum Stress by Down-Regulating Bcl2 and Perturbing the Cellular Redox State Gadd153 Sensitizes Cells to Endoplasmic Reticulum Stress by Down-Regulating

Bcl2 and Perturbing the Cellular Redox State. *Molecular and Cellular Biology*, 21(4), pp.1249–1259.

Mechler, B. & Vassalli, P., 1975. Membrane bound ribosomes of myeloma cells. I. Preparation of free and membrane bound ribosomal fractions. Assessment of the methods and properties of the ribosomes. *Journal of Cell Biology*, 67(6), pp.1–15.

Meusser, B. et al., 2005. ERAD: the long road to destruction. *Nature cell biology*, 7(8), pp.766–772.

Mili, S., Moissoglu, K. & Macara, I.G., 2008. Genome-wide screen reveals APC-associated RNAs enriched in cell protrusions. *Nature*, 453(7191), pp.115–119.

Mishiba, K. et al., 2013. Defects in IRE1 enhance cell death and fail to degrade mRNAs encoding secretory pathway proteins in the Arabidopsis unfolded protein response. *Proceedings of the National Academy of Sciences of the United States of America*, 110(14), pp.5713–8. Available at: http://www.pubmedcentral.nih.gov/articlerender.fcgi?artid=3619347&tool=pmcentrez&rendertype=abstract.

Mor, A. et al., 2010. Dynamics of single mRNP nucleocytoplasmic transport and export through the nuclear pore in living cells. *Nature cell biology*, 12(6), pp.543–552. Available at: http://dx.doi.org/10.1038/ncb2056.

Mori, K. et al., 1993. A transmembrane protein with a cdc2+/CDC28-related kinase activity is required for signaling from the ER to the nucleus. *Cell*, 74(4), pp.743–756.

Munro, T.P. et al., 1999. Mutational analysis of a heterogeneous nuclear ribonucleoprotein A2 response element for RNA trafficking. *The Journal of biological chemistry*, 274(48), pp.34389–34395.

Okamura, K. et al., 2000. Dissociation of Kar2p/BiP from an ER sensory molecule, Ire1p, triggers the unfolded protein response in yeast. *Biochemical and biophysical research communications*, 279(2), pp.445–450.

Ollion, J. et al., 2013. TANGO: A generic tool for high-throughput 3D image analysis for studying nuclear organization. *Bioinformatics*, 29(14), pp.1840–1841.

Palacios, I.M. & St Johnston, D., 2002. Kinesin light chain-independent function of the Kinesin heavy chain in cytoplasmic streaming and posterior localisation in the Drosophila oocyte. *Development (Cambridge, England)*, 129(23), pp.5473–

5485.

Paquin, N. & Chartrand, P., 2008. Local regulation of mRNA translation: new insights from the bud. *Trends in Cell Biology*, 18(3), pp.105–111.

Patel, V.L. et al., 2012. Spatial arrangement of an RNA zipcode identifies mRNAs under post-transcriptional control. *Genes and Development*, 26(1), pp.43–53.

Pehar, M. et al., 2012. SLC33A1/AT-1 protein regulates the induction of autophagy downstream of IRE1/XBP1 pathway. *Journal of Biological Chemistry*, 287(35), pp.29921–29930.

Peschek, J. et al., 2015. A conformational RNA zipper promotes intron ejection during non-conventional XBP1 mRNA splicing. *EMBO reports*, pp.1–11. Available at: http://www.ncbi.nlm.nih.gov/pubmed/26483401.

Pincus, D. et al., 2010. BiP binding to the ER-stress sensor Ire1 tunes the homeostatic behavior of the unfolded protein response. *PLoS Biology*, 8(7).

Plumb, R. et al., 2015. A functional link between the co-translational protein translocation pathway and the UPR. *eLife*, 4, pp.1–18. Available at: http://elifesciences.org/lookup/doi/10.7554/eLife.07426.

Pool, M.R., 2005. Signal recognition particles in chloroplasts, bacteria, yeast and mammals (review). *Molecular membrane biology*, 22(1-2), pp.3–15.

Powers, T. & Walter, P., 1997. Co-translational protein targeting catalyzed by the Escherichia coli signal recognition particle and its receptor. *The EMBO Journal*, 16(16), pp.4880–4886. Available at: http://www.nature.com/emboj/journal/v16/n16/abs/7590466a.html\nhttp://www.nature.com/emboj/journal/v16/n16/pdf/7590466a.pdf.

Pyhtila, B. et al., 2008. Signal sequence- and translation-independent mRNA localization to the endoplasmic reticulum. *RNA (New York, N.Y.)*, 14(3), pp.445–53. Available at: http://rnajournal.cshlp.org/content/14/3/445.short.

Reid, D.W. et al., 2014. The Unfolded Protein Response Triggers Selective mRNA Release from the Endoplasmic Reticulum. *Cell*, 158(6), pp.1362–1374. Available at: http://www.sciencedirect.com/science/article/pii/S0092867414010435\nhttp://ac.els-cdn.com/S0092867414010435/1-s2.0-S0092867414010435-main.pdf?_tid=641b7d34-7294-11e4-8384-00000aacb35e&acdnat=1416694418_7aa2c8250c07e059bcce88f400df6cf7.

Reid, D.W. & Nicchitta, C. V., 2012. Primary role for endoplasmic reticulum-bound ribosomes in cellular translation identified by ribosome profiling. *Journal of Biological Chemistry*, 287(8), pp.5518–5527.

Reimold, A.M. et al., 2000. An essential role in liver development for transcription factor XBP-1. *Genes & development*, 14(2), pp.152–7. Available at: http://www.pubmedcentral.nih.gov/articlerender.fcgi?artid=316338&tool=pmcentrez&rendertype=abstract.

Ritter, A.T., Angus, K.L. & Griffiths, G.M., 2013. The role of the cytoskeleton at the immunological synapse. , pp.107–117.

Romero-Ramirez, L. et al., 2009. X box-binding protein 1 regulates angiogenesis in human pancreatic adenocarcinomas. *Translational oncology*, 2(1), pp.31–38.

Ron, D., 2009. Targeting of mRNAs to Their Sites of Unconventional Splicing in the Unfolded Protein Response. *Molecular Cell*, 34(2), pp.133–134. Available at: http://dx.doi.org/10.1016/j.molcel.2009.04.003.

Ron, D. & Walter, P., 2007. Signal integration in the endoplasmic reticulum unfolded protein response. *Nature reviews. Molecular cell biology*, 8(7), pp.519–529.

Rüegsegger, U., Leber, J.H. & Walter, P., 2001. Block of HAC1 mRNA translation by long-range base pairing is released by cytoplasmic splicing upon induction of the unfolded protein response. *Cell*, 107(1), pp.103–114.

Rutkowski, D.T. & Hegde, R.S., 2010. Regulation of basal cellular physiology by the homeostatic unfolded protein response. *Journal of Cell Biology*, 189(5), pp.783–794.

Samson, F. et al., 1979. Nocodazole action on tubulin assembly, axonal ultrastructure and fast axoplasmic transport. *The Journal of pharmacology and experimental therapeutics*, 208, pp.411–417.

Schindler, A.J. & Schekman, R., 2009. In vitro reconstitution of ER-stress induced ATF6 transport in COPII vesicles. *Proceedings of the National Academy of Sciences of the United States of America*, 106(42), pp.17775–17780.

Schmid, M. et al., 2006. Coordination of Endoplasmic Reticulum and mRNA Localization to the Yeast Bud. *Current Biology*, 16(15), pp.1538–1543.

Shen, Z. et al., 2009. Nuclear shuttling of She2p couples ASH1 mRNA localization to its translational repression by recruiting Loc1p and Puf6p. *Molecular biology of the cell*, 20(8), pp.2265–75. Available at:

http://www.ncbi.nlm.nih.gov/pubmed/19244342.

Shepard, K. a et al., 2003. Widespread cytoplasmic mRNA transport in yeast: identification of 22 bud-localized transcripts using DNA microarray analysis. *Proceedings of the National Academy of Sciences of the United States of America*, 100, pp.11429–11434.

Sidrauski, C., Cox, J.S. & Walter, P., 1996. tRNA ligase is required for regulated mRNA splicing in the unfolded protein response. *Cell*, 87(3), pp.405–413.

Sidrauski, C. & Walter, P., 1997. The transmembrane kinase Ire1p is a site-specific endonuclease that initiates mRNA splicing in the unfolded protein response. *Cell*, 90(6), pp.1031–9. Available at: http://www.ncbi.nlm.nih.gov/pubmed/9323131.

Siegel, V. & Walter, P., 1988. The affinity of signal recognition particle for presecretory proteins is dependent on nascent chain length. *The EMBO journal*, 7(6), pp.1769–75. Available at: http://www.pubmedcentral.nih.gov/articlerender.fcgi?artid=457167&tool=pmcentrez&rendertype=abstract.

Sikorski, R.S. & Hieter, P., 1989. A system of shuttle vectors and yeast host strains designed for efficient manipulation of DNA in Saccharomyces cerevisiae. *Genetics*, 122(1), pp.19–27.

So, J.S. et al., 2012. Silencing of lipid metabolism genes through ire1??-mediated Mrna decay lowers plasma lipids in mice. *Cell Metabolism*, 16(4), pp.487–499. Available at: http://dx.doi.org/10.1016/j.cmet.2012.09.004.

Sriburi, R. et al., 2007. Coordinate Regulation of Phospholipid Biosynthesis and Secretory Pathway Gene Expression in XBP-1 (S) -induced Endoplasmic Reticulum Biogenesis * □. , 282(10), pp.7024–7034.

Sriburi, R. et al., 2004. JCB : REPORT. , 167(1).

Sugimoto, Y. et al., 2015. hiCLIP reveals the in vivo atlas of mRNA secondary structures recognized by Staufen 1. *Nature*, 519(7544), pp.491–4. Available at: http://dx.doi.org/10.1038/nature14280.

Tam, A.B., Koong, A.C. & Niwa, M., 2014. Ire1 Has Distinct Catalytic Mechanisms for XBP1/HAC1 Splicing and RIDD. *Cell Reports*, 9(3), pp.850–858. Available at: http://linkinghub.elsevier.com/retrieve/pii/S2211124714007840.

Tassan, J.P. & Le Goff, X., 2004. An overview of the KIN1/PAR-1/MARK kinase

family. *Biology of the Cell*, 96(3), pp.193–199.

Thandapani, P. et al., 2013. Defining the RGG/RG motif. *Molecular cell*, 50(5), pp.613–23. Available at: http://linkinghub.elsevier.com/retrieve/pii/S1097276513004085.

Tian, P.G. et al., 2015. Spliced XBP1 promotes macrophage survival and autophagy by interacting with Beclin-1. *Biochemical and Biophysical Research Communications*, 463(4), pp.518–523. Available at: http://dx.doi.org/10.1016/j.bbrc.2015.05.061.

Travers, K.J. et al., 2000. Functional and genomic analyses reveal an essential coordination between the unfolded protein response and ER-associated degradation. *Cell*, 101(3), pp.249–258.

Upton, J.-P. et al., 2012. IRE1α cleaves select microRNAs during ER stress to derepress translation of proapoptotic Caspase-2. *Science (New York, N.Y.)*, 338(6108), pp.818–22. Available at: http://www.ncbi.nlm.nih.gov/pubmed/23042294.

Valdés, P. et al., 2014. Control of dopaminergic neuron survival by the unfolded protein response transcription factor XBP1. *Proceedings of the National Academy of Sciences of the United States of America*, 111(18), pp.6804–9. Available at: http://www.ncbi.nlm.nih.gov/pubmed/24753614.

Valenzuela, V. et al., 2012. Activation of the unfolded protein response enhances motor recovery after spinal cord injury. *Cell Death and Disease*, 3(2), p.272. Available at: http://dx.doi.org/10.1038/cddis.2012.8.

Vicente-Manzanares, M. et al., 2009. Non-muscle myosin II takes centre stage in cell adhesion and migration. *Nature Reviews Molecular Cell Biology*, 10(11), pp.778–790. Available at: http://www.nature.com/nrm/journal/v10/n11/abs/nrm2786.html.

Voeltz, G.K. et al., 2006. A class of membrane proteins shaping the tubular endoplasmic reticulum. *Cell*, 124(3), pp.573–586.

Wakatsuki, T. et al., 2001. Effects of cytochalasin D and latrunculin B on mechanical properties of cells. *Journal of cell science*, 114(Pt 5), pp.1025–1036.

Walter, P. & Blobel, G., 1983. Disassembly and reconstitution of signal recognition particle. *Cell*, 34(2), pp.525–533.

Walter, P., Gilmore, R. & Blobel, G., 1984. Protein translocation across the

endoplasmic reticulum. *Cell*, 38(1), pp.5–8. Available at: http://www.sciencedirect.com/science/article/pii/0092867484905208\nhttp://www.sciencedirect.com/science?_ob=MiamiImageURL&_cid=272196&_user=618624&_pii=0092867484905208&_check=y&_origin=article&_zone=toolbar&_coverDate=31-Aug-1984&view=c&originContentFami.

Walter, P. & Johnson, A.E., 1994. Signal sequence recognition and protein targeting to the endoplasmic reticulum membrane. *Annual review of cell biology*, 10, pp.87–119. Available at: http://www.ncbi.nlm.nih.gov/pubmed/7888184.

Walter, P. & Ron, D., 2011. The Unfolded Protein Response: From Stress Pathway to Homeostatic Regulation. *Science*, 334(6059), pp.1081–1086.

Weickert, J., 1999. Coherence-enhancing diffusion of colour images. *Image and Vision Computing*, 17(3-4), pp.201–212.

West, M. et al., 2011. A 3D analysis of yeast ER structure reveals how ER domains are organized by membrane curvature. *Journal of Cell Biology*, 193(2), pp.333–346.

Woo, C.W. et al., 2009. Adaptive suppression of the ATF4-CHOP branch of the unfolded protein response by toll-like receptor signalling. *Nature cell biology*, 11(12), pp.1473–1480. Available at: http://dx.doi.org/10.1038/ncb1996.

Yanagitani, K. et al., 2009. Cotranslational Targeting of XBP1 Protein to the Membrane Promotes Cytoplasmic Splicing of Its Own mRNA. *Molecular Cell*, 34(2), pp.191–200. Available at: http://dx.doi.org/10.1016/j.molcel.2009.02.033.

Yanagitani, K. et al., 2011. Translational pausing ensures membrane targeting and cytoplasmic splicing of XBP1u mRNA. *Science (New York, N.Y.)*, 331(6017), pp.586–589.

Yoshida, H. et al., 2003. A time-dependent phase shift in the mammalian unfolded protein response. *Developmental Cell*, 4(2), pp.265–271.

Yoshida, H. et al., 2001. XBP1 mRNA is induced by ATF6 and spliced by IRE1 in response to ER stress to produce a highly active transcription factor. *Cell*, 107, pp.881–891.

Zaessinger, S., Busseau, I. & Simonelig, M., 2006. Oskar allows nanos mRNA translation in Drosophila embryos by preventing its deadenylation by Smaug/CCR4. *Development (Cambridge, England)*, 133(22), pp.4573–4583.

Zhang, Y. & Stefanovic, B., 2016. LARP6 Meets Collagen mRNA: Specific

Regulation of Type I Collagen Expression. *International Journal of Molecular Sciences*, 17(3), p.419. Available at: http://www.mdpi.com/1422-0067/17/3/419.

Zhou, C. et al., 2014. Organelle-based aggregation and retention of damaged proteins in asymmetrically dividing cells. *Cell*, 159(3), pp.530–42. Available at: http://www.ncbi.nlm.nih.gov/pubmed/25417105.

Zhou, J. et al., 2006. The crystal structure of human IRE1 luminal domain reveals a conserved dimerization interface required for activation of the unfolded protein response. *Proceedings of the National Academy of Sciences of the United States of America*, 103(39), pp.14343–14348.